ABSTRACT

Title of Document:

The Development of Food Polymer-Based Nanocomposites as

Novel Antimicrobial Agents and Sustainable Packaging Materials

Boce Zhang, Doctor of Philosophy, 2012

Directed by:

Professor Qin Wang
Department of Nutrition and Food Science

Nanocomposites developed from food polymers are an emerging technology, which has shown plenty of promising applications in worldwide food related markets. The dissertation first investigated how protein modification determined structural and functional properties of nanocomposites. The study then developed simple preparation methods for food polymer nanocomposites with two potential novel applications, including low toxic antimicrobial agent and high performance sustainable packaging material.

First, the study investigated the effects of chemical modification on protein structures and properties. The glutamine rich protein, zein, was selected to study how deamidation via acid and base may affect structural, mechanical, and antioxidant properties of zein. High cysteine protein, alpha-lactalbumin (ALA), was then used to investigate how redox modification of cysteine groups may determine the functional property of ALA.

The first potential application of food polymer nanocomposites is to lower the toxicity of silver-based antimicrobial agent. Although silver has renowned broad-spectrum antimicrobial activities, the use was still restricted by its toxicity from low biocompatibility and argyria (skin discoloration). In this study, silver-zein and silver-ALA nanocomposite showed promising capability to substantially reduce the toxicity of silver. The silver/protein nanocomposites may find a solution for the current challenge of silver-based antiseptics.

Another potential application of food polymer nanocomposites is to modify sustainable film made of food polymers to develop biodegradable plastic materials with improved mechanical and barrier properties. Theoretical studies have proven that a well-ordered nanocomposite structure could provide maximum functionality improvement, but such structure was largely unachieved. A simple and cost effective method was developed in this study using ferromagnetic nanoplatelet as nanofiller materials to achieve highly-arranged structure. Thus prepared zein/Fe3O4 nanocomposite had improved mechanical and gas barrier properties.

The Development of Food Polymer-Based Nanocomposites as Novel

Antimicrobial Agents and Sustainable Packaging Materials

By

Boce Zhang

Dissertation submitted to the Faculty of the Graduate School of the

University of Maryland, College Park, in partial fulfillment

of the requirements for the degree of

Doctor of Philosophy

2012

Advisory Committee:

Professor/Chair	Wang, Qin
Professor	Castonguay, Thomas
Doctor	Luo, Yaguang
Professor	Tao, Yang
Professor	Yu, Liangli (Lucy)

Dedication

This is lovingly dedicated to my wife, Haiqi, and our parents who have been my constant source for encouragement and inspiration.

Acknowledgements

Though only my name appears on the cover, a great many people have contributed to this dissertation and deserve special mention.

Foremost among them, I offer my deepest gratitude to my advisor, Dr. Qin Wang. My graduate life has been an amazingly fortunate journey to have an advisor who inspired and guided me with her tremendous knowledge, passion and patience, while at the same time giving me the freedom to explore the world of unknown.

I would like to thank my dissertation committee members, Drs. Thomas Castonguay, Yaguang Luo, Yang Tao, and Liangli (Lucy) Yu, for their guidance and support in finishing this dissertation. Their insightful suggestions broadened my professional experience and prepared me for future challenges.

Special thank also goes to to my labmates, Yangchao (Albert) Luo, Zhenlei Xiao, Zi (David) Teng, and Yunpeng (Roc) Wu, to make our lab a convivial place to work. Together, I had a memorable graduate life with all of your support, collaboration and companionship.

I'm also grateful to the University of Maryland for fostering a fantastic academic community, where I've been able to participate in interdisciplinary cooperation with renowned researchers in advanced science and engineering programs. Particularly, I would like to thank the Graduate School and our beloved Dean Dr. Charles Caramello, who have supported and accredited my enthusiasm to my entire graduate research experience through the Ann G. Wylie Dissertation Fellowship.

Finally, and most importantly, I would like to thank my family for their unending encouragement, support and love. I'm particularly thankful to my wife, Haiqi for her unwavering encourangement, patience, and her unyielding devotion and love, which were undeniably the cornerstone of my life for the past five years. I'm greatly indebted to my parents for their faith in me and their sacrifices to provide me a life that includes one of the best education and opportunities. Also, I thank Haiqi's parents for their encouragement and guidance on our life and career.

Table of Contents

List of Tables

List of Figures

Introduction

Biopolymer nanocomposite is an emerging technology. As one of the biopolymer nanocomposites category, food polymer nanocomposites have shown plenty of promising applications in worldwide food related markets. The dissertation first investigated the relationship between physiochemical properties of modified protein and nanocomposite structure, as well as their influences on nanocomposites functionalities. The study then developed simple preparation methods for food polymer nanocomposites with two potential novel applications, including low toxic antimicrobial agent and high performance sustainable packaging material.

The first objective of the study is to investigate the effect of chemical modification on protein's structures and physiochemical properties. The glutamine rich protein, zein, was selected to study how deamidation via acid and base may affect structural, mechanical, and antioxidant properties of zein. High cysteine protein, alpha-lactalbumin (ALA), was then used to investigate how redox modification of cysteine groups may determine the functional properties of food polymer.

The second objective is to develop silver/protein nanocomposites to address the toxicity of silver-based antimicrobial agents, which may induce immunological response and argyria (skin discoloration) when it bound to blood cysteine via the intake and release of silver in blood vessel. Both zein (high glutamine content) and ALA (high cysteine content) were biocompatible and used to increase silver's hemocompatibility, while only ALA was investigated to deal with the silver release issue.

The third objective is to develop a simple and cost effective method to prepare well-ordered food polymer-based nanocomposite using a magnetic nanofiller via in situ external magnetic field reorientation. The effect of filler arrangement on the functional property change of the zein/Fe3O4 nanocomposites was evaluated, including mechanical, gas barrier, and electromagnetic properties etc.

CHAPTER 1. Literature Review

1.1   Overview of Nanocomposite Technology

A composite typically consists of a polymer matrix (continuous phase) and a discontinuous phase (filler) (Ray & Okamoto, 2003). The fillers could be fibers, platelets, and/or particles, which have been used for decades in polymer composites. The primary functionality changes of polymer composites are the enhanced mechanical, barrier and thermal properties. Recently, the advancement in nanotechnology brought a major breakthrough in composite materials, which was associated with a new term 'nanocomposites'. Nanocomposites are polymeric materials in which the filler has at least one dimension smaller than 100 nm (e.g. nanoparticle has three dimensions, nanotube has two dimensions, and nanoplatelet has one diemension). In the last decade, nanocomposite technology has shown various promising applications, such as antimicrobial agent, biodegradable packaging, fire retardant, optical device and semiconductor as memory material (Ray & Bousmina, 2005; Ray & Okamoto, 2003). Among those, the development of nanocomposite as novel antimicrobial agent and biodegradable packaging could be of the top interests. Elementary form of silver or silver compound was most studied as the antimicrobial nanofiller in polymeric matrices, because silver's broad spectrum antimicrobial activities. However, the application of silver/polymer nanocomposites was restricted to certain clinical application due to two long-existing tolerability concerns: low hemocompatibility and silver release induced argyria (Wright, Lam, & Burrell, 1998).

Moreover, the application of eco-friendly biopolymer in sustainable packaging is of great interests, whereas major challenges still exists due to the poor mechanical and gas barrier properties of the pure biopolymer film. Recently, methods to form exfoliated nanocomposites structure has been established to overcome these disadvantages. However, a further theoretical study (Bharadwaj, 2001) suggested that a well-distributed and well-ordered planar structure could substantially improve the mechanical and gas barrier properties of the nanocomposites. Unfortunately, there is lack of knowledge regarding the development of well-ordered nanocomposites as packaging materials. Therefore, in this study, chemical modification of nanofiller and protein matrices, as well as the rearrangement of ferromagnetic nanofiller were used to address these challenges in the application of antimicrobial agents and sustainable packaging.

1.2 Antimicrobial Agents

1.2.1 Overview of Silver-Based Antimicrobial Agents

Silver element and silver ions have been used as conventional antiseptics since ancient times due to their broad-spectrum bactericidal activities. They are proved to be effective against both Gram positive and Gram negative antibiotic-resistant bacteria, which have caused increasing concerns in both clinical and food applications (de Azeredo, 2009; Panacek, Kvitek, Prucek, Kolar, Vecerova, Pizurova, et al., 2006; Wright, Lam, & Burrell, 1998). Silver compounds, such as silver sulfadiazine (Wright, Lam, & Burrell, 1998), and novel silver-based composites with phosphate based glass (Valappil, Pickup, Carroll, Hope, Pratten, Newport, et al., 2007), stainless steel

(Charlot, Sciannamea, Lenoir, Faure, Jerome, Jerome, et al., 2009), carbon nanotubes(Akhavan, Abdolahad, Abdi, & Mohajerzadeh, 2011), or gold surface (Gordon, Slenters, Brunetto, Villaruz, Sturdevant, Otto, et al., 2010) showed bactericidal activities against bacteria in clinical applications. Both elementary form and compounds of silver were proven to have broad-spectrum antimicrobial activities, as for being extremely efficient against both Gram positive and Gram negative microorganisms (Akhavan, Abdolahad, Abdi, & Mohajerzadeh, 2011; Balogh, Swanson, Tomalia, Hagnauer, & McManus, 2001; Charlot, et al., 2009; Cho, Park, Osaka, & Park, 2005; de Azeredo, 2009; do Nascimento, Sampaio, Medeiros, & de Azevedo, 2009; Furno, Morley, Wong, Sharp, Arnold, Howdle, et al., 2004; Gordon, et al., 2010; Ho, Tobis, Sprich, Thomann, & Tiller, 2004; Jonas, Bloch, Zimmermann, Stadie, Gross, & Schad, 2007; Krishnaraj, Jagan, Rajasekar, Selvakumar, Kalaichelvan, & Mohan, 2010; R. Kumar & Munstedt, 2005; Panacek, et al., 2006; Romanov, Siu, Verkerk, Hopkinson, & Siu, 2010; Sanpui, Murugadoss, Prasad, Ghosh, & Chattopadhyay, 2008; Travan, Pelillo, Donati, Marsich, Benincasa, Scarpa, et al., 2009; Triebel, Vasylyev, Damm, Stara, Ozpinar, Hausmann, et al., 2011; Valappil, et al., 2007; Wei, Sun, Qian, Ye, & Ma, 2009; B. C. Zhang, Y. C. Luo, & Q. Wang, 2010), and even multiresistant bacterial strain (de Azeredo, 2009; Panacek, et al., 2006; Wright, Lam, & Burrell, 1998). However, their current applications were still rigorously restricted to specific medical condition (e.g. sever burn wounds), which was also limited to a small market size out of the total $25 billion global market of antimicrobial agents. This regulatory situation could be basically attributed

to two major tolerability concerns: silver-induced lethal immunological response due to its low hemocompatibility; and skin discoloration (argyria) after long-term exposure to and accumulation of the silver released from its matrix. (Wright, Lam, & Burrell, 1998)

1.2.2 Hemocompatibility and Silver Retaining Property

Recently, the approach of incorporating the silver compounds or silver nanoparticles into polymer-based matrix has been explored to address the aforementioned problems. Such polymers included both synthetic polymers and natural polymers. Balogh, etc. developed a synthetic dendrimer to trap silver ion and form nanocomposites, which acted as a water soluble antiseptic agent (Balogh, Swanson, Tomalia, Hagnauer, & McManus, 2001). Other researches either incorporated silver compounds into amphiphilic hyperbranched macromolecules (Aymonier, Schlotterbeck, Antonietti, Zacharias, Thomann, Tiller, et al., 2002), or conjugated silver into polymeric networks (Furno, et al., 2004; Ho, Tobis, Sprich, Thomann, & Tiller, 2004). Although these approaches immobilized or controlled the diffusion of silver content, they still couldn't improve silver's hemocompatibility. Thereafter, polysaccharides were applied to incorporate silver compounds or silver nanoparticles. To ensure the conjugation of silver, polysaccharides containing amino-groups are usually selected. Therefore, chitosan became the most studied and reported polysaccharide matrix to produce silver-chitosan composites. Travan and co-workers found that chitosan gel significantly reduced silver's cytotoxicity (Travan, et al., 2009). In other studies, different silver compounds (i.e. silver sulfadiazine and

silver (I)-imidazole) were incorporated into various forms of chitosan matrix, including solution (Sanpui, Murugadoss, Prasad, Ghosh, & Chattopadhyay, 2008), gel (do Nascimento, Sampaio, Medeiros, & de Azevedo, 2009), and film (Wei, Sun, Qian, Ye, & Ma, 2009). Unfortunately, chitosan has its limitation as the matrix material. Although chitosan applied in these experiments was 80% - 90% deacetylated, due to its lacking of amino groups, a relatively large quantity of polysaccharide was required to form a stable silver chitosan composite. Otherwise, leaking of silver was observed in aqueous solutions (do Nascimento, Sampaio, Medeiros, & de Azevedo, 2009; Travan, et al., 2009). The silver leakage again could cause skin discoloration, low hemocompatibility, and induce cytotoxicity. Proteins, another commonly used category of nature polymer, may be more desirable because they are not only hemocompatible, but also contain large amount of nitrogen in their peptide backbones which has potential to interact with silver. To the best of our knowledge, no studies have been published on silver protein composites.

Kumar, etc. (2005) found out that silver formed coordination bond with nitrogen in polyamide. The silver/polyamide composites were then proven to be antiseptically active against both Gram positive and Gram negative bacterial species. However, silver leakage was still observed due to polyamide's good water solubility. Even fewer studies were focused on silver/protein composites, which was expected to have potential to greatly improve silver's hemocompatibility due to the strong affinity between silver filler and protein matrices as well as the biocompatible nature of biopolymer. Based on the coordinative property of silver, two varieties of proteins

were selected to form the silver/protein nanocomposites – high glutamine protein (zein) and high cysteine protein (α-lactalbumin).

Although many approaches have been developed to increase the hemocompatibility of silver, few studies has been focused on the second major challenge of silver antiseptic agents - skin discoloration. Jonas, et al. (2007) reported that the skin discoloration was generated following a pathway shown in Figure 1.1.
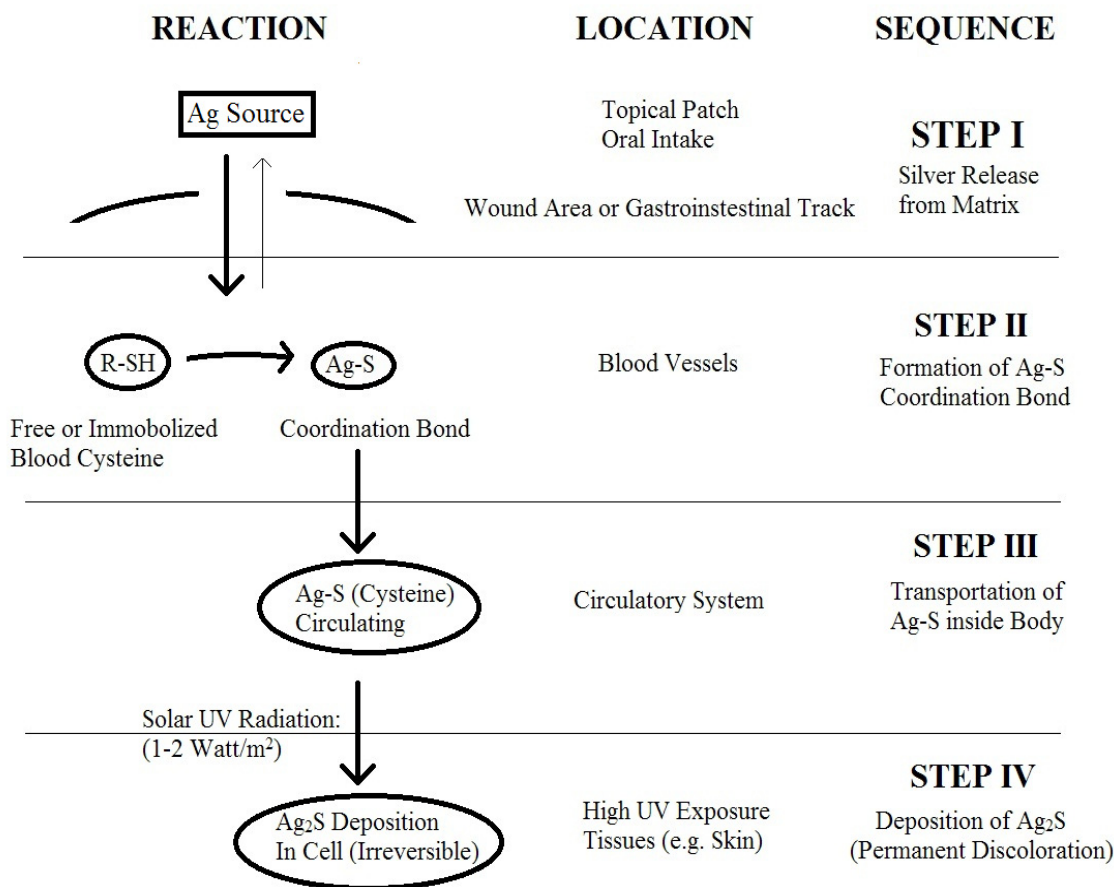
Figure 1.1 The mechanism of skin discoloration associated with silver release.

Derived from Jonas's mechanism study (2007).

First, the released stable Ag^+ (I) complexes migrate into human body through the mucosa of eyes, nose, gut or stomach (Jonas, Bloch, Zimmermann, Stadie, Gross,

& Schad, 2007). During the transportation of Ag^+ (I) inside body, it was further bound to amino acids, such as cysteine on proteoglycanes or collagen fibers. The accompanied silver deposition usually occurred at dermis cells, because the exposure to solar ultraviolet (UV) radiation could induce an irreversible chemical reaction that changes Ag^+ (I)-cysteine complexes to silver sulfide (Ag_2S), which caused skin discoloration (Jonas, Bloch, Zimmermann, Stadie, Gross, & Schad, 2007). Therefore, to prevent the discoloration of skin, it would be critical to prevent the binding between silver and blood cysteine, which is the first step of skin discoloration. Unfortunately, to the best of our knowledge, none of the previously studied polymers' matrix, either synthetic or biopolymer, had such silver retaining capabilities to compete with blood cysteine. (do Nascimento, Sampaio, Medeiros, & de Azevedo, 2009) Thermodynamically, the equilibrium constants of Ksp for Ag_2S is 6.0×10^{-51} and Kd for $Ag(NH_3)_2^+$ is 6.0×10^{-8}. The huge difference between these two constants indicated that the interaction of Ag^+ and S^{2-} (or RS^-) is much stronger and Gibbs free energy is lower than that of Ag^+ and NH_3. These suggested that silver is a strong sulfur affinitive metal. Therefore, the ordinary amine/amide-based polymers (e.g. chitosan and zein) may not fulfill the role of preventing the release of silver. Contrarily, high cysteine protein maybe good competitors to blood cysteine in the ability to retain silver and prevent skin discoloration. Proteins containing high percentage of cysteine then become a feasible solution to cope with the aforementioned two big challenges altogether, by bringing hemocompatibility to

silver and achieving high silver retention. To the best of our knowledge, there was no such studies have been published on this concept.

1.2.3 Protein Modification

Two types of proteins are selected in this study, which were zein and α-lactalbumin (ALA) to form silver/protein nanocomposites through electrostatic attraction and coordination bond. Zein is a maize prolamine protein, which is a major co-product of corn starch production. Zein is consisted of roughly one-third of hydrophilic (i.e. glutamine) and two-thirds of hydrophobic amino acid residues in its primary structure, which is closely related to its unique aqueous-alcohol solubility and film forming ability. Several studies have been published for applying zein as a matrix for different antimicrobial agents, including lysozyme (Gucbilmez, Yemenicioglu, & Arslanoglu, 2007; Zhong & Jin, 2009; Zhong, Jin, Davidson, & Zivanovic, 2009), thymol (Del Nobile, Conte, Incoronato, & Panza, 2008; Mastromatteo, Barbuzzi, Conte, & Del Nobile, 2009) and nisin (Hoffman, Han, & Dawson, 2001; Ku & Song, 2007). These food grade antiseptics were successfully incorporated in the zein matrix. The resultants were active in bacteria control of Gram positive (e.g. *Bacillus subtilis*, *Staphylococcus aureus*) and Gram negative (e.g. *Escherichia coli*, *Listeria monocytogenes*) species. For silver zein composites, besides solubility, pH-dependent properties of zein, including surface charge and morphology, could also be helpful (B. C. Zhang, Y. C. Luo, & Q. Wang, 2011).

ALA was selected as the high-cysteine protein for its outstanding biocompatibility and structural durability as a matrix material. ALA is a component of whey protein, and consists of eight cysteine residues in the form of four intra-molecular disulfide bonds. It should be noted that the affinity of silver to sulfur can vary dramatically depending on the redox states of sulfur (Högfeldt, 1983). As silver is a sulfur affinitive metal, and both the formation of silver/protein composites, its silver retaining properties, and hemocompatibility, etc involved the coordination bond between silver and donor items (e.g. S and N). Moreover, several studies also revealed that, in nanocomposites, the affinity between nanosized filler (i.e. nanoparticle, nanotube, and nanoplatelet) and protein matrices is the most dominating factor influencing the structure and functionalities. (Alexandre & Dubois, 2000; Carrado, 2000; Ray & Bousmina, 2005; Ray & Okamoto, 2003) The affinity may include hydrophobic- hydrophobic attraction, hydrogen bond, electrostatic force, and coordination bond. For silver specifically, the coordination bond between silver and polymer matrices would be the most dominating force. Therefore, it is necessary to systematically investigate the effects of cysteine redox states of ALA matrices on the nanocomposites' structural change and, therefore, induced functionality change.

1.3   Sustainable Packaging

1.3.1   Overview of Food Packaging Application of Biopolymer

Along with the arisen concern of environmental sustainability, the global sustainable packaging industry is growing much faster than traditional packaging industry. The market was expected to double in value from $88 billion in 2009 to

$170 billion in 2014. However, the total market share of sustainable packaging remained a small fraction of the entire global packaging industry with the anticipated value of $530 billion in 2014. Over the past decades, because of polymers' functionality, light weight, inexpensiveness and ease of processing, they have replaced conventional metal or ceramic materials in ubiquitous food packaging, where they provide physical, chemical, and biological protection from the environment and prolong product display. Examples of synthetic polymers most frequently used in food packaging are polyethylene (PE), polypropylene (PP), polystyrene (PS), polyvinyl chloride (PVC) and polyethylene terephthalate (PET). (Marsh & Bugusu, 2007) Due to arising interest in sustainable development, biopolymers are considered as potential replacements for these conventional plastic packaging materials due to their biodegradable nature. Biopolymers source primarily involve both plants, animals, microorganisms. The most studied plant based materials are polysaccharides (especially starch and cellulose) and proteins, and animal derived biopolymer also includes proteins and polysaccharides, while the most reported microbial products is polyhydroxybutyrate. An exception of biopolymer is polylactic acid which is a polymer synthesized chemically from lactic acid, which is naturally derived monomer. The most concerned application is the formation biopolymer-based edible films. Although previous studies have shown their enormous versatility (Marsh & Bugusu, 2007), a limiting property of polymers in packaging is their intrinsic mechanical property and permeability to gaseous substances, such as oxygen, CO_2, and organic volatile molecules. Specifically, similar to biopolymer, the application of

food polymers is greatly limited by its notoriously low mechanical strength and high water vapor permeability. These physical nature of the biopolymer materials resulted in great interests in developing new materials with enhanced gas or vapor barrier property by new preparation strategies and to carry out fundamental research assisting the understanding of the relationship between structure and barrier properties.

The most frequently adopted strategies to improve mechanical and gas barrier properties are the use of polymer blends, the coating of high barrier materials, and the use of multilayered films consisting a layer of high barrier film. For instance, aluminum foil is an effective high barrier material, which can be coated to polymer films and containers by several vapor deposition technologies. Multilayers can be formed by incorporating a layer of a high barrier material within other layers of structural polymers. Coatings and multilayers are efficient, whereas their application is limited to certain specific combinations due to the level of adherence between the materials involved. Therefore, another option is to add suitable filler into polymers matrix to form composites with enhanced barrier properties. Nanocomposites are innovative alternative to traditional technologies for improving polymer properties. Nanocomposites usually exhibit increased mechanical strength, increased gas/vapor barrier properties, and improved heat resistance compared to conventional composites and their neat polymers (Ray & Bousmina, 2005; Ray & Okamoto, 2003; Sorrentino, Gorrasi, & Vittoria, 2007).

Besides, various natural nanocomposites may inspire researchers to design a novel nanocomposite with improved mechanical, barrier, and thermal properties. The

naturally occurred nanocomposites, e.g. seashell and bone, usually have superior mechanical properties. Seashells have outstanding mechanical strength and toughness. The structure of seashells is composed of 95% aragonite, a carbonate mineral, and only 1% of organic biopolymer, which is considered as a reversed composite structure comparing to tradition concepts. Bone tissue is another example of natural nanocomposites. It serves as a reservoir of minerals (i.e. Calcium and Phosphates) and provides mechanical support to skeletal tissues (Boyle, Simonet, & Lacey, 2003). The building block is the collagen fibril, which is mineralized by orderly layered array of hydroxyapatite plates ($Ca_5(PO_4)_3OH$). For biomedical application, this structure has been developed as a model for biomimetic materials (Fratzl, Gupta, Paschalis, & Roschger, 2004).

1.3.2 Nanofiller

Particle fillers that are mostly used and reported include carbon nanotubes, graphene nanosheets, and nanoclays of MMT and kaolinite. MMT is one of the most popular organophilic clay fillers. The chemical composition is hydrated sodium calcium aluminium magnesium silicate hydroxide with the formula of $(Na,Ca)_{0.33}(Al,Mg)_2(Si_4O_{10})(OH)_2 \cdot nH_2O$. Structural-wise, MMT clays consist of nanoplatelets of magnesium aluminum silicate. The platelets have the dimension of 1 nm thick and 100-500 nm in diameter, which falls into the category of nano scale filler result in platelets of high aspect ratio (Uyama, Kuwabara, Tsujimoto, Nakano, Usuki, & Kobayashi, 2003). Clay structure is the stack of hundreds of layered platelets into particles or tactoids with a diameter around 8-10 μm. The effects of nano

filler on polymer matrix properties are mainly attributed to their high surface to volume ratio, because polymer-filler interactions are primarily governed by interfacial forces, such as electrostatic attraction and hydrogen bond. In order to take full advantage of the filler's high surface to volume ratio, clay particles should be completely exfoliated into individual platelets and then uniformly distributed within the polymer matrix (Ray & Okamoto, 2003).

When dispersed into polymer matrix, nanofillers create a maze-like structure that creates a tortuous path to gaseous molecules, greatly slowing the permeation rate (Bharadwaj, 2001). Additionally, layered silicate-polymer nanocomposites can improve mechanical characteristics and heat resistance compared to neat or conventional filled resins (Ray & Okamoto, 2003). Besides, traditional composite structures usually requires a large quantities of filler (~60 % vol), but in nanocomposites dramatic reduces in the demand of nanofiller loading are possible at substantially low level (<2 vol%).

Besides silicate nanoclays, another popular category is carbon-based nanofillers, including grapheme nanoplates (GNPs) and carbon nanotubes (CNTs). GNPs usually have a dimension of 20–60 nm in thickness and 0.5–25 μm in diameter, which were dispersed in polymer matrix by high-speed shearing methods. GNPs can form heat resistant and high gas barrier nanocomposites, which have promising application in food packaging industry. For instance, after dispersing 1–5 wt% GNPs in poly(methyl methacrylate) (PMMA), the nanofiller can increase the glass transition temperature for PMMA by 30 °C (Ramanathan, Abdala, Stankovich, Dikin,

Herrera-Alonso, Piner, et al., 2008). CNTs, whereas, have drawn considerable attention due to their unique mechanical and electrical properties. However, the application of CNTs in nanocomposites has been restricted by challenges in processing and dispersion, as well as their prohibitively high cost.

1.3.3 Food Polymer Matrices

Starch has been extensively investigated for a candidate of biopolymer food packaging, due to its nature of biodegradability, ease of production, and low in cost (Charles, Kao, & Huang, 2003; Ray & Okamoto, 2003). The addition of inorganic materials and synthetic polymers has been investigated, and the composites enhanced water resistance of starch (Avella, De Vlieger, Errico, Fischer, Vacca, & Volpe, 2005; Cyras, Manfredi, Ton-That, & Vazquez, 2008; Huang, He, Liu, Xu, Tay, & Chow, 2005; Ray & Okamoto, 2003). Starch-layered silicates are the most studied biodegradable nanocomposites for food packaging application (Avella, De Vlieger, Errico, Fischer, Vacca, & Volpe, 2005; B. Q. Chen & Evans, 2005; Cyras, Manfredi, Ton-That, & Vazquez, 2008; Huang, He, Liu, Xu, Tay, & Chow, 2005). With the addition of MMT clay, significant improvements in mechanical properties were achieved as the increase of both Young's modulus and tensile strength. Besides, a study reported a reduction in effective diffusion coefficient (water uptake) of starch film by adding MMT nano clay (Cyras, Manfredi, Ton-That, & Vazquez, 2008). A recent study reported a plasticized starch composite with carboxymethylcellulose (CMC) modified ZnO filler (Yu, Yang, Liu, & Ma, 2009). By adding 5 wt% of ZnO-CMC filler, the composite tensile strength increased 150% comparing to that of

neat polymer, whereas, the elasticity (elongation and break) reduced 38%. The water vapor barrier property was reported to increase significantly. The current status of starch nanocomposites is been summarized in a review regarding its properties, processing techniques and applications (Zhao, Torley, & Halley, 2008).

Polylactic acid (PLA) is a sustainable and biocompatible material with relatively better mechanical and optical properties than other biopolymers. PLA is unique because it is a synthetic polymer of lactic acid, which is a monomer obtained from fermentated carbohydrate feedstock. Because of its biodegradable nature, it is one of the potential options for disposable packaging that will replace the traditional petroleum-based plastics (Lunt, 1998). However, the large production of PLA as food packaging materials is still restricted by its low gas/vapor barrier properties and high cost comparing to conventional plastics. To cope with these disadvantages, nanocomposite technology has shown its potential to improve the functionalities and expand the applications of PLA (Lunt, 1998; Rhim, Lee, & Hong, 2007; Sinclair, 1996). PLA and layered silicate composite were investigated by Cabedo and others (2006) with modified Kaolinite. The study reported good interaction between polymer and clay, which contributed to a 50% increase in O_2 barrier properties. The study also applied plasticizers to overcome the inherent brittleness and increase the tensile strength of PLA. However, generally, plasticizer can reduce the gas/vapor barrier properties of the polymer film. In their study, the addition of clay filler counter-balanced the effects of plasticizer on gas barrier properties (Sinclair, 1996).

Proteins have been utilized in various industrial applications due to their good film-forming ability (Cuq, Gontard, & Guilbert, 1998). The natural protein source also includes plant and animal. Studies on plant based protein mostly involve soy protein, corn protein (zein) and wheat protein. Proteins from animal are mainly milk protein (casein and whey), collagen, egg white and myofibrillar protein from marine creatures (Zhao, Torley, & Halley, 2008). Compared with polysaccharide, proteins usually have better gas/vapor barrier properties (Miller & Krochta, 1997). However, protein's high modulus, high water adsorption and gas permeability still hindering its practical value as food packaging. Similarly, nanocomposite technology has been Significant efforts have been made to improve the properties of various proteins applying nanocomposites technology, mainly using nanoclays. Soy protein has good biodegradable and thermoplastic properties. However, its application is limited due to its low moisture resistance and high rigidity. Similarly to starch, plasticizers was blended with soy protein to reduce the brittleness of the polymer film, while increasing the gas/vapor permeability. Soy protein nanocomposite, on the other hand, counter-balanced the effects of plasticizer and increased the gas/vapor barrier properties, improved elastic modulus and tensile strength (P. Chen & Zhang, 2006; Dean & Yu, 2005; Miller & Krochta, 1997; Rhim, Lee, & Kwak, 2005). Zein is a prolamine protein, extracted from corn kernels. It is famous for its hydrophobicity and good film forming ability (Lawton, 2002; Winters & Deardorff, 1958). It is extensively used as edible and biodegradable coating in food industry. However, although zein is hydrophobic, it still shows high water vapor permeability and low

tensile strength, which greatly reduced its practical value as a food packaging. Similar to other cases of biopolymer, the combination of plasticizers (e.g. chloroacetic acid) and nanoclay could overcome the brittleness and low barrier properties of zein film. Exfoliated kaolinite filler are commonly applied to paper and paperboard to reduce the water uptake and increase the moister barrier properties (Rissa, Lepisto, & Yrjola, 2006). Kaolinite clay is expected to substitute fluorocarbons in extruded protein coatings.

1.3.4 Typical Structures of Nanocomposites

Nanocomposites rely on the high surface of the clay nanoplatelets (more than 750 m²/gram) and high aspect ratio (100 to 500). Commercially available MMT clays usually come in platelet clusters with low surface area exposed. Appropriate processing technologies are needed to de-aggregate or exfoliate the cluster to increase the interfacial surface area between nanofiller and polyer matrix.

There are three types of polymer-clay formations; a) tactoid, (b) intercalated and (c) exfoliated (Carrado, 2000; Ray & Okamoto, 2003) (Figure 1). Tactoid structures can be found in traditional composites. The formation of this type of structure can be attributed to two possibilities; a) the fillers were not treated with exfoliating process; b) when the interlayer space of the clay platelets does not expand, due to its poor affinity with the surrounding polymer matrix. Actually, the formed structure is a physical blend of two components, and no true nanocomposites are formed this way (Alexandre & Dubois, 2000). Intercalated structures have moderate expansion of the clay interlayer, in which polymer chains can penetrate the basal

spacing of filler, but the stacked shape of the nanoplatelets remains. The intercalated

structure is the result of moderate affinity between the polymer and clay.
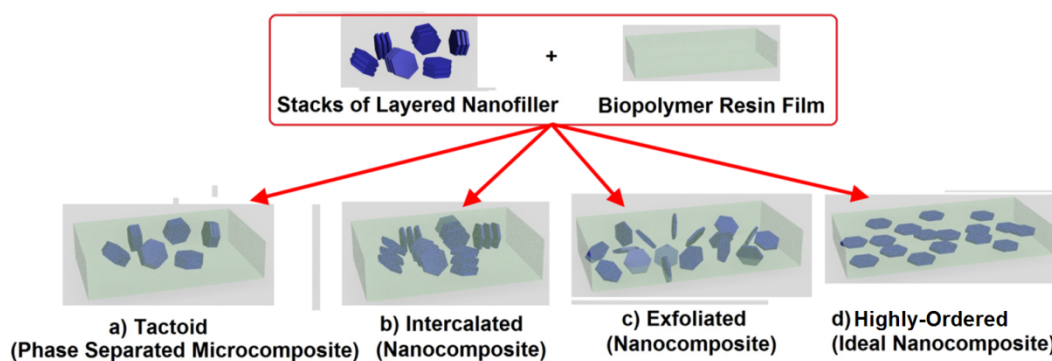
Figure 1.2 The three types of polymer-filler nanocomposite formations.

In exfoliated structures, clay clusters lose their layered structure and are well

dispersed into single platelets within the continuous polymer phase. This is the result

of a high affinity between polymer and filler (Figure 1). In exfoliated structure, clay

aggregates must be completely de-aggregated into single nanoplatelets and dispersed

homogeneously throughout the continuous phase to take full advantage of nanofiller's

high surface area (Ray & Bousmina, 2005; Ray & Okamoto, 2003). Dispersion of

clay nanoplatelets into the polymer matrix is affected by mismatches between the

hydrophobic/hydrophilic character of both filler and the continuous phase. Typically,

polymers are hydrophobic, and clays are hydrophilic. Therefore, the surfaces of

nanoclays are often chemically modified with fatty acid to improve the

hydrophobicity and the compatibility with polymer matrix.

1.3.5   Well-Ordered Structure

As mentioned earlier, the current 'ideal' structures for biopolymer

nanocomposites are intercalated and exfoliated structures. However, although the

exfoliated structure is consisted of well-distributed nanofillers in biopolymer matrices, the less of filler orientation sacrificed the optimum functionalities, such as mechanical properties, gas permeability, electronic, and catalytic properties etc. Recently, plenty of studies claimed the significance of synthesizing a truly well ordered nanocomposite. More importantly, well-ordered nanocomposites has shown promising capabilities of improving matrix film's mechanical property and gas permeability, which were two critical characteristics to biopolymer-based food packaging. By comparing the elastic modulus of well-ordered and disordered carbon nanotubes, a study concluded that the well-ordered structure can considerably improve a material's mechanical properties, and disordered structure was claimed as structural defects (Salvetat, Kulik, Bonard, Briggs, Stockli, Metenier, et al., 1999; Wong, Sheehan, & Lieber, 1997).

Bharadwaj (2001) established a theoretical model to explain the relationship between gas permeability and the nanofiller arrangement. The equation is shown in Equation 1.1. In which, Ps and Pp represented the gas permeability of polymer-nanofiller composite and pure polymer respectively. Φs was the volume fraction of filler to entire nanocomposites. Letters L and W were designated to the length and width of the nanofiller. Besides, S stood for the arrangement of the nanofiller (Equation 1.2), and can be calculated by substituting difference angular value (θ) into Eq. 2. In a complete disordered filler arrangement, S was assigned as 0. In an ideal orthogonal arrangement, θ is 90°, so S equals to -1/2. In an ideal planar arrangement, where nanofillers were incorporated parallel to the nanocomposite interface, θ is to 0° and S equals to 1.

$$\frac{P_s}{P_p} = \frac{1-\Phi_s}{1+\frac{L}{2W}\Phi_s\left(\frac{2}{3}\right)\left(S+\frac{1}{2}\right)}$$ Equation 1.1

$$S = \frac{1}{2}(3\cos^2\theta - 1)$$ Equation 1.2
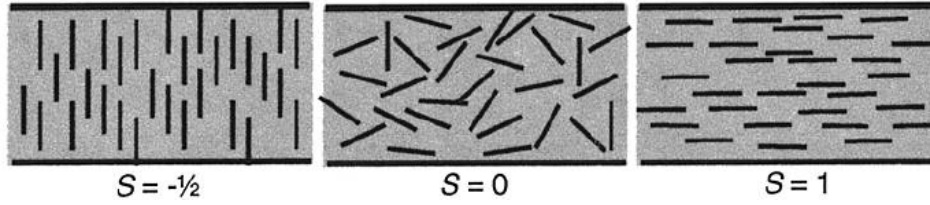
Figure 1.3 The nanofiller arrangement in polymer matrices.
Left: orthogonal; Middle: disordered; Right: Planar (Bharadwaj, 2001)

By the mathematical modeling, the author concluded that the gas permeability can be proportionally decreased by elongate the length of nanofiller, increase volumetric fraction of nanofiller, and achieve an ideal planar filler arrangement. Furthermore, mathematically, when fixing the value of L/W and Φs, and considering the aspect ratio of L/W is infinite, the gas permeability of planar arrangement (S=1) can be three fold smaller than that of disordered arrangement (S=0). In other words, by adding same amount of identical nanoplatelets, the gas barrier property of planar arrangement can be three fold better than that of exfoliated structure. In summary, the arrangement of nanofiller was critical to the mechanical property and gas barrier property of the biopolymer-based nanocomposite, and a highly ordered structure may significantly alter the physical property of the composite film.

Although the arrangement of nanofiller is important and may provide substantial improvement in functional properties than exfoliated structure, only a few studied have been endeavored in this concept. To the best of our knowledge, no experimental

study has been focused on the development of well-ordered nanocomposites for food

packaging application. Currently, several methods has been established in the

formation of well-ordered nanocomposites, such as lithography (Gao, Rodriguez, Liu,

Birajdar, Pantel, Ziese, et al., 2010), layer-by-layer deposition (Tian, Park, Cheng,

Liang, Zhang, & Wang, 2009) and rearrangement in external magnetic field (G. H.

Chen, Zhao, Tang, & Wang, 2007). Gao et al. (2007) established an pulse laser

deposition method that incorporated layers of $CoFe_2O_4$ nanoarray in a continuous

$Pb(Zn, Ti)O_3$ alloys, and the as-prepared nanocomposite exhibited strong

piezoelectric signals and magnetoelectric coupling. Tian and his colleagus (2009)

developed a method adopting electrostatic interaction. The well-ordered structure was

obtained by layer-by-layer deposition of positively charged poly(ethylamine) and

single wall carbon nanotube functionalized with negatively charged sodium

dodecylbenzenesulfonate. Although these two methods could form well-ordered

structures of nanocomposite coating, their feasibility in food packaging application is

questionable due to the complexity of the technique and impracticability in the

production of free standing film or even food containers. The third method (G. H.

Chen, Zhao, Tang, & Wang, 2007), however, is more practical by using external

magnetic field to trigger rearrangement of nanofiller. In Chen's study (2007), Fe

doped graphite nanoplatelets were mixed with the monomer solution of epoxy

polyester. The solution was then placed in 800T magnetic field for filler

rearrangement during the polymerization of epoxy resin and the solidification of

nanocomposite.

Therefore, in this study, the well-ordered biopolymer nanocomposites will be prepared using the filler rearrangement method under uniform external magnetic field to obtain a food packaging material with enhanced mechanical and gas barrier properties.

CHAPTER 2. Effect of Acid and Base Treatments on Structural, Rheological, and Antioxidant Properties of Alpha-Zein

2.1   Abstract

Five pH levels were experimented to study its effect on zein structural, rheological, and antioxidant properties. Structural changes, including secondary structures, surface charge, molecular weight, particle size distribution, and morphology were evaluated using a spectrum of instruments. Zein rheology, including the viscosity and viscoelastic property, was examined by a rheometer. The antioxidant efficacy was determined by measuring the scavenging activity of 1,1-diphenyl-2-picrylhydrazyl free radical and the reducing power of 1,10-penanthroline–iron with a spectrophotometer. Results indicated that under proper acidic or basic conditions, zein structures, rheological behavior, and antioxidant properties changed significantly. Decreased contents for α-helix, β-sheet, and β-turn were detected by the Fourier transform infrared spectroscopy for zein samples at acidic and basic conditions comparing to those in a near neutral condition, which were attributed to the deamidation of glutamine to glutamic acid / glutamate in zein. However, no obvious zein fragmentation or oligomerization was detected by the sodium dodecyl sulfate– polyacrylamide gel electrophoresis. The mild deamidation without fragmentation led to a decreased viscosity and an improved antioxidant property of zein. Modified rheological behavior and enhanced antioxidant properties

resulting from a pH treatment may facilitate novel application development of zein in food and pharmaceutical industries.

2.2   Introduction

Zein protein found in maize endosperm is a major co-product of bio-fuel industry. Zein is classified into α, β, γ, and δ-zein, based on its solubility and amino acid sequence homology. α-zein is the most abundant form that accounts for more than 80% of total zein protein. α-zein (refers as zein from this point on) is aqueous-alcohol soluble and contains roughly two-thirds of hydrophobic and one-third of hydrophilic amino acid residues (i.e. glutamine) in its primary structure (Argos, Pedersen, Marks, & Larkins, 1982). The amino acid composition of zein was determined by Pomes (1971). They found that zein contained 21.4% glutamine, 19.3% leucine, 9.0% proline, 8.3% alanine, 6.8% phenylalanine, 6.2% isoleucine, and 5.7% serine, and 5.1% tyrosine. The protein molecule is amphiphilic, with a proposed dimension around $17\times4.5\times1.2$ nm^3 (Matsushima, Danno, Takezawa, & Izumi, 1997) and a molecular weight of 19 and 21 kDa (Shewry & Tatham, 1990).

Zein is generally recognized as safe (GRAS) and is well known for its film-forming ability (Hernandez-Izquierdo & Krochta, 2008), biodegradability (McGowan, Padua, & Lee, 2005; Sessa, Selling, Willett, & Palmquist, 2006; Y. Wang & Padua, 2003), and biocompatibility (Hurtado-Lopez & Murdan, 2006; H. J. Wang, Gong, & Wang, 2008). Therefore, zein finds many potential applications in food and pharmaceutical industries including but not limited to tablet coating and free-standing packaging materials (Hernandez-Izquierdo & Krochta, 2008), emulsifier (Cabra,

Arreguin, Vazquez-Duhalt, & Farres, 2007; Casella & Whitaker, 1990; Yong, Yamaguchi, Gu, Mori, & Matsumura, 2004), chewing-gum base (Liu, Sun, Wang, Zhang, & Wang, 2005), antioxidant (Chiue, Iwami, Kusano, & Ibuki, 1994; Zhu, Chen, Tang, & Xiong, 2008), drug encapsulant (Guo & Shi, 2009; Hurtado-Lopez & Murdan, 2005; Liu, Sun, Wang, Zhang, & Wang, 2005; Zhong & Jin, 2009), and tissue scaffold (Gong, Wang, Sun, Xue, & Wang, 2006; Tu, Wang, Li, Dai, Wang, & Zhang, 2009; H. J. Wang, Gong, Lin, Fu, Xue, Huang, et al., 2007; H. J. Wang, Gong, & Wang, 2008). Many of these applications (e.g., chewing-gum base and antioxidant) are counted on zein's native property, which is high in aliphatic indexes and surface hydrophobicity (Argos, Pedersen, Marks, & Larkins, 1982; Cabra, Arreguin, Vazquez-Duhalt, & Farres, 2007) and high in fatty acid-binding capacity (Chiue, Kusano, & Iwami, 1997). Whereas, for other applications (e.g., emulsifier), modified zein structures with enhanced functional properties (e.g. water solubility, foaming and emulsifying properties) (Cabra, Arreguin, Vazquez-Duhalt, & Farres, 2007; Casella & Whitaker, 1990; Yong, Yamaguchi, Gu, Mori, & Matsumura, 2004) are preferred.

Moderate modification of zein structures by enzymatic and chemical treatments is desired for partially unfolding zein molecules to improve its functional properties. However, uncontrolled modifications would lead to reduced functionality (Chiue, Iwami, Kusano, & Ibuki, 1994; Chiue, Kusano, & Iwami, 1997) due to fragmentation and truncation of zein backbone (Zhu, Chen, Tang, & Xiong, 2008). Therefore, studying changes of zein structure under different chemical and physical conditions would provide fundamental knowledge for predicting its properties and

then facilitate its application development. Zein structures were found to be influenced by many physico-chemical parameters, such as temperature, concentration, salt type, pH, and solvent type. It was reported that high temperatures ($90°C$) would denature zein's secondary structure and result in zein oligomerization (Cabra, Arreguin, Vazquez-Duhalt, & Farres, 2007). Different cations (i.e. Na^+, K^+, NH_4^+ and Mg^{2+}) were found strengthening zein's selectivity and interaction with nonionic surfactants (Cserhati, Forgacs, & Illes, 2003).Various alcohols, e.g. methanol, ethanol and isopropyl, were concluded to modify the morphology, diameter and distribution of zein fibers from electrospinning (Selling, Biswas, Patel, Walls, Dunlap, & Wei, 2007).

Building on the aforementioned progress, this work will focus on the effect of pH on zein structures and properties that has less been studied. In the limited literature, Cabra et al. (2007) reported that different pH treatments (0.5-2 N hydrochloric acid or sodium hydroxide, NaOH) with or without applying heat would induce zein deamidations, resulting in an improved emulsifying property. Under the similar pH conditions (0.05 N hydrochloric acid with heat), Chiue et al. (1994) found a decreased zein's fat-binding capacity leading to the loss of radical scavenging ability. Severe pH levels employed in these studies, however, are not representative in most systems that zein is used for. Therefore, in this work, effect of mild acid and base treatments (0.0005 - 0.002 N hydrochloric acid or NaOH) were investigated on zein's structural changes, rheological behavior, and antioxidant properties. The results

will add knowledge of zein science and engineering and thus guide developments of new zein products.

2.3   Materials and Methods

2.3.1   Materials and Chemicals

Zein sample with a minimum protein content of 97% was purchased from Showa Sangyo (Chiyoda-ku, Tokyo, Japan). Chemicals, such as hydrochloric acid, NaOH, 2,2-diphenyl-1-picrylhydrazyl radical (DPPH·), and 1,10-Phenanthroline–iron(II), were purchased from Sigma-Aldrich (St. Louis, MO, USA). The sodium dodecyl sulfate – polyacrylamide gel electrophoresis (SDS-PAGE) system (NuPAGE) and its accessories including gel, loading and running buffers, staining kit and reducing agent were purchased from Invitrogen (Carlsbad, CA, USA).

2.3.2   Sample Preparation

0.1 mg/mL zein solution in 70% ethanol-water solvent was used throughout the study except for rheological measurements (100 mg/mL zein was used instead). Five pH levels were prepared, which included one near neutral pH (pH~6.5), two acidic pHs (2.7 and 3.3) adjusted by hydrochloric acid, and two basic pHs (10.5 and 12.5) adjusted by NaOH solution (1N). The respective five treatments were named as Z2.7, Z3.3, Z6.5, Z10.5, and Z12.5. To minimize the interference from insoluble component, all 0.1 mg/mL zein solutions were filtered through a GF 25 mm Syringe Filter Paper 410 (particle retention = 1 with GF/0.45μm GHP membrane, VWR). The

prepared samples were allowed for reaction at room temperature (20 °C) for 24 hrs before sample characterization and evaluation.

2.3.3   Fourier Transform Infrared Spectroscopy (FTIR)

A FTIR was used to measure the change in secondary structure of the prepared pH-treated zein samples. The samples were first lyophilized for 24 hrs (RVT 4104-115, Refrigerated Vapor Trap, Thermo Savant, Waltham, MA, USA), and then were ground into homogeneous powders, re-suspended in a 70% ethanol, and dried on an ATR crystal under dry nitrogen. The spectra were acquired at 400-4000 cm^{-1} wavenumbers with a $1cm^{-1}$ resolution utilizing a Jasco 4200 series FTIR spectrophotometer (Jasco Inc. Easton, MD, USA) equipped with an ATR cell. The FTIR spectra were baseline corrected and normalized according to the modified Forato's method (Forato, Bernardes-Filho, & Colnago, 1998), in which each spectrum baseline was corrected by subtracting the average absorbance values of 1900 and 2100 cm^{-1} and then normalized as each absorbance value ($\times100$) from 1200 to 1800 cm^{-1} was divided by the sum of the absorbance values in the same region.

The resolution of the collected normalized FTIR spectra was enhanced using the 2nd derivative and Fourier self-deconvolution (FSD), which were related to changes in protein conformation (Forato, Bernardes, & Colnago, 1998). With the 2nd derivative and FSD, it has been identified that the signal of α-helix in zein appeared around the wavenumber of 1648-1659 cm^{-1}; β-sheet was at 1627-1629,1681-1682, and 1694-1697 cm^{-1}; while random coil and β-turn structures were respectively detectable at 1638-1640 and 1681-1682 cm^{-1} (Forato, Bicudo, & Colnago, 2003;

Singh, Georget, Belton, & Barker, 2009; Yong, Yamaguchi, Gu, Mori, & Matsumura, 2004).

2.3.4 Sodium Dodecyl Sulfate – Polyacrylamide Gel Electrophoresis (SDS-PAGE)

SDS-PAGE (NuPAGE, Invitrogen, Carlsbad, CA, USA) was used to examine the change in molecular weight of the treated zein samples. The sample was re-suspended in a solution of 19.5 μL deionized water, 7.5 μL lithium dodecyl sulfate (LDS) sample buffer and 3 μL reducing agent. The mixtures were then heated at 70℃ for 10 minutes. The SDS-PAGE was carried on 4-12% (w/v) Bis-Tris Mini Gel stained with colloidal blue staining kit (SimplyBlue SafeStain). The molecular weight standards (Novex Sharp Pre-Stained Protein Standards) are as follows: myosin (200 kDa), β-galactosidase (116.3 kDa), phosphorylase B (97.4 kDa), bovine serum albumin (66.3 kDa), glutamic dehydrogenase (55.4 kDa), lactate dehydrogenase (36.5 kDa), carbonic anhydrase (31 kDa), trypsin inhibitor (21.5 kDa), lysozyme (14.4 kDa), aprotinin (6 kDa), insulin B chain (3.5 kDa), and insulin A chain (2.5 kDa).

2.3.5 Surface Charge

A laser Doppler velocimetry (Zetasizer Nano ZS90, Malvern, UK) was used to evaluate the electrophoretic mobility of zein samples. Zeta potential was obtained by converting the measured mobility using the Smoluchowski theory:

$$\upsilon_E = 4\pi\varepsilon_0\varepsilon_r\frac{\zeta}{6\pi\mu}(1 + \kappa r)$$

Equation 2.1

Where υ_E is mobility, ε_0 is the relative dielectric constant, and ε_r is the electrical permittivity. ζ represents the zeta potential, μ is the liquid viscosity, κ is the Debye–Hückel parameter, and r is the particle radius. The prepared zein sample was first well mixed and then filled in a fold capillary cuvette (Folded Capillary Cell - DTS1060, Malvern, UK) with a syringe. The whole cuvette is mounted on the measuring chamber. All measurements were carried out at 20 °C. Three replications were obtained and results were used for statistical analysis.

2.3.6 Particle Size and Morphological Properties

Hydrodynamic diameter of pH treated zein particles and particle distribution were assessed by a dynamic light scattering instrument (DLS, BI-200SM, Brookhaven Instruments Corporation, Holtsville, NY, USA). DLS is equipped with a 35 mW HeNe laser beam at a wavelength of 637 nm. All DLS measurements were performed at 20°C. Reflective index and viscosity of a 70% ethanol solution are 1.3617 and 2.592, respectively, which were used for calculate effective diameter from autocorrelation. The reported values were averaged from three replicates.

A scanning electron microscopy (SEM, SU-70 SEM, Hitachi, Pleasanton, CA, USA) was used to characterize and compare the morphologies of dried zein samples under the different pH treatments. The treated zein samples were first cast-dried on an aluminum pan and then were cut into small pieces, adhered to conductive carbon tapes (Electron Microscopy Sciences, Ft. Washington, PA, USA), and mounted on specimen stubs. The whole stub was coated with a thin (<20 nm) conductive gold and

platinum layer using a sputter-coater (Hummer XP, Anatech, CA, USA). Digital images of the samples were obtained and reported.

2.3.7 Rheological Behavior

A rheometer (AR 2000ex Rheometer, TA Instrument, Leatherhead, UK) was used to characterize the viscoelastic properties of the treated zein samples. The samples were dissolved and well mixed in 70% ethanol solution at a concentration of 100 mg/mL. The shear viscosity of all samples were then conducted at 25 ℃ with a 60 mm 0.59^o steel at a changing shear rate from 1 to 100 s^{-1}, and the dynamic oscillatory test was performed as a function of shear frequency (1 to 100 rad/s). The used strains were within the linear viscoelasticity limit. All rheological experiments were repeated three times. Since no distinct difference was observed, only one figure was presented for each sample.

2.3.8 Antioxidant Activity

Antioxidant activity was tested against the 2,2-diphenyl-1-picrylhydrazyl radical (DPPH·) and hydrogen peroxide. In the case of DPPH·, all experiments were performed immediately after pH-treated zein samples were prepared. DPPH· assay was examined according to previous method (Zhu, Chen, Tang, & Xiong, 2008). Equal volume of 0.1 mg/ml zein sample solution and 0.042 M DPPH· in a 70% ethanol solution were well mixed and then placed in a dark place for reaction at 4℃. The radical scavenging of DPPH· over time was examined with the optical density at 517 nm against a reagent blank of 70% ethanol using a spectrophotometer (Beckman Coulter, DU-730, Fullerton, CA, USA).

In the second set of experiments, different pH-treated zein samples were evaluated for their abilities to prevent 1,10-penanthroline–iron(II) complex ($[Fe(o\text{-phen})_3]^{2+}$) from oxidation by hydrogen peroxide. All zein samples were prepared in a 70% ethanol. The oxidation of Fe (II) is pH sensitive, so the samples were first reacted under different pH conditions at 20℃ for 24 hrs and then adjusted to a near neutral condition with pH around 6.5. During the experiment, $[Fe(o\text{-phen})_3]^{2+}$ (1 mM) was prepared by adding 1,10-phenanthroline to $FeSO_4$ in a 70% ethanol. Thereafter, 1 mL 70% ethanol was added to 2 mL complex, which served as the control, as compared to the treated cases in which 0.5 ml 3% (w/v) of each neutralized zein solutions plus 0.5 mL 70% ethanol were added to 2 mL complex. After solutions were well-mixed, 1 ml 0.025% H_2O_2 in a 70% ethanol solution was added. The prepared solutions were heated in a water bath at 37℃ for 60 minutes. The optical density of a reagent blank of 0.5 mM $[Fe(o\text{-phen})_3]^{2+}$ in 70% ethanol was collected using the spectrophotometer at 508 nm. Then, the optical density decrease of $[Fe(o\text{-phen})_3]^{2+}$ for each treatment was examined against the blank by subtracting the treatment reading from the blank reading.

These two antioxidant assays were repeated three times and statistical analysis was performed according to the method described in section *2.9*.

2.3.9   Statistical Analysis

All the experiments were conducted in triplicate with data reported as mean ± standard error. Experimental statistics were performed using the SAS software (Version 9.2, SAS Institute Inc., Cary, NC, USA). The analysis of variance (ANOVA)

was used to compare the treatment means. Secondary structural FTIR information of different treatments was tested against control (Z6.5) by ANOVA Dunnett's test. When pH was the only variable, the ANOVA Tukey's multiple comparison test was used in analysis of ζ-potential, particle size distribution and antioxidant activity. In the free radical scavenging test where both pH and reaction time were variables, the ANOVA Tukey's Studentized Range (HSD) test was selected. The probability of a test statistic (P) was set at 0.05.

2.4. Results and Discussion

2.4.1 Structural changes

(1) FTIR Analysis
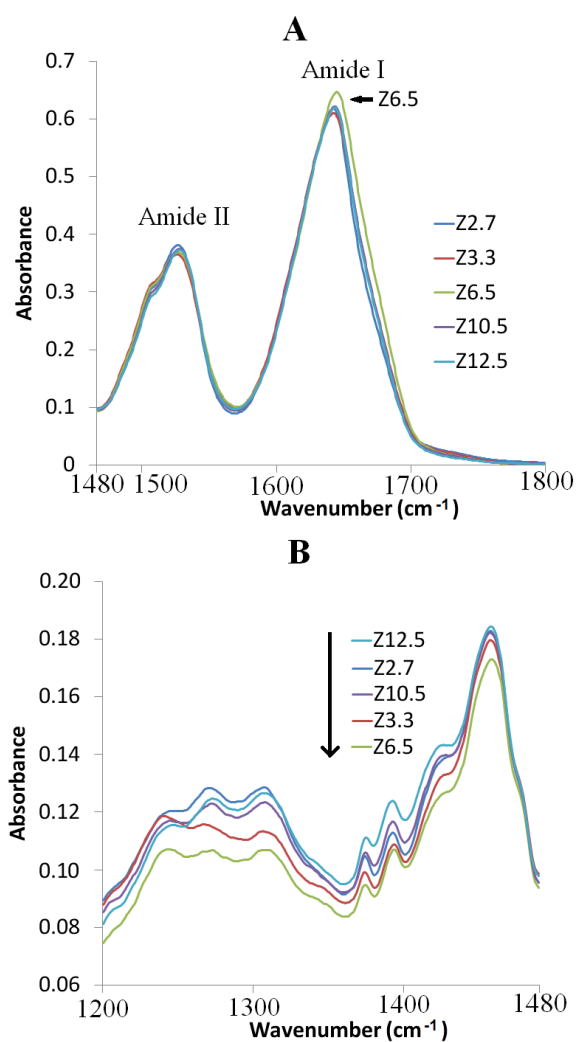
Figure 2.1 FTIR results for pH-treated zein samples.
A. wavenumber 1480-1800 cm^{-1}; and B. wavenumber 1200-1480 cm^{-1}.

Figure 2.1 presents the normalized FTIR data of three secondary structures for

five pH-treated zein samples. It can be seen that, in comparison to the absorbance of

near neutral pH zein (Z6.5), the absorbance dropped at the Amide I region but was

relatively unchanged at the Amide II region for both acid and base treated zein

samples (Figure 2.1A). At the same time, an increase of absorbance was observed in

acidic and basic zein samples at the wavenumbers between 1200 cm^{-1} and 1480 cm^{-1}

(Figure 2.1B). This area was considered to be the fingerprint area for a protein, which

was related to single bonds (e.g., C-H, and N-H) vibration (Bruno & Svoronos, 2006)

and tautomerism of amide structure (El-Gamel, Seyfarth, Wagler, Ehrenberg, Schwarz, Senker, et al., 2007).
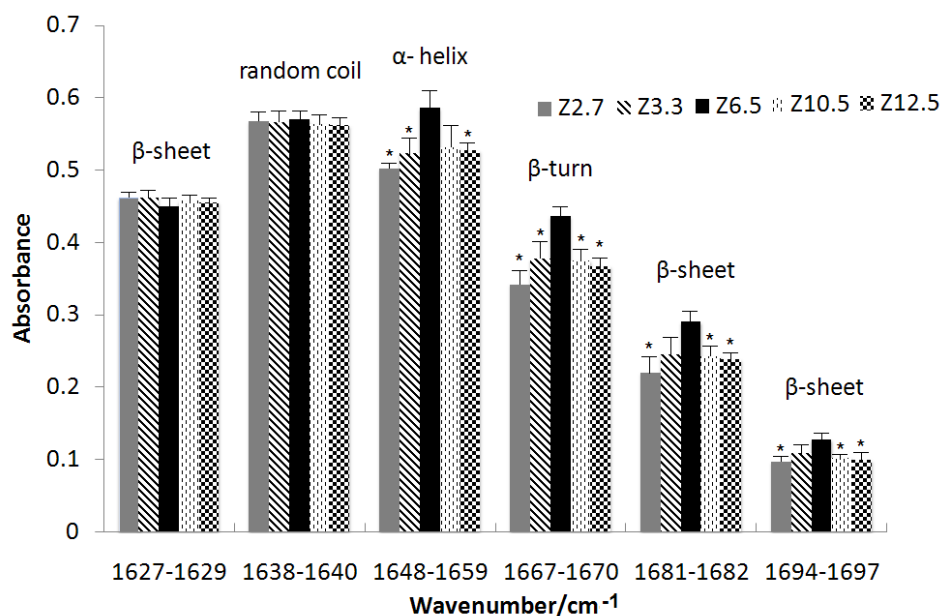
Figure 2.2 Secondary structural change of zein determined by FTIR spectroscopy. * indicated the treatment is significantly different from control (Z6.5) upon ANOVA Dunnett's test (P<0.05)

The spectra in Figure 2.1A could reflect significant difference in protein secondary structures. At the wavenumber of 1648-1659 cm^{-1}, the absorbance of α-helix contents showed significant decrease by 14% and 11% respectively for samples of Z2.7 and Z12.5, comparing to that of Z6.5 (Figure 2.2). The diminished α-helix structure was attributed to the deamidation of glutamine, which was critical in the formation of antiparallel helices of zein molecules (Matsushima, Danno, Takezawa, & Izumi, 1997). Through a pH-induced reaction, positively charged glutamine were deamidated to negatively charged glutamate residue (shown in Figure 2.3), and thus may weaken the electrostatic balance in the glutamine-rich turns. Such

balance was believed to be a major constraint affecting the stability of α-helix (Nelson & Cox, 2004).
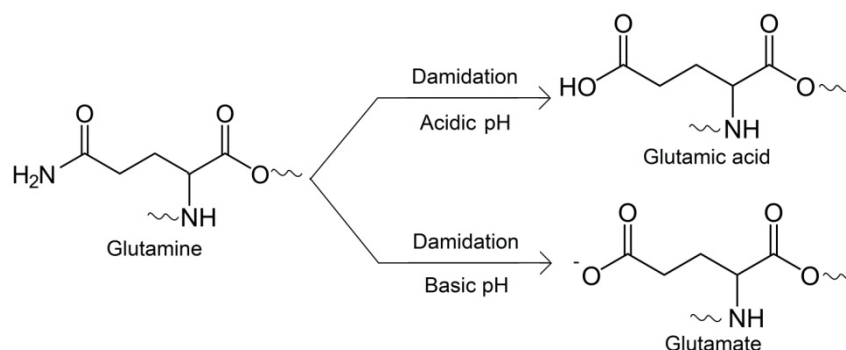
Figure 2.3 Deamidation reaction of glutamine.

Glutamic acid and glutamate residues were expected to have fewer propensities to form β-turn and β-sheet than glutamine based on the Chou–Fasman algorithm (H. Chen, Gu, & Huang, 2006; Jiang, Guo, Peng, & Sun, 1998). Therefore, the significant decrease in absorbance of Z2.7, Z3.3, Z10.5 and Z12.5 at 1667-1670, 1681-1682, and 1694-1697 cm^{-1} was attributed to the diminishing content of glutamine and the formation of glutamic acid / glutamate (Shown in Figure 2.3) However, pH seemed to have no significant influence on random coil at 1638-1640 cm^{-1}.

Two mechanisms of glutamine deamidation were studied by Joshi, Sawai, Kearney, & Kirsch (2005). Both 'direct hydrolysis of the amide side chain' and 'formation of a cyclic imide intermediate' were compared based on protein structure. They found that glutamine would easily undergo direct hydrolysis in acidic condition. A different mechanism of cyclic imide intermediate formation was established for basic deamidation. The reaction rate of intermediate formation depended on steric

bulk of neighboring amino acid groups. Less steric hindrances could increase the deamidation rate of glutamine in basic solutions. In zein structure, glutamine residues sufficiently exposed to solvent because it positioned as turns between antiparallel α-helix structures (Matsushima, Danno, Takezawa, & Izumi, 1997). Therefore, both direct hydrolysis and formation of cyclic imide intermediate could easily trigger deamidation of glutamine in acidic and basic conditions.

Although absorbance change in fingerprint area (1200 cm^{-1} to 1480 cm^{-1}) was related to single bond vibration (Bruno & Svoronos, 2006) and tautomerism of amide structures (El-Gamel, et al., 2007), the spectrum in fingerprint area can be unique for each compound. To explore the structural reason for increased absorbance intensity of pH-treated zein in the fingerprint area, further study is needed to identify which bond vibration and tautomerism of amide corresponds to the changes of absorbance spectra.

(2) ζ-potential
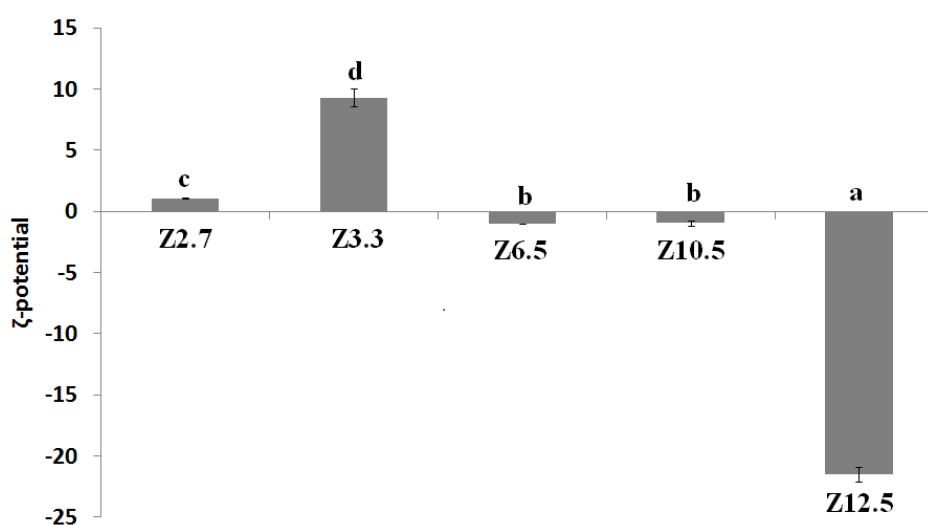
Figure 2.4 ζ-potential of pH-treated zein samples.
Means marked with different letters indicated significant difference between each other upon the ANOVA Tukey's test (P<0.05).

Another evidence of zein deamidation was obtained from the ζ-potential data (Figure 2.4). ζ-potential for Z6.5 is -0.94 mV indicating that zein surface can be regarded to carry no charges at near neutral pH, which is expected since native zein does not contain glutamate residue but is high in glutamine residues. After the treatment in a mild acidic condition (Z3.3), zein surface was positively charged possibly due to the protonation of side amide group on glutamine residues. Interestingly, when pH decreased to 2.7 (Z2.7), the surface charge dropped significantly, which was consistent with the findings by Guo, Heinämäkib, & Yliruusi (2008). Deamidation of glutamine into glutamic acid was thought to be responsible for the dramatic change of surface charge. Because the pKa value of glutamic acid is around 4.1, at pH 2.7 it would be protonated and carry no charges. In a previous study, the cutoff pH for the deamidation of asparagine was found to be near 3.0 (Peters & Trout, 2006), which was in good agreement to the observed deamidation pH (between 2.7 and 3.3) of zein glutamine.

In a mild basic solution (pH 10.5), glutamine was in its native stage, and no surface charge was measured. However, when pH increased to 12.5, a large reduction to -21 mV in zeta potential was observed as a consequence of the deamidation process. Deprotonated carboxylic groups on glutamate resulted in a great negative charge on zein molecule surface.

(3) SDS-PAGE Analysis

Both FTIR and ζ-potential results indicated the occurrence of zein deamidation under certain pH treatments. Further information is needed to assure that the deamidation does not cause further oligomerization on zein structures (e.g., peptide bond scission) and polymerization of zein molecules. For this purpose, the SDS-PAGE method was applied to evaluate protein oligomerization and polymerization in its denatured structure, and results were presented below. During sample preparation, zein was denatured and its original structures may be altered.

In **Figure 2.5**, all pH-treated zein samples shared the same band pattern as the native zein at pH = 6.5, which clearly contained monomer (19 and 22 kDa) and dimer α-zein (38 and 44 kDa) bands. A shift of protein bands toward upper region of slab gel was previously reported in acid-deamidation on wheat gliadins and enzymatic modification by protein-glutaminase on zein (Bollecker, Viroben, Popineau, & Gueguen, 1990). However, such phenomenon was not found in our zein samples, indicating that zein retained its primary structure upon the mild pH treatment. Although FTIR and zeta–potential results showed that zein underwent deamidation, especially at the conditions of pH = 2.7 and pH = 12.5, the band pattern of protein electrophoresis for monomer and dimer zein indicated that the deamidation of glutamine did not change the zein molecular weight, which agreed with the results of alkaline deamidated zein by Cabra et al. (2007). Besides, no increase in molecular weight was observed as well, which indicates that no polymerization of zein molecules occurred in mild pH solutions.
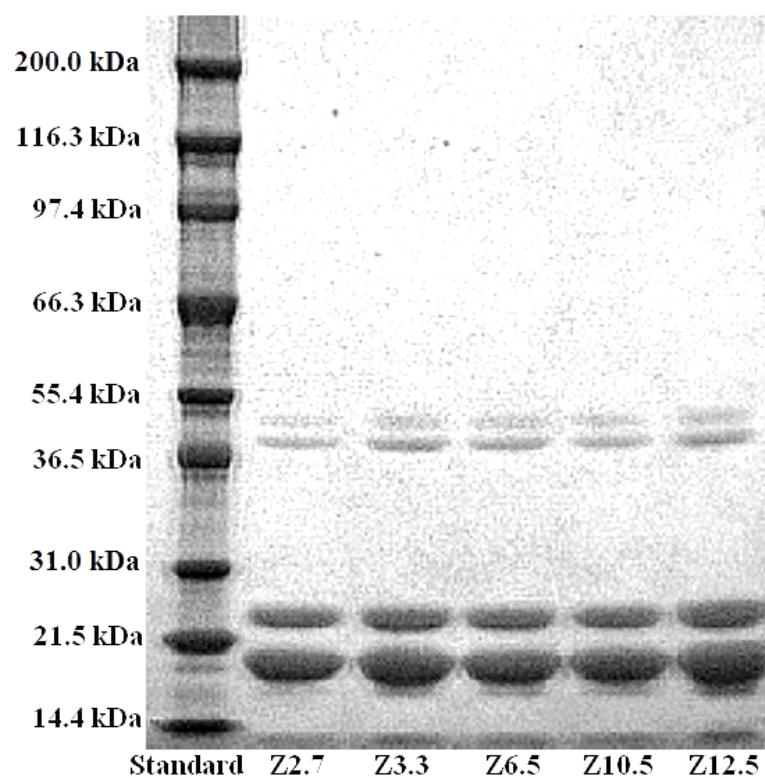
Figure 2.5 SDS-PAGE analysis of pH-treated zein samples.
The loaded amount of protein was 0.5 μg; and the gel was Coomassie stained.

(4) Particle Size and Morphology

Table 2.1 Effective diameter and polydispersity of different zein samples.

Sample	Effective Diameter* (nm)	Polydispersity
Z2.7	970d ± 49	0.145±0.004
Z3.3	470c ± 10	0.292±0.015
Z6.5	243a ± 9	0.077±0.003
Z10.5	283a ± 17	0.076±0.008
Z12.5	383b ± 16	0.105±0.012

* The reported data includes standard error of the mean for three replications. a, b and c indicate that each category is significantly different from the others using ANOVA Tukey's test ($\alpha=0.05$).

Particle size and its morphology are important physical properties of zein. Accurate characterization of these properties would provide theoretical foundation to zein application development. In this study, particle size distribution of zein samples was measured by DLS, and its morphology was characterized by SEM. Results of hydrodynamic diameter and polydispersity were shown in **Table 2.1**. It can be seen that zein in acid solutions tended to form remarkably bigger particles with larger polydispersity comparing with other zein samples in near neutral and basic solutions. Hydrodynamic diameters of zein in acid solutions (970 nm for Z2.7 and 470 nm for Z3.3) and Z12.5 (383 nm) were found statistically larger than that in near neutral condition (243 nm). In previous section, SDS-PAGE thoroughly destroyed protein's structures and was able to provide molecule weight information. However, DLS and the following SEM methods captured zein's original structures in solution and after drying respectively. An increase of original surface hydrophobicity caused by zein deamidation was thought to account for the increment of zein particle sizes in acidic solution (Cabra, Arreguin, Vazquez-Duhalt, & Farres, 2007). Besides, the hydrophobicity increase could also derive from the change in ionization of ionizable amino acids. However, based on zein's original amino acid sequence (Pomes, 1971), 69.7% of total amino acid were non-ionizable, but, other than the most abundant glutamine (21.4%), only 8.9% was ionizable amino acids (6% of acidic and 2.9% basic amino acids). Protonation of acidic amino acid in low pH condition could

increase hydrophobicity of zein, whereas basic amino acid could reversely affect surface hydrophobicity. Therefore, the hydrodynamic diameter change of zein in acidic solution could be primarily associated with deamidation of glutamine residues. Deamidated zein with higher hydrophobicity should have less interaction with ethanol but higher protein-protein interaction, resulting in low stabilities of zein particles and thus promoting zein coagulation in the acid solutions. This effect was amplified after sample was dried as evidenced by the SEM results presented below.

After cast drying, the acidic treated zein formed films with holes (Figures 2.6A and B), which were also found when zein treated with chloroacetic acid (Q. Wang, Yin, & Padua, 2008) and acetic acid (Shi, Kokini, & Huang, 2009) were cast-dried on smooth surfaces. Whereas, zein treated under the near neutral and basic conditions formed uniform particles ranging from 100-400 nm (Figures 2.6C-E). Detailed mechanism of such phenomena has yet to be found but we thought it must be related to physico-chemical properties of zein surface. In the drying process, ethanol evaporated first, followed by water, resulting in a rapid increase of environment polarity. Zein molecules tended to expose their hydrophilic residues towards solvent to minimize the surface tension. Therefore, negative charges, even weak, on zein surface (Z6.5, Z10.5, and Z12.5) would help minimize hydrophobic interaction between proteins and promote protein-water interaction. Subsequently, small particles were stabilized through electrostatic force (Guo, Heinamaki, & Yliruusi, 2008). Otherwise, hydrophobic interaction and Van-der Waals force would make protein coagulate resulting in the film formation (Z2.7 and Z3.3).
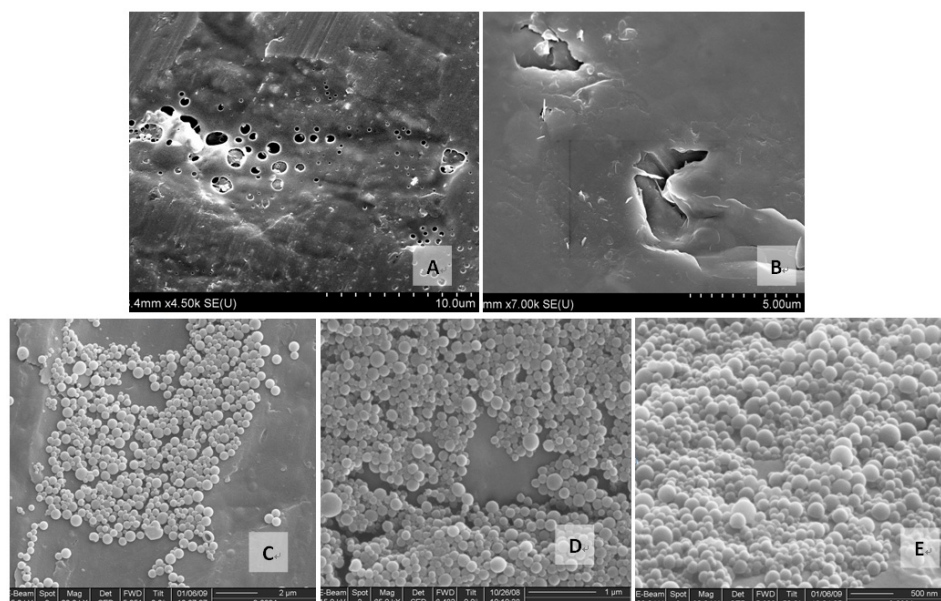
Figure 2.6 SEM images of pH-treated dried zein samples.
A. Z2.7; B. Z3.3; C. Z6.5; D. Z10.5; and E. Z12.5.

2.4.2 Rheological Property

Rheological behavior is a major physical property and an important parameter, which determines the processing ability of a polymer material. In this study, rheological properties of pH-treated zein samples were examined by a rheometer. Figure 2.7 showed viscosity changes vs. shear rate of five zein samples at the 10% protein concentration in 70% ethanol at 25 °C. It can be seen that viscosities of all samples decreased with an increasing shear rate, suggesting that zein treated at the experimented pH conditions was non-Newtonian. Z6.5 had the largest viscosity among 5 samples and its viscosity was approximately 6 and 10 times more than that of Z2.7 and Z12.5, respectively, at the shear rate of 1 s^{-1}. This indicated that pH had a significant influence on zein viscosity – both acidic and basic conditions would decrease it. Conformational changes, i.e., decreased contents of ordered α-helix, β-sheets, and β-turns as evidenced by the FTIR results, were believed to account for

the viscosity decrease. Conformational changes may partially unfold zein and thus cause the increase of surface hydrophobicity (Cabra, Arreguin, Vazquez-Duhalt, & Farres, 2007). As a result, more hydrophobic zones on zein molecules would expose to and interact with the solvent leading to less aggregation or polymerization.

Shear thinning index (*m*) is a measure of non-Newtonian-ness of a solution and can be derived from the Ostwald-de Waele model:

$$\eta = K\gamma^{m-1}$$
<div align="right">Equation 2.2</div>

Where η is the apparent viscosity (Pa·s), K is the consistency (Pa·s^m), and γ is the shear rate (s^{-1}). The shear thinning index is 1 for a Newtonian fluid and between 0 and 1 for a shear thinning solution. The smaller the *m* value, the stronger the shear thinning behavior.
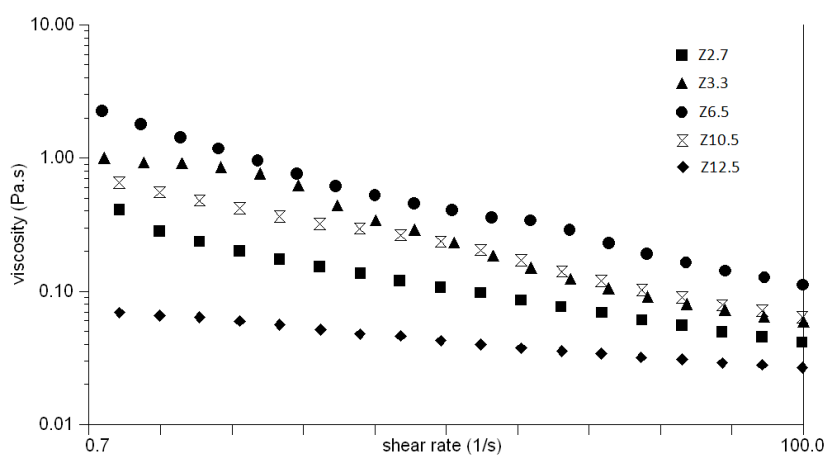
Figure 2.7 Viscosity of pH-treated zein samples.
(10% w/v) at 25℃ in double log scale

Table 2.2 Shear Thinning Index (m) and Conssistency (K) values for different pH-treated zein samples.

At 25℃ and shear rates between 0.7 and 100 s-1.		
Sample	m*	K* (Pa s^m)

Z2.7	0.948c ± 3.302E-4	1.584c ± 3.225E-2
Z3.3	0.923a ± 2.126E-4	1.432b ± 1.207E-2
Z6.5	0.931b ± 2.055E-4	2.118d ± 1.385E-2
Z10.5	0.935b ± 1.769E-4	3.187e ± 2.567E-2
Z12.5	0.975d ± 2.722E-5	0.073a ± 5.129E-5

Table 2.2 summarized *m* and K values derived from Figure 2.7 at the shear rate between 0.7 and 100 s^{-1} for all pH-treated zein samples at 25℃. It can be seen that *m* values were between 0.9 and 1, confirming that all pH-treated zein in this study had weak shearing thinning behavior, which was consistent with what Selling et al. (2005) had reported on apparent viscosity of native zein solutions. Samples Z12.5 and Z2.7 ranked 1 and 2 in *m* value suggesting that their rheological behaviors were close to a Newtonian solution. K value for Z12.5 was 0.07, which was more than one order of magnitude smaller than that of other treatments, indicating lowest viscosity happened at a 0.02 N basic condition.

A dynamic oscillatory test at the linear viscoelasticity strain% was performed to obtain values and trend of elastic modulus (G') and viscous modulus (G'') (Figure 2.8). Figures 2.8 A-E showed the G'/G'' changes of samples Z2.7, Z3.3, Z6.5, Z10.5, and Z12.5, respectively. It should be noted: 1) in general, G' was larger than G'' indicating a predominance of elastic characteristics; 2) pH had a visible effect on viscoelastic property of zein – either acidic or basic treatment would reduce it by

several orders of magnitude; 3) both modulus of Z6.5 were nearly independent of the frequency, whereas G' and G'' of zein samples treated under acidic and basic conditions became frequency-dependent and increased gradually with increase in frequency. These viscoelastic behavior changes were attributed to conformational changes of zein samples in non-neutral pH conditions. A decrease of ordered structures made pH treated zein behave more like a liquid.
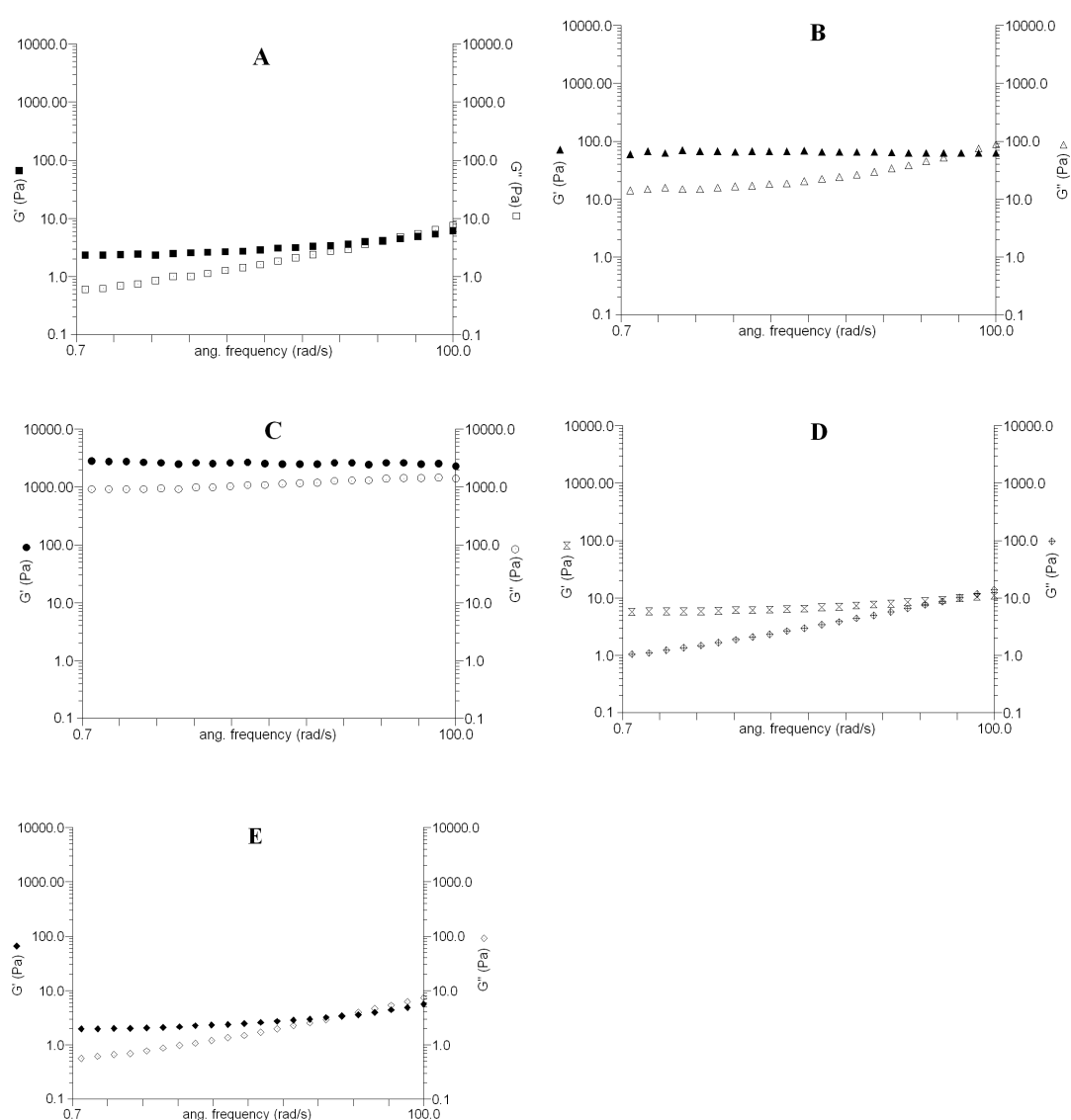
Figure 2.8 Elastic modulus (G') and Viscous modulus (G") of pH-treated zein samples.

(10% w/v): A. Z2.7; B. Z3.3; C. Z6.5; D. Z10.5; and E. Z12.5. (double log scale).

By and large, modified rheological behaviors of the pH-treated zein samples, i.e. dramatic viscosity decrease and viscoelastic property change, are expected to have a remarkable influence on zein application processes, such as power requirements of agitation, pumping, and extruding, and to provide guidance to zein purification and processing in future application development.

2.4.3 Antioxidant Properties

Previous studies have demonstrated that certain amino acids residues or short peptides were related to the radical scavenging activity (RSA) of proteins or peptides (Chan, Decker, Lee, & Butterfield, 1994; H. M. Chen, Muramoto, Yamauchi, & Nokihara, 1996; Hernandez-Ledesma, Amigo, Recio, & Bartolome, 2007; Marcuse, 1960). Zein's RSA was attributed to the presence of His, Arg, Ala, Val, Met, and Leu amino acid residues that had strong antioxidant activity both in free forms and as residues in peptides and proteins (H. M. Chen, Muramoto, Yamauchi, Fujimoto, & Nokihara, 1998; Hernandez-Ledesma, Amigo, Recio, & Bartolome, 2007; Pena-Ramos, Xiong, & Arteaga, 2004). However, zein fragmentation by severe deamidation was found to have a negative effect on its antioxidant properties due to diminution in its fatty acid-binding capacity (Chiue, Iwami, Kusano, & Ibuki, 1994; Chiue, Kusano, & Iwami, 1997; Yong, Yamaguchi, Gu, Mori, & Matsumura, 2004) and thus limit its application. Therefore, retaining or improving antioxidant property is an important consideration of zein modification.

FTIR and ζ-potential analysis indicated that mild zein deamidation happened under the pH treatments experimented in this work. Though no evidence showed that zein fragmentation or oligomerization occurred through the SDS-PAGE analysis, it was of great interest to see if the zein's RSA deteriorated upon mild pH treatments. In this section, the RSA (with DPPH˙ assay) and reducing power (using ferric-ion spectrophotometric assay) of five pH treated zein samples were investigated to evaluate their antioxidant activities.

(1) DPPH˙ Assay

The free radical scavenging study of zein was carried out using a DPPH˙ assay and the results were illustrated in Figure 9. Both short (Figure 9A) and long (Figure 9B) period of time were studied to compare the difference of DPPH radical scavenging properties of pH treated zein samples. The interesting findings included: 1) the optical density of all samples decreased with time, indicating a decrease of DPPH free radicals; 2) different samples had different decreasing rates. The faster the optical density was dropping, the better the scavenging activity against DPPH˙ was. DPPH free radicals in the control (70% ethanol) were scavenged naturally without zein. However, addition of zein accelerated the DPPH˙ scavenging. Similar result was observed for zein hydrolysates from alcalase treatment by Zhu et al. (2008). Although in short time (Figure 9A), a large variation in DPPH˙ decreasing rate was observed among different samples with Z12.5 (2.5 fold of the control) showing the best RSA, the DPPH˙ decreasing rate of Z12.5 and Z2.7 converged at day 2 (Figure 9B) and was

approximately 1.8 times larger than that of the other three samples (Z3.3, Z6.5, and Z10.5) which showed similar RSA as time evolved.

Saiga, Tanabe, and Nishimura (2003) found that short peptides rich in aspartic acid and glutamic acid exhibited strong antioxidant activities. Therefore the increased RSA of Z2.7 and Z12.5 samples was possibly attributed to the mild deamidation of glutamine and the formation of glutamic acid / glutamate residues in zein. In addition, no zein fragmentation also helped retaining its RSA property.
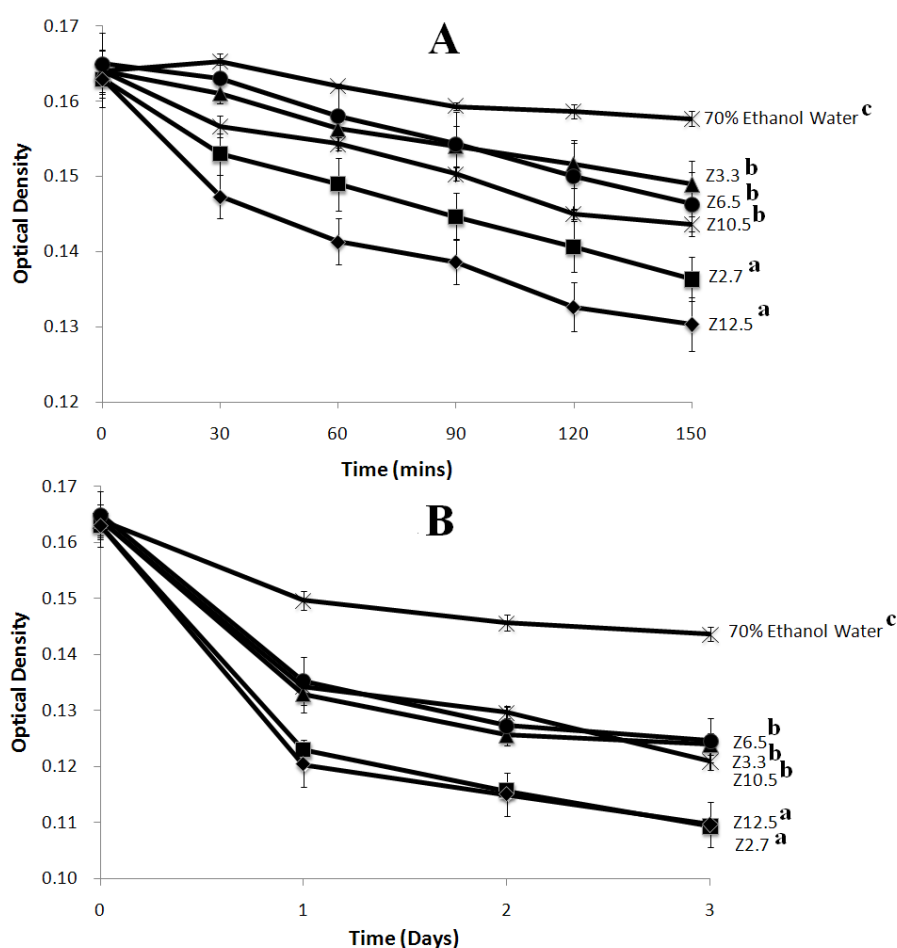
Figure 2.9 DPPH radical scavenging results of different zein samples
A. Short reaction time from 0-150 minutes; B. Long reaction time from 0-3 days. Means marked with different letters indicated significant difference between each other upon the ANOVA Tukey's Studentized Range Test (P<0.05).

(2) Ferric-ion Spectrophotometric Assay

51
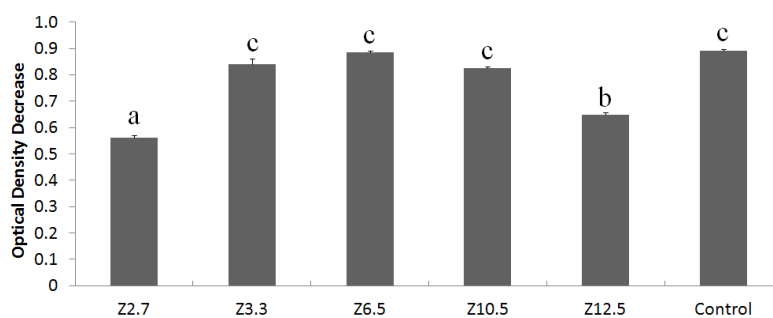
Figure 2.10 Antioxidant activity of different zein samples against hydrogen peroxide and the formation of hydroxyl radicals.
Means marked with different letters indicate significantly different between each other upon the ANOVA Tukey's test (P<0.05). The optical density decrease was determined between original samples and incubated (37 °C for 60 mins) samples.

In addition to evaluating the scavenging property of zein on DPPH· (a nitrogen radical), ferric-ion spectrophotometric assay was also applied to study the antioxidant activity of zein against the formation of hydroxyl radical (OH·). $[Fe(o\text{-}phen)_3]^{2+}$ can be oxidized by hydrogen peroxide to generate OH· by Fenton's reaction (Goldstein, Meyerstein, & Czapski, 1993; Walling, 1998). Fe(III) produced from the Fe(II) oxidation can no longer form a coordination compound with ligand o-phen, and hence the optical density will decrease. The magnitude of decrease is proportional to the quantity of the generated hydroxyl radical. Figure 2.10 showed that, as compared with that of the control experiment in which no zein was added, the optical density, hence the OH· generation, decreased by 38% and 27% for samples Z2.7 and Z12.5, respectively. The presence of glutamic acid / glutamate residues was effective in preventing Fe (II) oxidation because of their high antioxidant activity (Saiga, et al., 2003). Therefore, deamidation of glutamine upon mild pH treatment of zein was also believed to contribute to the significant improvement of Z2.7 and Z12.5 samples on antioxidant activities.

In summary, pH has been found important to determine the free radical scavenging properties of zein against the nitrogen radicals DPPH· and the antioxidant activity that prevents the generation of OH·. The effects can be attributed to the zein deamidation without protein fragmentation in the experimented acidic and basic conditions.

2.5 Conclusions

Mild pH (0.0005 – 0.002 N hydrochloric acid or NaOH) treated zein would maintain its structural and functional properties, change its rheological behavior, and enhance its antioxidant properties due to mild zein deamidation. In comparison to the near neutral zein sample (Z6.5), secondary structure of zein (i.e. α-helix, β-sheet, and β-turns) decreased by 10 ~ 20% likely due to deamidation of glutamine residues. However, no protein oligomerization or polymerization was found in these experimented pH conditions. These conformational changes had a significant effect on rheological behaviors of the pH-treated zein as evidenced by its decreased viscosity, elastic modulus (G'), and viscous modulus (G"). Furthermore, the antioxidant properties of zein samples, as expressed as RSA against DPPH· and the reducing power of 1,10-penanthroline–iron, improved significantly in the experiment time range up to 3 days.

This finding may facilitate novel applications of zein in food and pharmaceutical industries, e.g., food flavor and drug encapsulation. In the future, experiments designed for investigating the synergistic effect of pH, temperature, and solvent type on zein physical and chemical properties will further improve

understandings of zein science and technology, and may provide optimized operation conditions for zein application development.

2.6 Acknowledgements

CHAPTER 3. Development of Silver-Zein Composites as A Promising Antimicrobial Agent

Adapted from Zhang, B., Luo Y., and Wang Q. (2010). Biomacromolecules, 11, 2366-2375.

3.1 Abstract

Recently, silver, a traditional broad-spectrum antiseptic, drew increasing attentions as a solution against antibiotic resistant bacteria. Various synthetic polymers and nature polymers were applied to form silver polymer composite in order to cope with the defects (e.g. low hemocompatibility) of silver loaded antimicrobial agents. In this study, an alcohol soluble prolamine, zein, was applied to prepare silver zein composites as novel antiseptics. Both zein in silver (Z]A) and silver nanoparticles (AgNP) in zein (A']Z) structures at two pH conditions (i.e. pH=3.3 and pH=6.5) were successfully prepared. Several characterization methods (i.e. zeta potential, FTIR, SEM, and turbidity) confirmed the formation of silver zein composites through nitrogen silver coordination bond and electrostatic interaction. It was found that low pH was critical in facilitating formation and increasing stability of the silver zein composites probably by inducing electrostatic interaction between silver and zein. The antiseptic activities (i.e. growth inhibition and bactericidal activity) of different silver zein composites were studied against Gram negative *E. coli* and Gram positive *S. aureus*. It was revealed that the silver zein composites showed similar or better results against both types of bacteria comparing to those of $AgNO_3$ and AgNP, except for the sample of A']Z-Ac. It had better growth inhibition

activity, but inferior bactericidal activity than that of AgNP because of its decreased solubility in aqueous medium. Furthermore, addition of zein was proven to be capable of dramatically increasing hemocompatibility of silver loaded antiseptic agents. Therefore, silver-zein composites prepared in this work may find applications in wound care and food packaging areas.

3.2 Introduction

Silver element and silver ions have been used as conventional antiseptics since ancient times due to their broad-spectrum bactericidal activities. They are proved to be effective against both Gram positive and Gram negative antibiotic-resistant bacteria, which have caused increasing concerns in both clinical and food applications (de Azeredo, 2009; Panacek, et al., 2006; Wright, Lam, & Burrell, 1998). Silver compounds, such as silver sulfadiazine (Wright, Lam, & Burrell, 1998) and silver (I)-imidazole (Melaiye, Sun, Hindi, Milsted, Ely, Reneker, et al., 2005), showed bactericidal activities against bacteria in clinical applications. However, concentration-wise, they didn't show substantial improvement comparing to traditionally used 5 mg/ml silver nitrate ($AgNO_3$) (Melaiye, et al., 2005; Wright, Lam, & Burrell, 1998). A novel category, known as silver nanoparticles (AgNP), was found to be 10-100 times more efficient than traditional $AgNO_3$. This translated that to be as effective as $AgNO_3$, only 0.05 – 0.5 mg/ml of the silver was needed in AgNP (J. S. Kim, Kuk, Yu, Kim, Park, Lee, et al., 2007; Sondi & Salopek-Sondi, 2004). However, when using silver as an active bactericidal agent, some problems still exist even after

the conventional silver compounds have been replaced by silver nanoparticles. For example, silver containing antiseptic agents can cause permanent discoloration (argyria) if silver directly contacts with skin (Wright, Lam, & Burrell, 1998)[1], and it may also trigger allergic reactions in human body (Mohungoo & Gawkrodger, 2009; Ozkaya, 2009). Accumulation of silver on skin wound area and immune response inside human body could be attributed to the release of silver element from matrix and the migration to the blood circulation system.

Recently, the approach of incorporating the silver compounds or silver nanoparticles into polymer-based matrix has been explored to address the aforementioned problems. Such polymers included both synthetic polymers and natural polymers. Balogh, etc. developed a synthetic dendrimer to trap silver ion and form nanocomposites, which acted as a water soluble antiseptic agent(Balogh, Swanson, Tomalia, Hagnauer, & McManus, 2001). Other researches either incorporated silver compounds into amphiphilic hyperbranched macromolecules (Aymonier, et al., 2002), or conjugated silver into polymeric networks (Furno, et al., 2004; Ho, Tobis, Sprich, Thomann, & Tiller, 2004). Although these approaches immobilized or controlled the diffusion of silver content, they still couldn't improve silver's hemocompatibility. Thereafter, polysaccharides were applied to incorporate silver compounds or silver nanoparticles. To ensure the conjugation of silver, polysaccharides containing amino-groups are usually selected. Therefore, chitosan became the most studied and reported polysaccharide matrix to produce silver-chitosan composites. Travan and co-workers found that chitosan gel

significantly reduced silver's cytotoxicity (Travan, et al., 2009). In other studies, different silver compounds (i.e. silver sulfadiazine and silver (I)-imidazole) were incorporated into various forms of chitosan matrix, including solution (Sanpui, Murugadoss, Prasad, Ghosh, & Chattopadhyay, 2008), gel (do Nascimento, Sampaio, Medeiros, & de Azevedo, 2009), and film (Wei, Sun, Qian, Ye, & Ma, 2009). Unfortunately, chitosan has its limitation as the matrix material. Although chitosan applied in these experiments was 80% - 90% deacetylated, due to its lacking of amino groups, a relatively large quantity of polysaccharide was required to form a stable silver chitosan composite. Otherwise, leaking of silver was observed in aqueous solutions (do Nascimento, Sampaio, Medeiros, & de Azevedo, 2009; Travan, et al., 2009). The silver leakage again could cause skin discoloration, low hemocompatibility, and induce cytotoxicity. Proteins, another commonly used category of nature polymer, may be more desirable because they are not only hemocompatible, but also contain large amount of nitrogen in their peptide backbones which has potential to interact with silver. To the best of our knowledge, no studies have been published on silver protein composites.

Kumar, etc. (2005) found out that silver formed coordination bond with nitrogen in polyamide. The silver/polyamide composites were then proven to be antiseptically active against both Gram positive and Gram negative bacterial species. However, silver leakage was still observed due to polyamide's good water solubility. Thus, in this study, zein protein was explored for its ability to form silver-zein composite. Zein is a maize prolamine protein, which is a major co-product of corn

starch production. Zein is consisted of roughly one-third of hydrophilic (i.e. glutamine) and two-thirds of hydrophobic amino acid residues in its primary structure, which is closely related to its unique aqueous-alcohol solubility and film forming ability. In our previous study (B. C. Zhang, Y. C. Luo, & Q. Wang, 2011), zein showed different pH-dependent properties, including morphology and surface charge. Several studies have been published for applying zein as a matrix for different antimicrobial agents, including lysozyme (Gucbilmez, Yemenicioglu, & Arslanoglu, 2007; Zhong & Jin, 2009; Zhong, Jin, Davidson, & Zivanovic, 2009), thymol (Del Nobile, Conte, Incoronato, & Panza, 2008; Mastromatteo, Barbuzzi, Conte, & Del Nobile, 2009) and nisin (Hoffman, Han, & Dawson, 2001; Ku & Song, 2007). These food grade antiseptics were successfully incorporated in the zein matrix. The resultants were active in bacteria control of Gram positive (e.g. *Bacillus subtilis*, *Staphylococcus aureus*) and Gram negative (e.g. *Escherichia coli*, *Listeria monocytogenes*) species. For silver zein composites, besides solubility, pH-dependent properties of zein, including surface charge and morphology, could also be helpful (B. C. Zhang, Y. C. Luo, & Q. Wang, 2011).

The objective of this study is to prepare and characterize two types of silver zein composites to develop a novel silver-loaded zein antiseptic with strong antimicrobial activities and improved hemocompatibility. The effect of pH (i.e. neutral and acidic) and particle size of silver compounds (i.e. $AgNO_3$ and AgNP) on the stabilities, antimicrobial activities and hemocompatibility of the silver zein composites were evaluated. Some of the obtained composites were then proven to be

conducive to improve silver antiseptic's stability and antiseptic activities, as well as hemocompatibility. This study provided a novel solution for reducing side effects of silver containing antiseptic reagents and expanding the application of silver-based antiseptics in clinics and packaging industry.

3.3 Materials and Methods

3.3.1 Materials and Chemicals

Zein sample with a minimum protein content of 97% was obtained from Showa Sangyo (Tokyo, Japan). Chemicals, including acetic acid (AcOH), calcium chloride, ethanol, silver nitrite, and sodium citrate were purchased from Sigma-Aldrich (St. Louis, MO). *E. Coli* and *S. aureus* were purchased from ATCC (Manassas, VA), while all broth and agar were bought from Difco (Franklin Lakes, NJ). For QCM-D experiment, gold and silver coated quartz crystals were ordered from Q-Sense (Glen Burnie, MD); pooled human plasma and human Immunoglobulin G (IgG) were purchased from Innovate Research (Novi, Michigan), and rabbit anti-human C3c antibody was brought from Dako (Carpinteria, CA), while Veronal buffer (VBS and VBS++) were from Boston BioProducts (Ashland, MA).

3.3.2 Sample Preparation

Two types of silver-zein composites were successfully prepared using different methods. They were zein in silver (Z]A) and AgNP in zein (A']Z) structures.

For Z]A sample preparation, 1 mg/ml zein was prepared in advance in 70% ethanol aqueous solution. Then, various amounts of silver nitrite were added to obtain different weight percentage of zein vs. silver nitrite. An acidified zein in silver samples (Z]A-Ac) were prepared by adjusting the pH of final solutions to 3.3 by AcOH.

A']Z was obtained by first preparing AgNP core following Lee's method (Lee & Meisel, 1982). Briefly, 10 mL of 38.8 mM sodium citrate aqueous solution was added dropwise within 2 min into 490 mL of 347 mM boiling $AgNO_3$ aqueous solution under vigorous stirring. Afterwards, the solution was boiled for 1 hr, and heat was removed to cool the reaction solution to room temperature. Then, ethanol was well mixed with the aqueous AgNP solution to form 70% ethanol aqueous environment for zein dissolution. The as-prepared AgNP had the particle size around 116 nm. Thereafter, different quantities of zein were introduced to AgNP solution to form AgNP in zein composites. Acidified AgNP in zein samples (A']Z-Ac) were again prepared by adjusting the pH of final solutions to 3.3 with AcOH.

The final concentrations and pHs of difference compositions of silver zein samples were reported in Table 1.

3.3.3 Surface Charge

A laser Doppler velocimetry (Zetasizer Nano ZS90, Malvern, UK) was used to characterize the electrophoretic mobility of different samples. Zeta potential was further converted from the measured mobility using the Smoluchowski theory. During

the experiment, samples with different treatments were first well mixed and filled in a fold capillary cuvette (Folded Capillary Cell - DTS1060, Malvern, UK). The whole cuvette was then mounted onto the measuring chamber at 20 °C. For each sample, three replications were obtained and results were statistically analyzed.

3.3.4 Infrared Analysis

A Jasco 4100 series Fourier Transform Infrared Spectroscopy (FTIR) with an attenuated total reflection (ATR) cell (Jasco Inc. Easton, MD) was used to monitor structural changes of different samples. The samples were first cast-dried on an aluminum tray for 24 hrs, and then mounted directly on an ATR crystal. The spectra were acquired at 400-4000 cm^{-1} wavenumbers with a 4 cm^{-1} resolution. The spectra were further analyzed by OMNIC software (version 8.0, Thermo Scientific).

3.3.5 Morphology and Elemental Analysis

A scanning electron microscopy with energy-dispersive X-ray spectrometer (SEM/EDS, SU-70, Hitachi, Pleasanton, CA) was used to obtain morphology change and elemental analysis of different samples. The samples were first cast-dried on an aluminum tray and then were cut into small pieces and mounted on specimen stubs by conductive carbon tapes. The whole stub was coated with an infinitesimal (<20 nm) conductive gold and platinum layer using a sputter-coater (Hummer XP, Anatech, CA). EDS was used to obtain elemental information of sample surfaces. Both typical SEM and EDS digital images of the samples were reported.

3.3.6 Stability

The stability of the samples in 70% ethanol aqueous solution was evaluated using a turbidimeter (ONION AQ4500, Thermo Scientific, Beverly, MA). After preparation, samples were stored in the room temperature under daylight lamps and their turbidities were measured at day 0, 1, 2, 3, 4, and 5. The reading was taken right after 15 s of vortex. Before measuring turbidity of the samples, water was used as a blank to set the turbidity value to zero. Z (1.0 mg/ml), $AgNO_3$ (5.0 mg/ml) and AgNP (5.4×10^{-2} mg/ml) stored at the same conditions were used as controls for comparison.

3.3.7 Antimicrobial Activities

The antimicrobial activities of different samples were evaluated by two assays, i.e. growth inhibition and bactericidal efficacy assays, against both *E. coli* (ATCC# 53323) and *S. aureus* (ATCC# 29213). *E. coli* and *S. aureus* were selected as pathogen representatives because they are both well known pathogenic bacteria responsible for foodborne illness and clinical infections. In previous studies, minimal inhibitory concentration (MIC) and minimal bactericidal concentration (MBC) of $AgNO_3$ and AgNP have already been established [5]. Therefore, samples were prepared using the fixed concentrations of $AgNO_3$ (5.0 mg/ml) and AgNP (5.4×10^{-2} mg/ml) obtained from previous studies for antimicrobial activity evaluations.

(1) Growth inhibition Assay.

The growth inhibition for *E. coli* and *S. aureus* in solid medium was evaluated according to Travan's method [13]. A coating of silver-zein composites was first

produced by evenly spread 1 ml sample solutions on Tryptic Soy Agar (TSA) surface. After the solvent was evaporated and coating was dried, 10 μL of bacterial solution with the concentration of 10^8 CFU/mL was dripped onto coated TSA. After smearing bacteria with sterile cotton swabs, the solid media were incubated at 37 °C for 24 hrs. Original TSA agar was applied as the control at same bacterial inoculation and incubation conditions. To evaluate the bacterial growth in different samples, the appearance of agar colonies was photographed by a digital camera (Canon, A2100 IS, Lake Success, NY).

(2) Bactericidal Efficacy Assay.

Sample solutions of silver-zein composites with different treatments were first transferred into sterile vials, which all contained equal amount of zein (1.0 mg/ml) and AgNO$_3$ (5.0 mg/ml of Ag element) or AgNP (5.4×10^{-2} mg/ml of Ag element). The alcohol and water were then evaporated by incubating the vials for 72 hrs at 50 °C. The vials were then sterilized with UV irradiation (Class II A/B3 Biological Safety Cabinet, Forma Scientific, Marietta, OH) for 1 hr immediately before use. 5 ml of Luria-Bertani (LB) medium containing 10^6 CFU/ml bacteria of *E. coli* or *S. aureus* were well mixed with sterilized samples by vortexing the solution. After incubation at 37 °C for 24 hrs, the microorganism concentration was plate counted. LB medium was used as a control for both bacteria. Each sample was repeated for three times for statistical analysis.

3.3.8 Hemocompatibility

Hemocompatibility assay was conducted on an Quartz Crystal Microbalance with Dissipation function (QCM-D) platform (Q-Sense E1, Glen Burnie, MD), following the procedures of previously reported method, by Sellborn etc (2005). This method has been adapted in many materials studies, including inorganic materials, e.g. Titanium (Sellborn, Andersson, Hedlund, Andersson, Berglin, & Elwing, 2005) and silicon dioxide (Sellborn, Andersson, Fant, Gretzer, & Elwing, 2003); synthetic polymers, e.g. polystyrene (Sellborn, Andersson, Hedlund, Andersson, Berglin, & Elwing, 2005), nylon (Berglin, Olsson, & Elwing, 2008; Sellborn, Andersson, Fant, Gretzer, & Elwing, 2003); and biomaterials, e.g. cellulose (Fink, Faxalv, Molnar, Drotz, Risberg, Lindahl, et al., 2010).
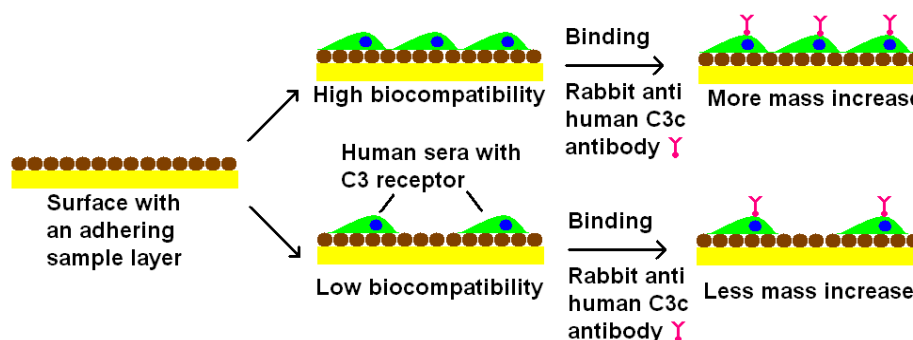
Figure 3.1 Schematic Mechanism of Biocompatibility Assay Using QCM-D.

To better understand the experimental mechanism of hemocompatibility assay utilizing QCM-D, Figure 3.1 was included. According to Sellborn's method (Sellborn, Andersson, Hedlund, Andersson, Berglin, & Elwing, 2005), as shown in Scheme 1, the assay can be divided into three steps, sample layer formation, attachment of human sera (Sera), and attachment of antibody C3c. Depending on the hemocompatibility of the sample layer, the specific attachment of Sera can be more or

less. Therefore, the mass increment of specifically bound C3c on the attached Sera (the third step) can be used to determine the hemocompatibility of sample layers. More C3c mass increase detected by QCM-D, more hemocompatible the sample was. Immunoglobulin G (IgG) was considered as a positive control, which had the best hemocompatibility, whereas inactivated human sera (iSera) had the worst hemocompatibility and acted as a negative control. Zein, silver and AgNP also performed as controls that were intended to conduct comparisons with silver-zein composites, i.e. Z]A, Z]A-Ac, A']Z, and A']Z-Ac. iSera was obtained by heating thawed human sera at 56 ℃ for 30 min. During the experiment, the quartz crystal was first saturated with the 70% ethanol aqueous solution, and sample solution was then pumped to the crystal surface. After the mass curve reached a plateau indicating a full coverage of the testing material on the crystal surface, Veronal Buffer Solution (VBS) was applied to wash off loosely bound sample materials. Afterwards, Sera solution was introduced to the sample-coated crystal surface, and the VBS was again used to remove unspecifically bound Sera cell. Last, the anti-human C3c antibody was introduced to interact with attached Sera. The mass change of specifically bound C3c was adopted for quantitatively analyzing the hemocompatibility. All measurements were carried out at 37 ℃ under a flow rate of 22.5 μL/min precisely controlled by a tubing pump (ISMATEC, REGLO Analog MS-2/12, Glattbrugg, Switzerland).

3.3.9 Statistical Analysis

Experiments, i.e. zeta potential, stability and bactericidal efficacy, were conducted in triplicate with data reported as mean ± standard error.   Experimental

statistics were performed using a SAS software (Version 9.2, SAS Institute Inc., Cary,

NC).

3.4 Results and Discussion

3.4.1 Preparation and Characterization of Silver-Zein Composites.

Different compositions of four groups of silver-zein composites, namely Z]A,

Z]A-Ac, A']Z, and A']Z-Ac, were summarized and presented in Table 3.1.

Physicochemical properties of samples such as surface charge, morphology, chemical

analysis, stability were characterized and discussed in following sections.

Table 3.1 The Composition and pH of silver zein Composites.
a) Z]A and Z]A-Ac

No.	Zein mg/ml	$AgNO_3$ mg/ml	pH	No.	Zein mg/ml	$AgNO_3$ mg/ml	pH (AcOH)
Z]A-1	1.0	0	6.5	Z]A-Ac-1	1.0	0	3.3
Z]A-2	1.0	1.0	6.5	Z]A-Ac-2	1.0	1.0	3.3
Z]A-3	1.0	3.0	6.5	Z]A-Ac-3	1.0	3.0	3.3
Z]A-4	1.0	5.0	6.5	Z]A-Ac-4	1.0	5.0	3.3
Z]A-5	1.0	7.0	6.5	Z]A-Ac-5	1.0	7.0	3.3
Z]A-6	1.0	10.0	6.5	Z]A-Ac-6	1.0	10.0	3.3
Z]A-7	0	5.0	6.5	Z]A-Ac-7	0	5.0	3.3

b) A']Z and A']Z-Ac

No.	Zein mg/ml	AgNP* mg/ml	pH	No.	Zein mg/ml	AgNP* mg/ml	pH (AcOH)
A']Z-1	0	5.4×10^{-2}	6.5	A']Z-Ac-1	0	5.4×10^{-2}	3.3
A']Z-2	5.0×10^{-2}	5.4×10^{-2}	6.5	A']Z-Ac-2	5.0×10^{-2}	5.4×10^{-2}	3.3

A']Z-3	0.1	5.4×10^{-2}	6.5	A']Z-Ac-3	0.1	5.4×10^{-2}	3.3
A']Z-4	0.5	5.4×10^{-2}	6.5	A']Z-Ac-4	0.5	5.4×10^{-2}	3.3
A']Z-5	1.0	5.4×10^{-2}	6.5	A']Z-Ac-5	1.0	5.4×10^{-2}	3.3
A']Z-6	2.0	5.4×10^{-2}	6.5	A']Z-Ac-6	2.0	5.4×10^{-2}	3.3
A']Z-7	1.0	0	6.5	A']Z-Ac-7	1.0	0	3.3

* This indicates the concentration of silver element.

(1) Zeta Potential.

Figure 3.2a showed the changes of surface charge when Z]A structure was formed. Zein (Z]A-1) carried no charge in 70% ethanol aqueous solution. Silver ion could form ion-water cluster in the solution and carried positive charge, however, the cluster was too small to be detectable in zeta potential measurement, which usually required the particle size larger than a few nanometer. Therefore, in Figure 3.2a and b, pure $AgNO_3$ solution (treatment 7) didn't have a true value from this measurement. After $AgNO_3$ was added to zein, the Z]A composites became positively charged (Z]A-2 to Z]A-6), indicating that the positively charged silver ions conjugated to the uncharged zein surfaces through Ag-N coordination bond. When silver ion concentration increased from 1.0 to 10.0 mg/ml, the composite surface charges declined slightly from 1.8 to 0.7 mV. Because free silver ions could not be detected by velocimetry, they had no effect on the overall zeta potential of the solution. Therefore, this slight declining of zeta potential indicated the neutralization of Z]A composites by addition of more silver ions.
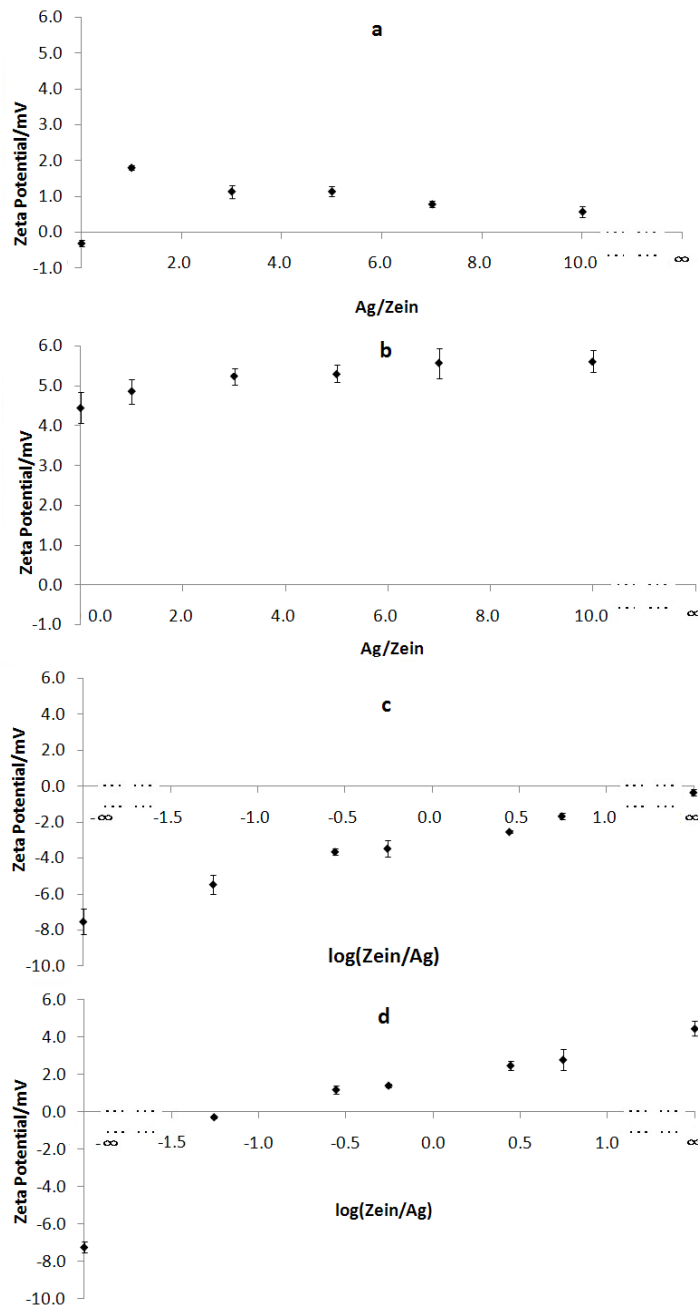
Figure 3.2 Zeta potential change of silver zein nanocomposites
a. Z]A; b. Z]A-Ac; c. A']Z; d. A']Z-Ac. For each composite, treatment 1 to 7
(shown in Table-3.1) were placed sequentially from left to right.

When silver ion concentration was low (Z]A-2), silver could interact with zein

without causing any zein aggregation. However, with the increase of silver ion

concentration, the interaction among silver and zein through Ag-N coordination bonds

was enhanced leading to the aggregation of silver-zein composites, which resulted in

the neutralization of particles in solution. The composite aggregations could also be supported by experimental results of appearance change (Figure 3.3a) for Z]A composite.

Zeta potential change of Z]A-Ac (in an acidic medium) was shown in Figure 3.2b. It had an opposite trend comparing with that of Z]A (in a neutral medium). Zein carried positive charges in acidic condition, due to the high glutamine residue exposure in its tertiary structure. Along with adhering more silver ions on zein surfaces, the zeta potential increased slightly from 4.5 to 5.5 mV. In the neutral solution, comparing to Z]A-1, addition of 1 mg/ml of $AgNO_3$ (Z]A-2) increased the surface charge by 2.0 mV. Whereas, in acidic solution, 1 mg/ml of $AgNO_3$ (Z]A-Ac-2) only induced an increment for 0.5 mV comparing to Z]A-Ac-1. The interaction of zein and silver ions in AcOH solution was thought to be hindered by electrostatic repulsive force as both zein and silver ion carried positive charges at acidic pH, which could weaken the formation of Ag-N coordination bonds, and therefore preventing the zein aggregations. The composites were thought to be stabilized by the AcOH considering there was no aggregation or neutralization occurred even at high silver concentrations, which was also consistent to appearance change (Figure 3.3b) results of the Z]A-Ac composites.
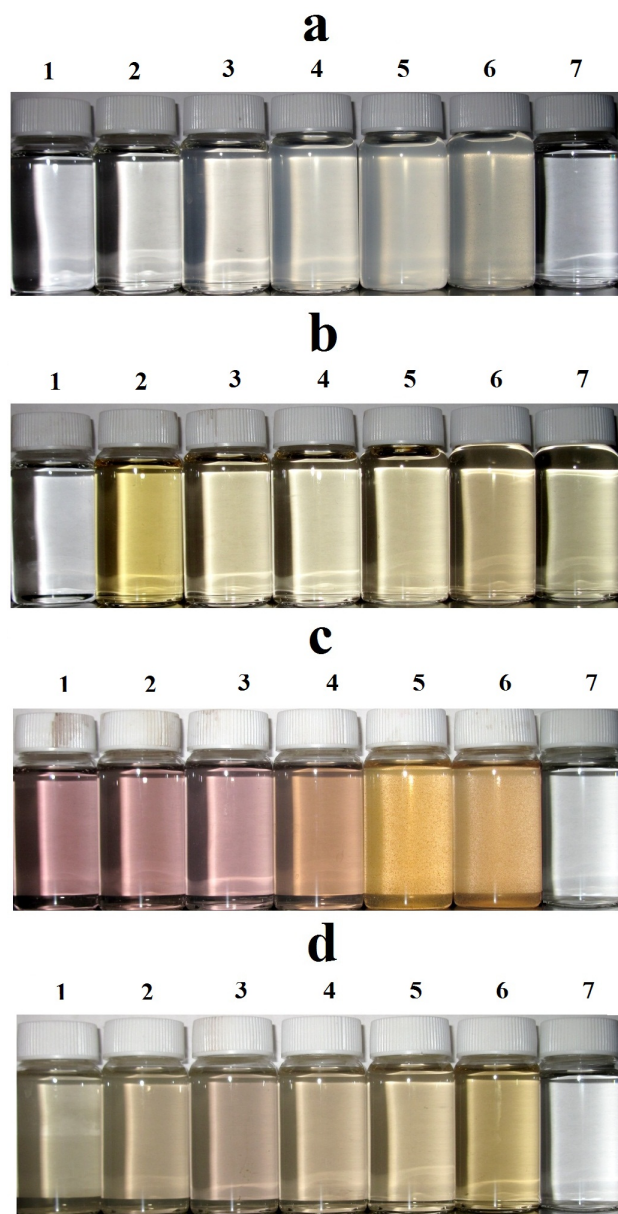
Figure 3.3 Color change of silver zein nanocomposites
a. Z]A; b. Z]A-Ac; c. A']Z; d. A']Z-Ac. For each composite, treatment 1 to 7
(shown in Table-3.1) were placed sequentially from left to right.

Figures 3.2c and 3.2d showed surface charge changes of A']Z and A']Z-Ac

composites. It can be seen that surfaces of AgNP (A']Z-1 and A']Z-Ac-1) had similar

negative charges in both neutral and acidic pH. Because zein had neural and positive

charges at pH 6.5 and 3.3, addition of zein neutralized charges on AgNP surfaces

through electrostatic interaction and surface charges of silver-zein composites fell

between those of AgNP and zein. However, comparing to the zeta potential increases of A']Z composites at pH 6.5, that of A']Z-Ac at pH 3.3 was more dramatic ranging from -7.2 mV to 2.6 mV. This difference could also be ascribed to the contribution of pH. The electrostatic attractive force (in AcOH condition) between negatively charged AgNP and positively charged zein played an important role in facilitating the formation of silver zein coordination complexes.

These surface charge results provided the evidence that silver-zein composites could be formed through silver nitrogen coordination bond between protein and silver.

(2) Appearance.

Figure 3 illustrated appearance of different silver-zein composites in 70% ethanol after they were stored at room temperature for one week under daylight lamps. In Z]A samples (shown in Figure 3a), along with the increase of silver concentration, the clearness of the solution decreased (Z]A-1 to Z]A-6), caused by the silver-zein composite aggregation, which supported the discussion in surface charge changes of Z]A composites. The presence of AcOH in Z]A-Ac composites generated yellowish color in the solution (shown in Figure 3b). The clearness of the solutions was maintained better than Z]A (Figure 3a), indicating the stabilization effect of AcOH.

Figure 3c showed the color change of A']Z, which was related to the zein concentration. Sample c-1, containing solely AgNP, was purple in 70% ethanol aqueous solution. After zein was introduced into the system, the color changed from purple to yellow, indicating the increase of particle size of the composites due to the

coordination between AgNP and zein. Visible particles were presented in samples A']Z-5 and A']Z-6, due to the aggregation of AgNP in zein solutions. This phenomenon was consistent with previous studies of silver-chitosan composites (Travan, et al., 2009), it was found that the color was closely related to the composition of silver compound and the particle size of AgNP (Dubas & Pimpan, 2008). Figure 2d showed that the color of AgNP diminished by adding AcOH to the composites. The acidified solution at pH = 3.3 appeared clearer than A']Z because of the stabilizing effect of AcOH.

Based on the aforementioned results, Z]A-4, Z]A-Ac-4, A']Z-5 and A']Z-Ac-5 samples were selected as representatives of composite category of Z]A, Z]A-Ac, A']Z, and A']Z-Ac respectively. And these four samples were denoted as their category name for further characterization. The selection was based on two criteria. First, they all contained same quantity of zein, which would minimize the variation induced by zein concentration. Second, the silver ion and AgNP concentrations were kept consistent to the concentrations that were reported and adopted in antiseptic applications (J. S. Kim, et al., 2007; Melaiye, et al., 2005; Sondi & Salopek-Sondi, 2004; Wright, Lam, & Burrell, 1998). By using these concentrations as comparisons to commonly used silver-loaded antiseptics, the study was able to illustrate that silver-zein composites could enhance the stability and hemocompatibility of silver-based antiseptics without reducing their antimicrobial activities.

(3) FTIR.
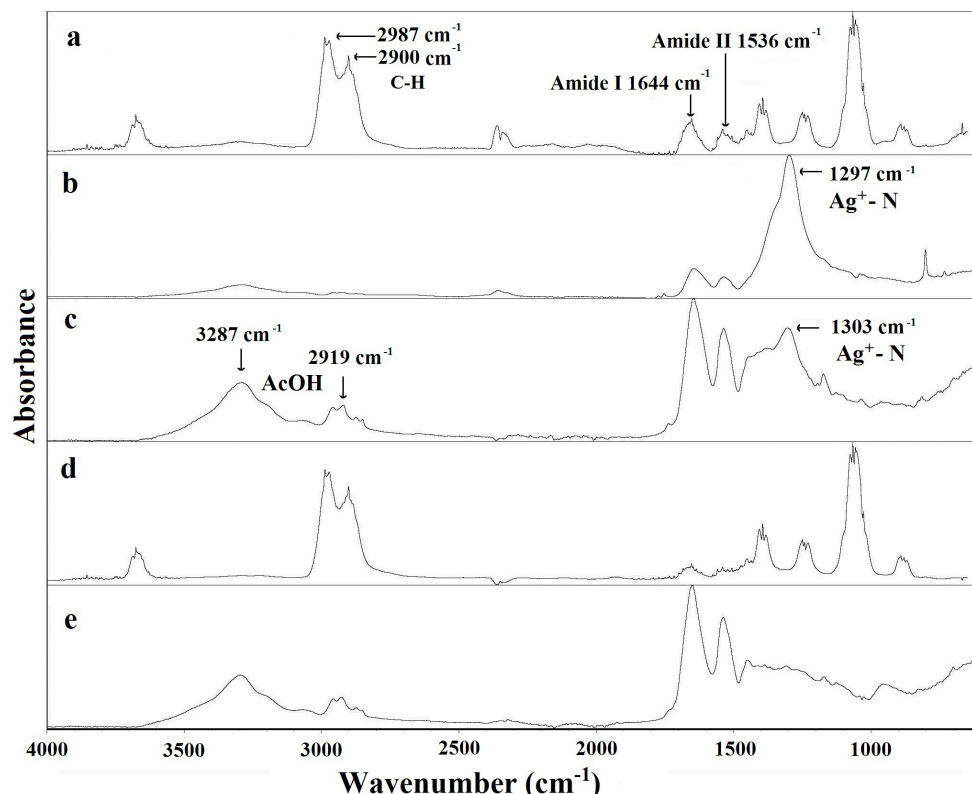
Figure 3.4 FTIR spectra of silver zein nanocomposites
a. Z; b. Z]A; c. Z]A-Ac; d. A']Z; e. A']Z-Ac. The peaks in same wavenumbers
were only marked once.

FTIR spectra of zein (Z), Z]A, Z]A-Ac, A']Z, and A']Z-Ac were collected after samples were casting dried and results were shown in Figures 3.4 a-e, respectively. In original zein spectrum, the peaks observed at 2987 cm^{-1} and 2900 cm^{-1} were considered as C-H stretching from CH_3 and CH_2 functional groups (Figure 3.4a). Several author indicated that these peaks were probably derived from free fatty acids that present in commercial zein (Forato, Bernardes, & Colnago, 1998; Forato, Bicudo, & Colnago, 2003). Besides, amide I (1644 cm-1) and amide II (1536) bands were also observable in zein's original spectra (Figure 3.4a) (B. C. Zhang, Y. C. Luo, & Q. Wang, 2011).

For zein in silver composites, it can be seen that C-H bands disappeared in both Z]A (Figure 3.4b) and Z]A-Ac (Figure 3.4c) samples, which confirmed the interaction of silver ion and zein. The increase of molecular weight of the biopolymer (e.g. zein and chitosan) resulting from the binding of silver, could also cause the reduction of vibration intensity of these bonds (Morgado, 1992; Wei, Sun, Qian, Ye, & Ma, 2009). Moreover, an intensive new band around 1297 and 1303 cm^{-1} was observed in both Z]A and Z]A-Ac, which may be generated by the newly formed Ag$^+$-N coordination bonds, because these peaks were not appeared on either original zein spectrum or spectra of A']Z and A']Z-Ac (Figure 3.4d and 3.4e). However, Z]A-Ac had dramatic different spectra profile due to the addition of AcOH. Comparing to the spectrum of Z]A, two new humps were discovered in Z]A-Ac spectra (Figure 3.4c), which were located at 3287 cm^{-1} and 2919 cm^{-1}. In addition, the vibration intensity at 1644 cm^{-1} and 1536 cm^{-1} increased dramatically, indicating the acidic environment facilitated the C=O stretching (amide I, 1644 cm^{-1}) and N-H bending (amide II, 1536 cm^{-1}). These two bands were contributed by hydrogen bonded O-H stretching of AcOH (Hu, Fu, & Bernstein, 2006). Therefore, addition of silver ion and AcOH dramatically altered the FTIR spectra of zein due to silver-zein composite formation.

For AgNP in zein composites, FTIR spectra were also affected by AgNP and AcOH, but not as dramatic as AgNO$_3$, maybe because they did not have free silver ions in solution. In A']Z composite (Figure 3.4d), C-H bands preserved original zein signals. The result was because AgNP solution doesn't contain Ag$^+$, and the total

amount of silver used in AgNP was only 1.1% of that of AgNO$_3$ used in Z]A samples. The only difference between spectra of Z (Figure 3.4a) and A']Z (Figure 3.4d) was that amide I and amide II at 1644 cm^{-1} and 1536 cm^{-1} in A']Z diminished, indicating the binding of AgNP to the zein molecules (Morgado, 1992; Wei, Sun, Qian, Ye, & Ma, 2009). Z']A-Ac (Figure 3.4e) was similar to Z]A-Ac (Figure 3.4c), that amide I & amide II were increased by adding AcOH, which also included new bands at 3287 cm^{-1} and 2919 cm^{-1}. Furthermore, compared with zein in silver composites (Figure 3.4b and 3.4c), no peak near 1297 cm^{-1} was found for A']Z (Figure 3.4d) and A']Z-Ac (Figure 3.4e) samples because the Ag$^+$-N coordination bond cannot be formed due to the lack of silver ion in these samples. In summary, FTIR results further confirmed the interaction between silver and zein molecules.

(4) Morphology and Elemental Analysis.

Figure 3.5 shows the morphology and elemental distribution of silver-zein composites. In the EDS images (right column), carbon was used as an indicator of zein, and was marked in green, whereas silver was in red. With EDS analysis, it was possible to clarify how silver and zein interacted position-wise with each other in micro scale. A clear view of core shell structure was captured in Figure 3.5a for sample Z]A, in which 1-2 micron zein particles were surrounded by Ag ions (EDS image). The connection between silver and protein again was attributed to the formation of Ag-N coordination bond. Figure 3.5b showed how silver incorporated into wrinkled zein film in the presence of AcOH. This morphological character was similar to previous findings that zein formed films in acidic environments (Mizutani,

Matsumura, Imamura, Nakanishi, & Mori, 2003). Therefore, the zein, as an isolated

core in neutral condition (Z]A), transformed into a continuous film during the drying

process and incorporate silver ions in it.
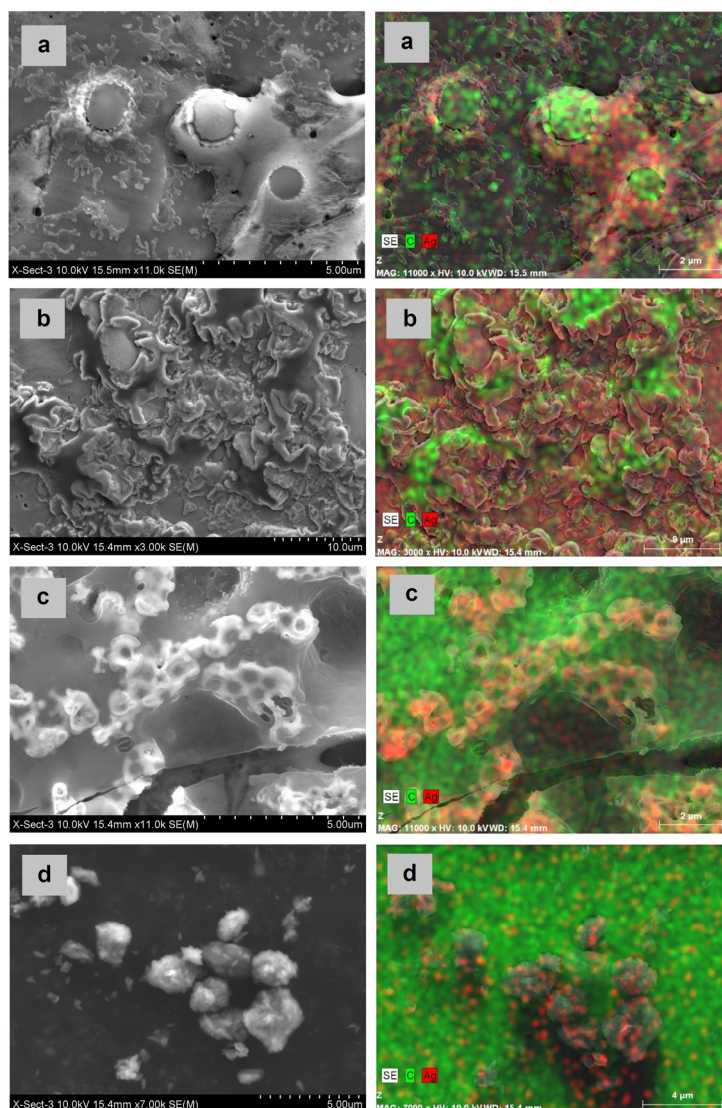
Figure 3.5 SEM (left column) and EDS (right column) images of silver zein
nanocomposites.
a. Z]A; b. Z]A-Ac; c. A]Z; d. A]Z-Ac.

In Figure 3.5c and 3.5d, reversed structures were captured when AgNP served

as core materials. It was found AgNP was imbedded into zein films. However, A']Z

and A']Z-Ac samples had different morphology for both AgNP and zein. A slight

increase in the size of AgNP was observed for A']Z-Ac, which could be ascribed to the presence of AcOH. AgNP reacted with AcOH and formed silver acetate, which was an unstable and photosensitive material that may result in bigger silver particles (Travan, et al., 2009). On the other hand, zein was also affected by AcOH, a smooth and uniform zein film formed in A']Z-Ac, which was expected based on previous studies (Mizutani, Matsumura, Imamura, Nakanishi, & Mori, 2003).

(5) Stability Assay.
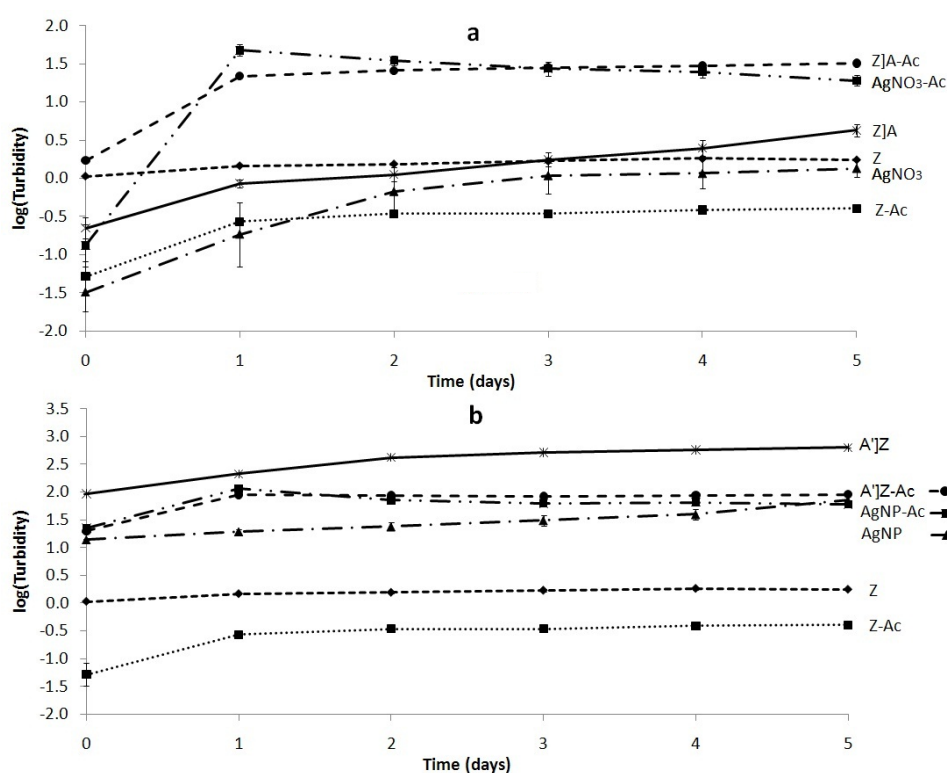
Figure 3.6 Turbidity change of silver zein composites and controls over 5 days
a. Z]A, Z]A-Ac, and controls (i.e. Z, Z-Ac, AgNO$_3$, and AgNO$_3$-Ac) ; b. A']Z, A']Z-Ac and controls (i.e. Z, Z-Ac, AgNP, and AgNP-Ac).

The stability of the sample solutions with different treatments was characterized by utilizing a turbidimeter. The change of turbidity over time was used as an indicator to evaluate the stability of the samples. The more increase in the

turbidity value, the less stable the sample was. Results were presented in Figure 3.6. In Figures 3.6a and 3.6b, both zein (Z) and zein in AcOH (Z-Ac) were included as controls for comparison purpose. Z solution had low turbidity and was stable over 5 days. Turbidity of Z-Ac was lowest among all samples and it increased in the first day, and remained stable for the rest 4 days. $AgNO_3$ (in Figure 3.6a) and AgNP (in Figure 3.6b) were also presented as controls in both neutral ($AgNO_3$ and AgNP) and acidic conditions ($AgNO_3$-Ac and AgNP-Ac). $AgNO_3$ was unstable in 70% aqueous ethanol solution that the log turbidity value continuously increased from -1.5 to 0 over five days. On the contrary, $AgNO_3$-Ac had high turbidity and increased dramatically in the first day and decreased slightly in the rest of 4 days, indicating the stabilizing effect of AcOH (in Figure 3.6a). AcOH also showed stabilizing effect on AgNP (in Figure 3.6b) that the turbidity of AgNP-Ac remained declining after the first day, whereas that of AgNP was steadily increasing tenfold (one log scale) over the five days.

In Figure 3.6a, zein in silver composites (Z]A and Z]A-Ac) were compared with different control samples. Among the samples and controls, Z]A-Ac and $AgNO_3$-Ac exhibited the greatest turbidity values, due to the reaction between silver and AcOH. The turbidity values of Z]A-Ac increased 10 folds from day 0 to day 1 and reached stable status throughout the rest of days (day 2 to day 5). Z]A, on the other hand, had clear and transparent solution with a relatively low turbidity value at day one, and turbidity increased gradually over time, which indicated continuous aggregations of silver-zein composites.

79

Figure 3.6b showed the stability results of two silver nanoparticles in zein samples (A']Z and A']Z-Ac) and four controls. Similar to turbidity of Z]A and Z]A-Ac, that of A']Z-Ac increased 5 folds in the first day and became stable in the rest of days, whereas A']Z structure was unstable that resulted in a constantly increased turbidity value.

As a conclusion, $AgNO_3$ and AgNP were not stable in solution, and zein had little effect on stabilizing them. However, AcOH acted as a stabilizer for $AgNO_3$, AgNP, as well as silver-zein composites. The stabilizing effect of AcOH may be attributed to the electrostatic repulsion, as silver-zein composites in acidic condition had relatively larger surface charges (shown in Figure 3.2).

3.4.2 Antimicrobial Activities.

Silver is a broad-spectrum antiseptic agent (J. S. Kim, et al., 2007). In previous studies, silver and AgNP were proven to be effective in controlling both Gram positive and Gram negative microorganisms (J. S. Kim, et al., 2007; Melaiye, et al., 2005; Sondi & Salopek-Sondi, 2004; Wright, Lam, & Burrell, 1998). In this study, the concentration of $AgNO_3$ and AgNP was chosen to be consistent to previous studies (J. S. Kim, et al., 2007; Melaiye, et al., 2005; Sondi & Salopek-Sondi, 2004; Wright, Lam, & Burrell, 1998). Therefore, the antimicrobial activities of silver-zein composites (i.e. Z]A, Z]A-Ac, A']Z, and A']Z-Ac) were evaluated by growth inhibition and bactericidal assays against bacteria of Gram positive - *E. coli* and Gram

negative - *S. aureus*. Results were compared with medium (control), zein and previous studied silver loaded antiseptics.

(1) Growth Inhibition Assay on Gel Media.
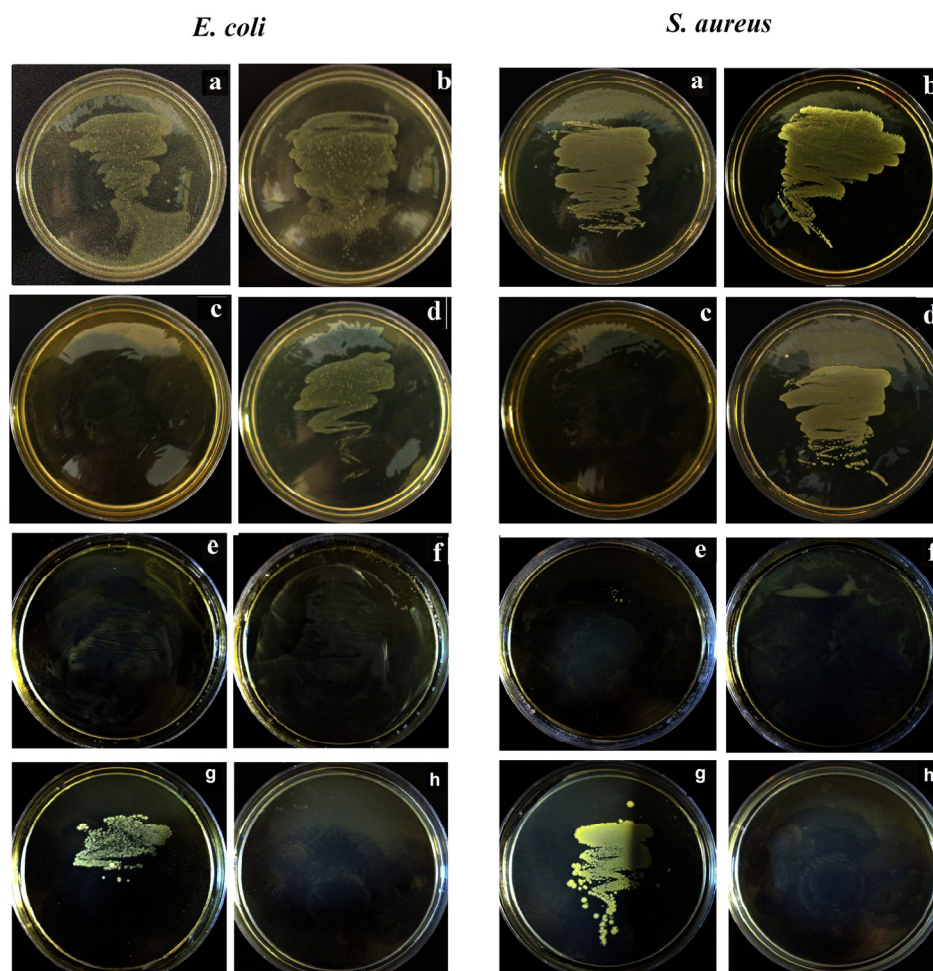
E. coli   S. aureus

Figure 3.7 Representative photographs for the bacterial activity against E. coli (left two columns) and S. aureus (right two columns)
a. TSA (control); b. Z; c. AgNO₃; d. AgNP; e. Z]A; f. Z]A-Ac; g. A']Z; h. A']Z-Ac. AgNO₃ (sample c) served as a control against zein in silver composites (sample e and f), while AgNP (sample d) were compared with AgNP in zein composites (sample g and h).

Figure 3.7 showed respectively the appearance of visible colonies of *E. coli* (left column) and *S. aureus* (right column) after agar coated with different samples were inoculated and incubated. Shown in Figure 3.7b, zein coated TSA plates had

81

similar pattern with original TSA plates (Figure 3.7a), suggesting that zein have no inhibition effect against either bacterial. AgNO$_3$ (Figure 3.7c) showed strong growth inhibition activities, as no colony pattern was observed. AgNP (Figure 3.7d) did not perform as well as AgNO$_3$ in the assay, which may be ascribed to the low concentration of AgNP (5.4×10^{-2} mg/ml) used throughout this study. Besides, AgNP did not perform well on TSA plate in comparison with previous studies using Luria–Bertani plate (Sondi & Salopek-Sondi, 2004), possibly because TSA provided a better surface for bacteria to grow on.

Zein in silver composites, i.e. Z]A (Figure 3.7e) and Z]A-Ac (Figure 3.7f) had dramatic inhibitory effects against both bacteria since there were not a single colony was observed on the corresponded *E. coli* and *S. aureus* agars. A']Z-Ac (Figure 3.7h) also showed a remarkable improvement comparing to original AgNP (Figure 3.7d), which could be attributed to the incorporated AcOH, which is a strong antimicrobial agent by providing an acidic environment. Another possible mechanism explaining these results was established by Stoimenov (Stoimenov, Klinger, Marchin, & Klabunde, 2002), Hamouda (Hamouda & Baker, 2000) and their co-workers that the strong growth inhibition efficacy was attributed to electrostatic interaction between negatively charged bacterial cells and positively charge antimicrobial materials (as shown in Figure 3.2a, 3.2b, and 3.2d). Only A']Z (Figure 3.7g) coating had slightly improvement in inhibitory effect comparing to AgNP, which was less effective in controlling bacterial growth on gel media than the other three silver zein composites. Although A']Z increased the surface charge of AgNP from -8.0 mv to -4.0 mv, it still

carried negative charges. The reduced electrostatic repulsion between A']Z and negatively charged bacterial cells could only slightly increase the efficacy of A']Z. Therefore, colony areas for both bacteria were successfully reduced, but not eliminated on respective agars. It can be concluded that by introducing AcOH, A']Z-Ac sample that had same concentration of AgNP and A']Z performed much better inhibitory effect against both bacteria. In summary, all four silver-zein composites had similar or better growth inhibition activities, comparing to $AgNO_3$ and AgNP controls. The results of growth inhibition of silver-zein composites were consistent to those of silver-chitosan composites (Travan, et al., 2009) against *E. coli* and *S. aureus*, suggesting that zein was capable of preserving or enhancing silver's antimicrobial activities by forming a silver-zein composite.

(2) Bactericidal efficacy in solution.

Table 3.2 Bacterial Level of Different Samples in LB Medium against E. coli.

Composite	Microorganism Concentration(CFU/ml)	Composite	Microorganism Concentration(CFU/ml)
Control	$1.01 \pm 0.11 \times 10^7$	Z	$1.06 \pm 0.22 \times 10^7$
$AgNO_3$	<1	AgNP	32.0 ± 2.50
Z]A	<1	A']Z	<1
Z]A-Ac	<1	A']Z-Ac	$9.67 \pm 0.58 \times 10^4$

Table 3.3 Bacterial Level of Different Samples in LB Medium against *S. aureus*.

Composite	Microorganism Concentration(CFU/ml)	Composite	Microorganism Concentration(CFU/ml)
Control	$1.53 \pm 0.07 \times 10^8$	Z	$1.10 \pm 0.50 \times 10^8$
$AgNO_3$	<1	AgNP	$2.32 \pm 0.46 \times 10^2$

Z]A	<1	A']Z	25.0 ± 1.25
Z]A-Ac	<1	A']Z-Ac	$2.90 \pm 0.26 \times 10^7$

Bacterial counts of control (LB medium) and sample solutions toward *E. coli* and *S. aureus* were presented in Table 3.2 and Table 3.3, respectively. Zein had similar bacterial count for *E. coli* or *S. aureus* comparing to the control, showing no effects in killing either bacteria. AgNP and $AgNO_3$ were also served as controls. $AgNO_3$ was found to have strong bactericidal efficacy by reducing microorganism concentrations in both two bacteria solutions down to less than 1 CFU/ml. However, similar to growth inhibition assay, AgNP had moderate efficiency in killing bacteria in solution, which was also discovered in previous studies (J. S. Kim, et al., 2007; Sondi & Salopek-Sondi, 2004), which was attributed to the decreased solubility or aggregation of AgNP in aqueous medium. For Z]A, and Z]A-Ac composites, bacterial counts decreased almost to zero from the initial bacteria concentration of 10^6 CFU/ml, indicating they were extremely effective in killing both bacteria. During the experiments, it was observed that these two composites were capable of forming emulsion, in which they had been sufficiently interacting with the microorganisms, and thus were able to kill the microorganisms. These results proved that zein and AcOH formulated in the zein in silver composites did not affect the bactericidal efficacies of traditional used $AgNO_3$.

The bactericidal efficacy of AgNP-loaded antiseptics (A']Z and A']Z-Ac) was inferior to that of Z]A and Z]A-Ac. They also exhibited different killing efficacies against *E. coli* and *S. aureus*. Although A']Z composite completely killed Gram

negative *E. coli*, it was slightly less effective against Gram positive *S. aureus*, evidenced by numerating *S. aureus* colonies shown in Table 3.3. However, it had better killing effect comparing to that of the control (AgNP) against both bacteria. This is expected due to the electrostatic interaction between AgNP and microbial cell, which was explained in the discussion of growth inhibition assay. A']Z-Ac, on the other hand, only reduced 100 fold of *E. coli* concentration, from 10^7 to 10^5 CFU/ml, whereas it showed even worse bactericidal effect against *S. aureus* by reducing less than 10 fold. These results were attributed to the decreased solubility of A']Z-Ac in aqueous-based LB medium, which dramatically decreased the contact chances between the composites and the bacteria, thus resulted in the inactivation of AgNP in water. The accumulation of AgNP in dead bacteria cells, proposed by Sondi, et al. in their study (Sondi & Salopek-Sondi, 2004), can be another reason, which may result in precipitation of AgNP and phase separation of A']Z-Ac and LB medium. Although AcOH by itself is a strong antimicrobial agent it did not show any bactericidal activity. There were three possible reasons: 1) the pH of dispersion of A']Z-Ac in LB medium (6.5 as measured) was larger than pKa of AcOH (3.5) so that hydrogen was dissociated, which made AcOH be in its inactivated form; 2) AcOH interacted strongly with the composite and did not get chance to release in the LB phase; 3) the total initial bacteria count in LB medium is 5×10^6 of bacteria, but there was only 1×10^6 of bacteria on TSA plat, so the 5 fold difference may also account for the odd behavior. Possibly, the insolubility, aggregation with dead cells, together with neutral pH level all contributed to the worst bactericidal scenario of the A']Z-Ac sample. In

brief, A']Z maintained the bactericidal efficacy of AgNP in LB medium, while A']Z-Ac significantly decreased its activity.

3.4.3 Hemocompatibility.

Good hemocompatibility refers to specific properties of a biomaterial that generates little or no adverse response of immune system when in contact with live tissue. It is highly related to this study since the proposed applications of silver-zein composites may require a good hemocompatibility if used as antiseptic agents or antimicrobial food packaging materials. Therefore, it was of great interest to evaluate the hemocompatibility of silver loaded antiseptics after it formed composites with zein. The hemocompatibility experiments were carried out on a QCM-D instrument followed a previously published protocol (Sellborn, Andersson, Hedlund, Andersson, Berglin, & Elwing, 2005). Four samples (i.e. Z]A, Z]A-Ac, A']Z. and A']Z-Ac) and five controls (i.e. human IgG, iSera, Z, AgNO$_3$ and AgNP) were tested as binding surfaces.
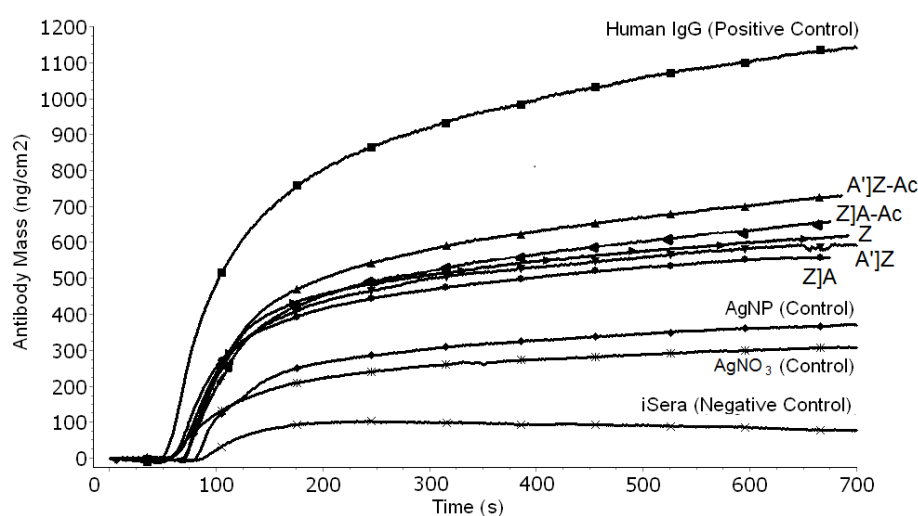
Figure 3.8 Hemocompatibilty of silver zein nanocomposite

Dynamic mass accumulation of antibody (C3c) on different samples. IgG and iSera acted as a positive and a negative control respectively; Z, $AgNO_3$, and AgNP were also applied as controls in comparison with silver-zein composites (i.g. Z]A, Z]A-Ac, A']Z, A']Z-Ac).

Figure 3.8 illustrated the difference of mass accumulation of antibody (C3c) among silver-zein composites and various controls. As described in materials and methods, human IgG and iSera were used respectively as a positive control and a negative control. As expected, they had highest and lowest mass changes respectively, and the values were consistent with what Sellborn and his collaborates' have found (Sellborn, Andersson, Hedlund, Andersson, Berglin, & Elwing, 2005). Mass accumulations of all other samples were in between those of the two controls. Silver and AgNP were unfavorable to the attachment of Sera so that only 200 and 300 ng/cm^2 of C3c adhered to the Sera surfaces. Mass of bonded C3c increased 2.5 and 3.0 times for Z]A and Z]A-Ac surfaces comparing to that of $AgNO_3$. While mass accumulation of C3c increased 1.7, and 2.0 times on Sera when A']Z and A']Z-Ac were used as testing surfaces, respectively, comparing to that of AgNP. These results strongly indicated that incorporating of zein into silver antimicrobial agent significantly improved its hemocompatibility. Besides, AcOH showed an improvement in the hemocompatibility of silver-zein composites, evidenced by increased mass accumulation of C3c on Z]A-Ac and A']Z-Ac. Among those, A']Z-Ac had the best hemocompatibility, which could be attributed to the low silver concentration and the presence of AcOH.

3.5 Conclusions.

Zein in silver and AgNP in zein composites at two pHs (i.e. pH=3.3 and pH=6.5) were prepared using two different preparation methods. Formation of silver-zein composites were evidenced by the results of zeta-potential, FTIR, morphology, and elemental analysis. AcOH was found to be an important ingredient in improving the formation, stability, antimicrobial activity and hemocompatibility of the silver-zein composites. Solubility property in water was discovered to be critical in deciding the bactericidal efficacy of silver-zein composites.

Among the four silver-zein composites, water soluble Z]A, Z]A-Ac and A']Z had similar or better antimicrobial activities comparing to those of AgNO$_3$ and AgNP, by showing strong growth inhibition and bactericidal activities against *E. coli* and *S. aureus*, in addition to the dramatically improved hemocompatibility. Therefore, they may provide an optimized option for clinic as wound care products, such as wound care patch and gel dressing. Contrarily, the water insoluble A']Z-Ac showed strong growth inhibition activity as dry coating, but trivial bactericidal effect in solution due to its reduced solubility in water. However, decreased solubility may have advantage to alleviate the skin discoloration by preventing release of silver from the composite matrix, and thus, reduce the risk of skin discoloration and immune response. Further study is necessary to prove A']Z-Ac's potential benefits in wound care products. Furthermore, the silver release profile and the cytotoxicity study of silver-zein composites are indispensible in future studies to comprehensively understand the novel antimicrobial agents.

3.6 Acknowledgement.

CHAPTER 4. Development of Silver/α-Lactalbumin Nanocomposites: A New Approach to Reduce Silver Toxicity.

4.1 Abstract.

The current use of silver is limited to certain medical applications, due to two major toxicity concerns: low hemocompatibility and silver release induced skin discoloration, both of which were attributed to the interaction between silver and blood cysteine. Therefore, in this study, silver/protein nanocomposites were prepared to address these challenges by usingα-lactalbumin (ALA), a high cysteine protein. The effect of cysteine redox states of ALA was evaluated on the physicochemical characteristics, and the nanocomposites were formed by Ag-S or Ag-N coordination bonds and electrostatic attractions. The optimum balance between antimicrobial efficacy and toxicity was achieved by treating freshly prepared silver and ALAred nanocomposite with UV radiation, which resulted in dramatic reduction in toxicity, and maintaining antimicrobial activity. We anticipated that these promising results may bring a great impact on broaden the clinical application of silver-based antimicrobial agents.

4.2 Introduction.

Silver-based antimicrobial agents are traditional antiseptics, with broad-spectrum antimicrobial activities against both Gram positive and Gram negative

microorganisms (de Azeredo, 2009; Jonas, Bloch, Zimmermann, Stadie, Gross, & Schad, 2007; R. Kumar & Munstedt, 2005; Panacek, et al., 2006; Romanov, Siu, Verkerk, Hopkinson, & Siu, 2010; Travan, et al., 2009; Wei, Sun, Qian, Ye, & Ma, 2009; Wright, Lam, & Burrell, 1998; B. Zhang, Y. Luo, & Q. Wang, 2010), and even multiresistant bacterial strain (Jonas, Bloch, Zimmermann, Stadie, Gross, & Schad, 2007; Wright, Lam, & Burrell, 1998). However, their current applications were still rigorously restricted to specific medical condition (e.g. sever burn wounds). This regulatory situation was attributed to two specific toxicity issues: acute silver-induced lethal immunological response due to its low hemocompatibility; and chronic skin discoloration (argyria) after long-term exposure and accumulation of released-silver from its matrix (Wright, Lam, & Burrell, 1998). In this study, a novel silver/protein nanocomposites were developed to address these two challenges.

In previous studies, improved hemocompatibility of silver was achieved by incorporated silver into natural polymers, i.e. polysaccharide and protein, through silver-amino coordination bond. The most studied polysaccharide was chitosan, because of its abundant amino groups. Various silver and silver compounds were incorporated into different forms of chitosan matrices (Travan, et al., 2009; Wei, Sun, Qian, Ye, & Ma, 2009). Polyamide and protein was another category of biopolymer that contained abundant amide groups, however, only a few studies were focused on the formation of silver-amide chelating complex (R. Kumar & Munstedt, 2005; Romanov, Siu, Verkerk, Hopkinson, & Siu, 2010; B. Zhang, Y. Luo, & Q. Wang, 2010). Although these studies found that biopolymer could improve the

hemocompatibility of silver and support mammalian cell growth, the release of silver content still remained an irresolvable problem (Travan, et al., 2009).

Jonas, et al. (2007) reported that the skin discoloration was generated following a pathway shown in Scheme-1.1. First, the released Ag^+ migrated into human body by binding to cysteine in blood vessels (Jonas, Bloch, Zimmermann, Stadie, Gross, & Schad, 2007). The accompanied silver deposition occurred at dermis cells, when the exposure to solar UV radiation irreversible converted Ag^+-cysteine complexes to silver sulfide, which caused skin discoloration (Jonas, Bloch, Zimmermann, Stadie, Gross, & Schad, 2007). Therefore, to prevent the skin discoloration, it would be critical to prevent the binding between silver and blood cysteine. Unfortunately, none of the previously studied polymer matrices had such silver retaining capabilities to compete with blood cysteine (Travan, et al., 2009), because the huge difference between two thermodynamic constants indicated that the interaction between Ag^+ and RS^- ($Ksp=6.0\times10^{-51}$) is much stronger than that of Ag^+ and RNH_2 ($Kd=6.0\times10^{-8}$) (Singh, Georget, Belton, & Barker, 2009). Contrarily, high cysteine protein maybe good competitors to blood cysteine in the ability to retain silver and prevent skin discoloration.

To address the two challenges, a hemocompatible high cysteine protein, α-lactalbumin (ALA), became a feasible solution. ALA accounts for 17.5% of whey protein, and consists of eight cysteine residues in the form of four intra-molecular disulfide bonds (R-S-S-R'). According to the Lewis acid-base theory (Carrado, 2000; Singh, Georget, Belton, & Barker, 2009), the affinity of silver to sulfur can vary

dramatically depending on the reduction-oxidation (redox) states of cysteine, Therefore, ALA was first modified with reduction and oxidation. Reduced ALA was denoted as ALAred, while oxidized ALA was obtained by further oxidation of ALAred and named as ALAox. Then, the physicochemical properties of the proteins and silver/protein nanocomposites were characterized, and the nanocomposites were further investigated for their toxicity (i.e. hemocompatibilities and silver retaining capabilities) and antimicrobial efficacy.

4.3   Experimental Section.

4.3.1 Materials and Chemicals.

ALA was isolated from whey protein isolate (obtained from Trueprotein, Oceanside, CA) using an established protocol (Alomirah & Alli, 2004). Gram positive *Staphylococcus aureus* (ATCC# 29213) and Gram negative *Escherichia coli* (ATCC# 53323) were purchased from ATCC (Manassas, VA), while all broth and agar were bought from Difco (Franklin Lakes, NJ). Pooled human plasma and human immunoglobulin G (IgG) were purchased from Innovate Research (Novi, Michigan), and rabbit antihuman C3c antibody was brought from Dako (Carpinteria, CA), while Veronal buffer (VBS and VBS++) were from Boston BioProducts (Ashland, MA). All other chemicals were purchased from Sigma-Aldrich (St. Louis, MO).

4.3.2 Sample Preparation.

(1) Modification of protein:

ALAred was prepared following a reduction method using Na_2SO_3. First, 2 mg/mL of protein aqueous solution was sufficiently mixed with 2 mg/mL of Na_2SO_3(Barone, Dangaran, & Schmidt, 2006). Then, the solution was water bathed at 40 °C for 1 hr, which was accompanied by a 24 hrs dialysis at 4 °C to remove Na_2SO_3 and Na_2SO_4. Thereafter, 30% H_2O_2 was added to 1 mg/mL ALAred at a volumetric ratio of 1:1 to produce ALAox. The reaction was controlled at 40 °C for 1 hr.

(2) Preparation of silver/protein nanocomposites:

1 mg/mL of protein solution (i.e. ALA, ALAred, or ALAox) was first dispersed in aqueous solution with 100 μg/mL of $AgNO_3$. After sufficient vortex, Ag-protein solution was water-bathed at 40 °C for 1 hr, and one hour of intensive ultraviolet (UV) radiation (15 Watt/m^2, λ=365nm) was applied to Ag/protein nanocomposites.

4.3.3 Characterization of Protein Modification and Formation of Ag-Protein Nanocomposites.

(1) Sodium Dodecyl Sulfate Polyacrylamide Gel Electrophoresis (SDS–PAGE):

SDS–PAGE (NuPAGE, Invitrogen, Carlsbad, CA, USA) was used to examine the change in molecular weight of the treated ALA samples. The sample was re-suspended in a solution of 20μl deionized water and 10μl lithium dodecyl sulfate (LDS) sample buffer. The mixtures were then heated at 70°C for 10 mins. The SDS–PAGE was carried on 4–12% (w/v) Bis–Tris Mini Gel stained with colloidal blue staining kit (SimplyBlue SafeStain).

(2) Zeta-Potential:

A laser Doppler velocimetry (Zetasizer Nano ZS90, Malvern, U.K.) was used to characterize the surface charge of different samples. During the experiment, samples were well mixed and filled in a fold capillary cuvette (Folded Capillary Cell - DTS1060, Malvern, U.K.). The whole cuvette was then mounted onto the chamber at 20 °C for measuring the mobility. For each sample, three replications were obtained and results were statistically analyzed.

(3) Fourier Transform Infrared Spectroscopy (FTIR):

A Jasco 4100 series FTIR with an attenuated total reflection (ATR) cell (Jasco Inc. Easton, MD) was used to monitor structural changes of different samples. The samples were first cast-dried on an aluminum tray for 24 hrs, and then mounted directly on the ATR. The spectra were acquired at 400-4000 cm^{-1} wavenumbers with a 4 cm^{-1} resolution. The spectra were further analyzed by 'Know It All' software (Version 8.1, Bio-Rad, CA, USA).

(4) Quantitative Chemical Analysis:

Chemical analysis was used to precisely identify the number of free sulfhydryl group (R-SH) on protein molecules (Petruccelli & Anon, 1995). According to Beveridge's study (Beveridg.T, Toma, & Nakai, 1974), fifty milligrams of the protein isolate was dissolved in 5 mL of 0.086 M Tris buffer, 0.09 M glycine, 0.004 M EDTA, and 8 M urea, pH 8. 40 mL of Ellman's reagent (4 mg/mL in methanol) was added to 1 mL aliquots, the absorbance being determined at 412 nm 15 mins later. In the case of the isolates containing Na_2SO_3, they were dissolved in water and then the

Na$_2$SO$_3$ was eliminated 24 hrs of dialysis at 4 °C. L-cysteine was used to generate standard curve.

(5) Scanning Electron Microscopy with energy-dispersive X-ray spectrometer (SEM/EDS):

A SEM/EDS (SU-70, Hitachi, Pleasanton, CA) was used to obtain morphology change and elemental analysis of different samples. The samples were first cast-dried on an aluminum tray, cut into small pieces and mounted on specimen stubs by conductive carbon tapes. The whole stub was coated with an thin layer of (<20 nm) conductive gold layer using a sputter-coater (Hummer XP, Anatech, CA).

4.3.4 In vitro Toxicity Assay

(1) Biomimic Silver Release Assay.

The Quartz Crystal Microbalance with dissipation (QCM-D, Q-Sense E1, Glen Burnie, MD) was used to measure real-time silver release. During the experiment, the quartz crystal was first saturated with DI water, and native ALA (1 mg/ml) or nanocomposite solutions (1 mg/ml protein and 100 μg/mL AgNO$_3$) was then pumped to the crystal surface, accompanied by 10 μg/mL L-cysteine solution used to mimic the blood in the Step II of silver release mechanism illustrated in the Scheme 1. All measurements were carried out at 37 °C under a flow rate of 22.5 μL/min precisely controlled by a peristaltic pump (ISMATEC, REGLO Analog MS-2/12, Glattbrugg, Switzerland). The frequency and dissipation changes were further convert to the mass changes of adhered sample layer by Q-Tool software.

(2) In vitro Hemocompatibility Assay.

In vitro hemocompatibility assay was also performed on QCM-D, referring to the procedures of a previously reported method by Sellborn et al (2003; 2005). Human immunoglobulin G (Human IgG) and $AgNO_3$ were considered as the positive control and the negative control respectively, which had the best and the worst hemocompatibility. During the experiment, the quartz crystal was first saturated with DI water, and sample in Veronal Buffer Solution (VBS) was then pumped to the crystal surface, accompanied by Sera solution. Last, the antihuman C3c antibody was introduced to quantify the attached Sera, which was propositional to hemocompatibility. All measurements were carried out at 37 °C under a flow rate of 22.5 μL/min precisely controlled by a peristaltic pump.

4.3.5 *in vitro* Antimicrobial Assay.

(1) Minimal Inhibitory Concentration Assay (MIC):

The MIC assay of $AgNO_3$ and silver/protein nanocomposites in Lysogeny broth (LB) medium was referred to Andrews' method (2001) against *E. coli* and *S. aureus*. Modified microdilution method was adopted to prepare a series of nanocomposites concentration, as 10, 20, 40, 80, 160, 320, and 640 μg/mL in LB medium. The MIC endpoint was determined by the lowest concentration at which no viable bacterial growth was detected in spectrophotometer at 550 nm after 24 hrs incubation at 37 ^{o}C.

(2) Minimal Bactericidal Concentration Assay (MBC):

The MBC assay was an adjunct to the MIC assay (Andrews, 2001; Ogrady, Murphy, & Pearson, 1983). For each concentration without visible bacteria growth,

100 μL aliquot of the broth was incubated in LB broth for 24 hrs at 37 °C. The subcultured broth was further examined by spreading solution on TSA plate for another 24 hrs at 37 °C. Visible bacterial growth indicated that the concentration was bacteriostatic instead of bactericidal. The MBC endpoint was determined at the lowest concentration with no visible colony appeared.

4.3.6 Statistical Analysis.

Experiments, that is, zeta potential and chemical analysis, were conducted in triplicate with data reported as mean ± standard error. Experimental statistics were performed using a SAS software (version 9.2, SAS Institute Inc., Cary, NC).

4.4   Results and Discussion.

4.4.1   Modification of Protein.

Table 4.1 Quantitative analysis of R-SH group and zeta potential of native and modified ALA.

	Theoretical numbers of R-SH group	Measured numbers of R-SH group	Zeta potential (mV)
ALA	0	0.16 ± 0.11	-5.52 ± 0.14
ALAred	4	3.25 ± 0.27	-15.00 ± 1.01
ALAox	0	0	-26.50 ± 2.30

Quantitative chemical analysis and surface charge were conducted to characterize redox state of native and modified ALA samples and results were displayed in Table 4.1. In each native ALA molecule, no free R-SH group was detected and the protein molecule carried slightly negative charge under neutral pH condition as its isoelectric point is 4.5 (Vanaman, Brew, & Hill, 1970). After reduction, the four R-S-S-R' bonds were changed to four R-SH groups and four sulfonic acid residues ($R-SO_3^-$):
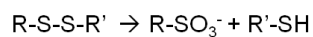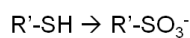
Quantitative analysis indicated that ~80% of theoretical free R-SH groups presented in each ALAred molecule. The zeta potential of ALAred dropped 9.48 mV from that of ALA supporting the structural change of non-charged R-S-S-R' bonds to negatively charged R-SO$_3^-$ groups. The oxidation further converted the free R-SH groups into R-SO$_3^-$ groups, which made up eight R-SO$_3^-$ groups in each ALAox molecule theoretically. Quantitatively analysis suggested that all R-SH groups were oxidized completely, and therefore the surface charge dropped an additional 15 mV.
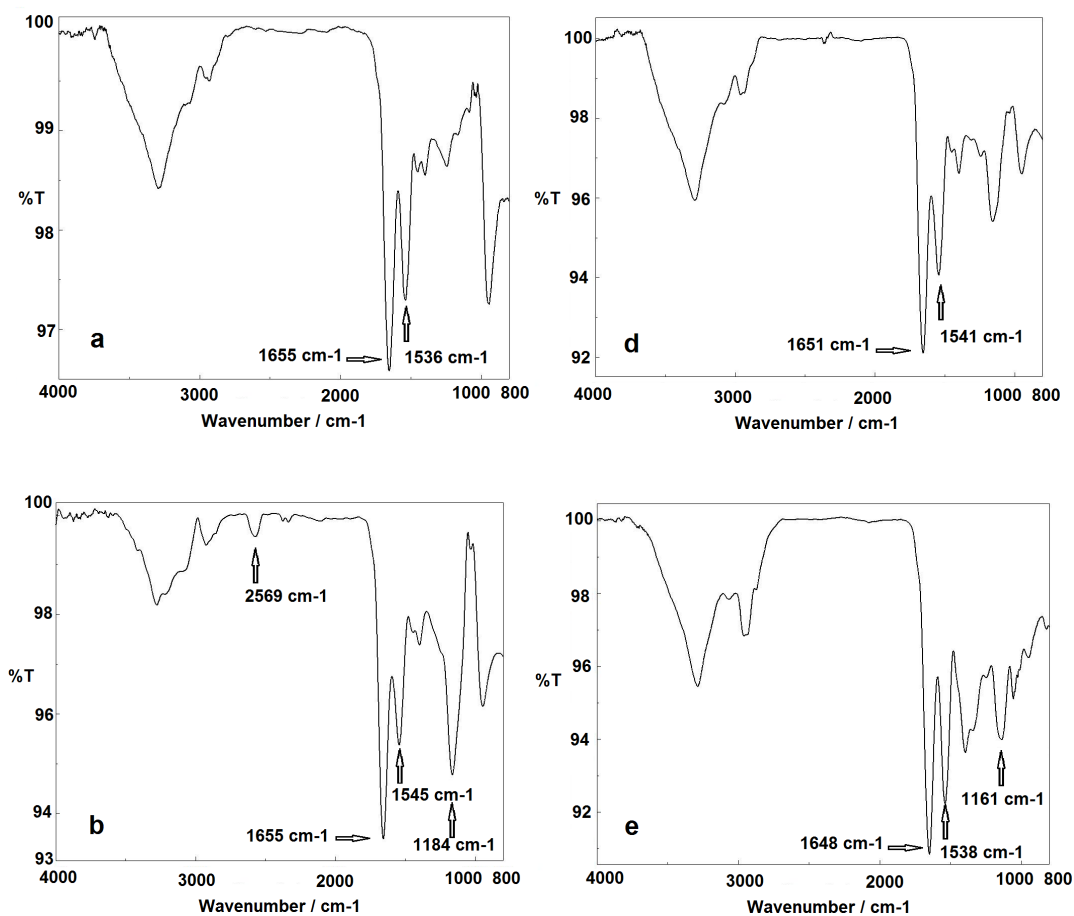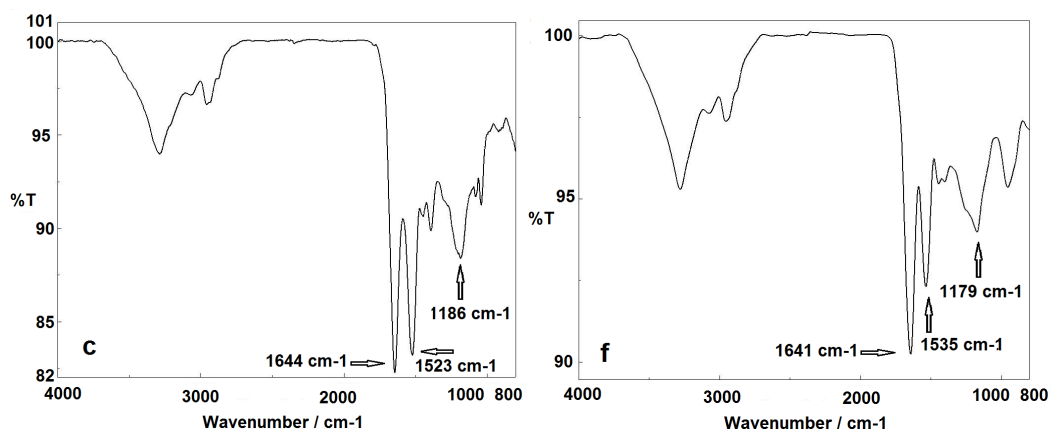
Figure 4.1 FTIR spectra of ALA and silver/protein nanocomposites native ALA (a), ALAred (b) and ALAox (c); FTIR spectra of silver/protein nanocomposites: ALA-Ag (d), ALAred-Ag (e) and ALAox-Ag (f).

Additionally, FTIR was used to identify the changes of functional groups and FTIR spectra of samples were presented in Fig 4.1. The native ALA (Fig 4.1a) showed high similarity with previously reported ALA spectra (Dzwolak, Kato, Shimizu, & Taniguchi, 2001). Two significant signal changes were observed in the spectrum of ALAred (Fig 4.1b). The new absorption peak at 2569 cm^{-1} can be used to indicate RS-H stretching, and the intensified peak at 1184 cm^{-1} acted as an index of S=O stretching of R-SO3$^-$ group (Stuart, 2004). In ALAox spectrum (Fig 4.1c), whereas, only the peak of R-SO$_3^-$ was observed at 1186 cm^{-1}, no RS-H peak around 2650-2550 cm^{-1} was found. The changes of FTIR bands provided additional evidence to modification of protein.

4.4.2 Formation of ALA-silver nanocomposites.

The formation of nanocomposites between proteins and Ag was supported by following analysis, chemical analysis by FTIR (Figure 4.1), surface charges by Zeta-Potential (Table 4.2), molecular weight determination by SDS-PAGE (Fig 4.2), and morphology examination by SEM (Fig 4.3).

Table 4.2 Zeta potential of silver/protein nanocomposites.

	ALA-Ag	ALAred-Ag	ALAox-Ag
Zeta potential (mV)	-3.45 ± 1.00	-9.50 ± 0.56	-7.63 ± 0.09
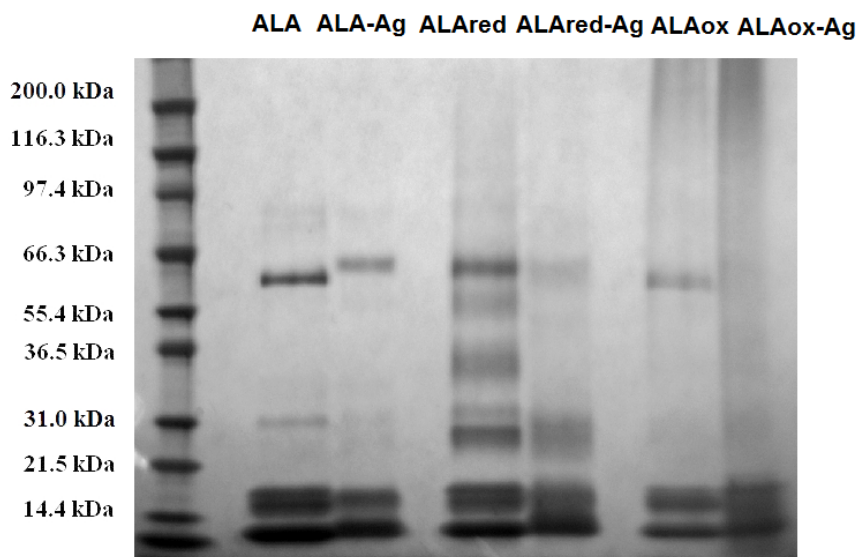
Figure 4.2 SDS-PAGE of native ALA, modified ALA and silver/protein nanocomposites.

The results of FTIR spectra (Fig 4.1) proved the formation of silver/protein nanocomposites. In ALA-Ag spectrum (Fig 4.1d), no significant change was found, so the formation of silver/protein nanocomposites did not affect the secondary and tertiary structures of protein. A significant difference was found between ALAred and ALAred-Ag samples. The specific absorption of RS-H stretching at 2650-2550 cm^{-1} presented in the ALAred sample (Fig 4.1b) was no longer observable in the ALAred-Ag sample (Fig 4.1e) indicating that the silver ions were bound to R-SH groups through Ag-S coordination bonds. The changed ratio of peak intensity of the Amide I to the Amide II in Figure 4.1e,f compared to Figure 4.1b,c, possibly indicating that there is co-ordination of Ag with the amide bonds of the protein backbone.
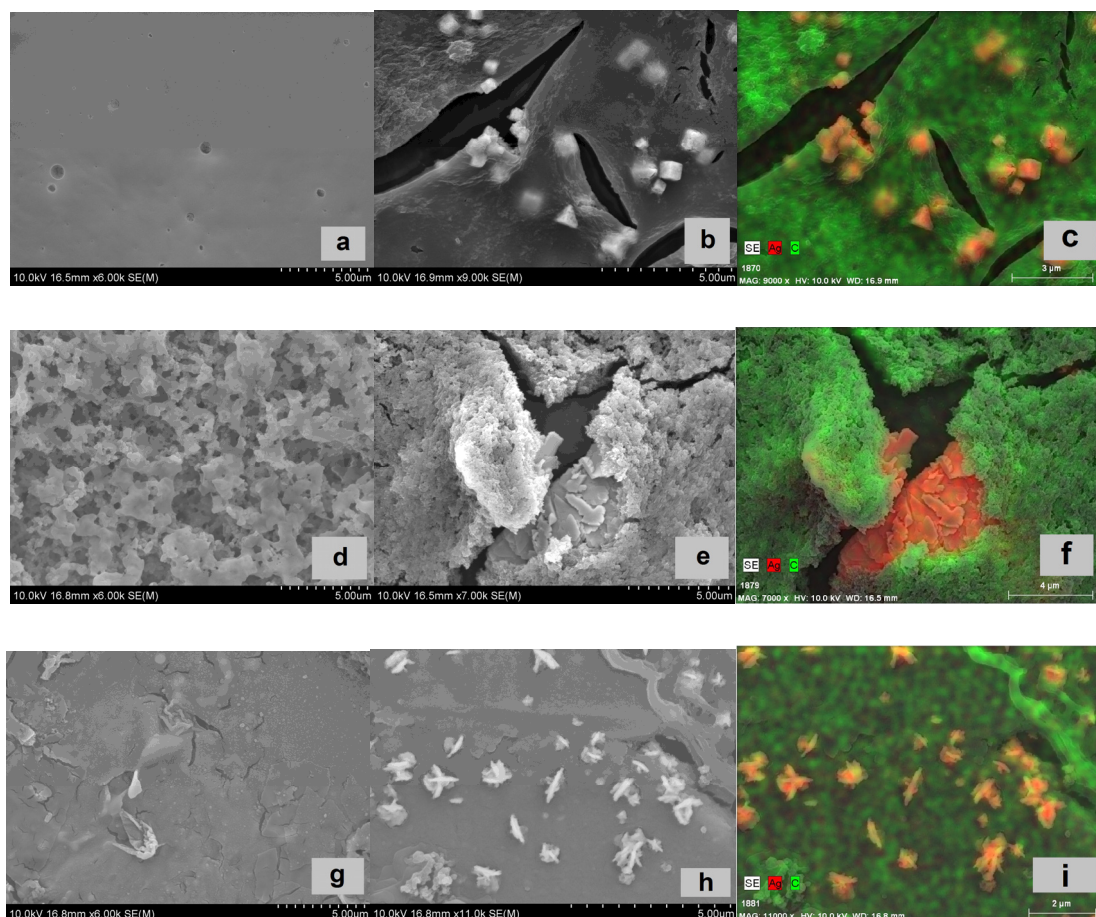
Figure 4.3 SEM images of native ALA, modified ALA and silver/protein nanocomposites.

native ALA (a), ALA-Ag nanocomposite (b), ALAred (d), ALAred-Ag nanocomposite (e), ALAox (g), and ALAox-Ag nanocomposite (h); EDS analysis of elemental distribution of Ag (red) and C (green) in ALA-Ag (c), ALAred-Ag (f) and ALAox-Ag (i) nanocomposites.

Furthermore, comparing to the zeta potential of the native and modified ALA (Table 4.1), Table 4.2 showed that the surface charges of proteins increased after the silver/protein nanocomposites were formed, which was attributed to the association between positively charged Ag^+ and negatively charged ALA in all three forms. Therefore, the formation of silver/protein nanocomposites was confirmed to be a result of both coordination bond formation and electrostatic attractions.

The molecular weight (MW) change of different treatments was shown in Fig 2. For the native ALA, the intensive band was around 14-15 kDa, and a small fraction (10%) of bovine serum albumin (BSA) at 66 kDa was also observed, which was in accordance with MW reported by other literatures (Alomirah & Alli, 2004). The formation of ALA-Ag nanocomposite did not affect the MW profile, which may indicate that no intermolecular coordination bond was formed between different ALA molecules. In ALAred, however, although significant change was observed in BSA fraction, the band at 14-15 KDa was not affected by reduction, since all R-S-S-R' bonds in ALA molecules were intramolecular in nature (Wei, Sun, Qian, Ye, & Ma, 2009). The band of ALAred-Ag was similar to that of the ALAred at 14-15 kDa on molecular weight profile. For the ALAox sample, the band distribution was similar to that of native ALA, and ALAox-Ag composites remained its molecular weight at 14-15 kDa, thus the addition of $AgNO_3$ did not affect the molecular weight distribution for ALAox.

In addition, SEM/EDS was further applied to study the morphology of cast-dried ALA samples with or without modification and their silver nanocomposites. The representative images were presented in Fig 4.3. For ALA-Ag nanocomposite, cubic and tetrahedral silver crystals around 500 nm were observed either on the surface of or embedded in the smooth ALA protein matrices (Fig 4.3a-c). The morphology of ALAred (Fig 4.3d) indicated the deformation of the protein film due to the reductive reaction. When forming the ALAred-Ag nanocomposite (Fig 4.3e,f), stacks of silver nanoplatelets, around 50 nm thick, were found fully incorporated in the ALAred film.

A relatively rough film structure was observed for the ALAox sample (Fig 4.3g). For the ALAox-Ag sample (Fig 4.3h,i), needle like silver crystals with diameter of 50 nm and length of 500 nm were observed on the surface of the ALAox matrices, which showed high structural similarity with the ALA-Ag nanocomposite. Therefore, the SEM/EDS results further verified the formation of silver/protein nanocomposites.

4.4.3   Toxicity.

During the preparation of silver/protein nanocomposites, the UV radiation process was found essential for the ALAred-Ag nanocomposite, however not for the ALA-Ag and ALAox-Ag samples. A mechanism study (J. Y. Kim, Lee, Cho, & Yoon, 2008) discovered that intensive UV radiation at 365 nm could convert Ag-S coordination bonds to R-S-S-R' bonds and silver element through a monoradical scavenging process (shown in Scheme 3). Therefore, the effects of UV treatment on the toxicity changes of ALAred-Ag nanocomposite were evaluated by adding an UV-free sample. The UV-free nanocomposite was denoted as ALAred-Ag-Fresh, and the UV-treated nanocomposite was still kept as ALAred-Ag.

(1) Silver Release:

In the silver release assay, the ALA acted as a control (Fig 4.4). Its small mass increase indicated the adsorption of cysteine onto the ALA protein layer, probably through hydrogen bond. The other four nanocomposites (i.e. ALA-Ag, ALAred-Ag, ALAred-Ag-Fresh, and ALAox-Ag) displayed an overall mass decrease. The mass change of each sample was a combined result of cysteine adsorption and silver content release from the nanocomposite matrix.
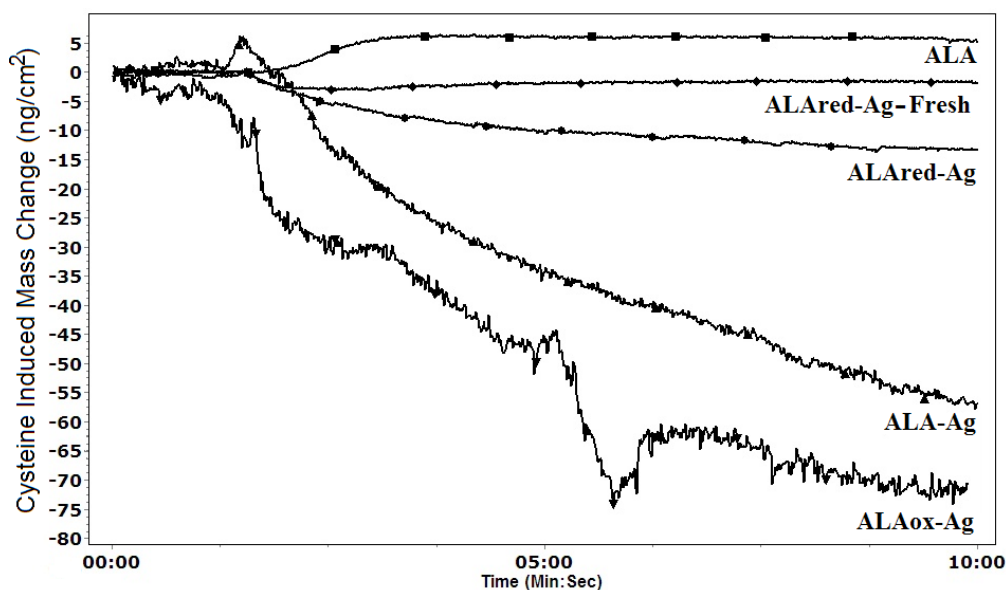
Figure 4.4 Monitored mass changes corresponding to the release of silver from silver/protein

After 10 mins of erosion by cysteine, approximately 55 ng/cm^2 of silver content were washed off from the ALA-Ag layer into the mobile phase, which indicated a relatively low silver retaining capability. In native ALA, most of silver molecules were bound to the nitrogen atoms on the amide groups of native ALA. Besides, as shown in Fig 4.3c, silver crystals were exposed to the environments on the surface of ALA-Ag composite, which enabled the sufficient interaction between silver filler and cysteine solution.

Both ALAred-Ag and ALAred-Ag-Fresh showed substantial improvement in retaining silver in their matrixes. ALAred-Ag-Fresh had the minimum silver release (<5 ng/cm^2) comparing to the other nanocomposites, indicating strong bindings between ALAred and silver without UV treatment. After being treated with UV radiation, its ability of retaining silver reduced slightly (about 10 ng/cm^2), because the UV treated nanocomposite (ALAred-Ag) converted most of free R-SH groups to

R-S-S-R' bonds through monoradical scavenging process as illustrated in Scheme 3. These results indicated that incorporating ALAred could become a solution for improving silver retaining property and further reduce the risk of Argyria.

For ALAox-Ag nanocomposite, about 75 ng/cm^2 of silver content was washed off by the cysteine solution after 10 mins. As all R-SH groups were converted to R-SO$_3$$^-$ in the ALAox sample, the protein lost its silver retaining capability. Therefore, a considerable amount of silver was released into the mobile phase of the cysteine solution. In summary, silver/protein nanocomposites with diverse redox states resulted in different silver release profiles. The difference was attributed to the functional groups in each sample, which were responsible for binding with silver and structural integrity of protein samples.

(2) In vitro Hemocompatibility:

The result of hemocompatibility assay was displayed in Fig 4.5, in which more sera attachment indicates that the binding surface is more hemocompatible. Fig 4.5 illustrated different mass accumulations of antibodies (C3c) for tested surfaces. As expected, IgG had the highest mass change, while AgNO$_3$ had the lowest one, and the obtained values were consistent with those reported in the previous studies (Sellborn, Andersson, Fant, Gretzer, & Elwing, 2003; B. Zhang, Y. Luo, & Q. Wang, 2010). ALA preformed outstanding hemocompatibility, which was very close to the positive control (IgG). Besides, all silver/protein nanocomposites exhibited a substantial antibody mass increase by 2.5 – 4 times when comparing to that of AgNO$_3$. The results suggested that these nanocomposites could significantly improve the

hemocompatibility of silver by incorporating a hemocompatible protein into the silver-based antiseptics.

Figure 4.5 Hemocompatibility of silver/protein nanocomposites
Dynamic mass accumulation of antibody (C3c) on different samples.

4.4.3   *in vitro* Antimicrobial property (MIC/MBC).

In previous sections, the silver/protein nanocomposites were proven to have low toxicity with better hemocompatibility and silver retaining properties. In order to evaluate their antimicrobial efficacy, MIC and MBC values were compared with AgNO$_3$ and results were displayed in Table-4.3. The result showed that ALA-Ag, ALAred-Ag and ALAred-Ag-Fresh samples suffered a depression of the antimicrobial efficacy of silver (Wright, Lam, & Burrell, 1998). However, the increase of MIC and MBC values were insignificant comparing to the commercial concentration of silver-based antiseptics at 50 mg/mL (Wright, Lam, & Burrell,

1998). This slight defect can be explained by several mechanism studies, both of which also involved the binding of silver to either N atom in DNA and RNA (Arakawa, Neault, & Tajmir-Riahi, 2001) or the cysteine residues on membrane transport protein (J. Y. Kim, Lee, Cho, & Yoon, 2008) through Ag-N and Ag-S coordination bonds. Therefore, this result was in consistent with silver release study that less silver was able to be released from these nanocomposite coatings and thereby less interaction with bacteria were expected.

Table 4.3 MIC/MBC values of ALA-silver nanocomposites against *E. Coli* and *S. aureus* in LB medium.

	E. Coli		*S. aureus*	
	MIC (µg/mL)	MBC (µg/mL)	MIC (µg/mL)	MBC (µg/mL)
AgNO$_3$	10	10	20	20
ALA-Ag	80	80	160	160
ALAred-Ag	80	160	160	160
ALAred-Ag-Fresh	160		160	
ALAox-Ag	10	10	40	40

However, UV radiation could have reverse effects on silver/ALAred nanocomposites (i.e. ALAred-Ag-Fresh and ALAred-Ag), thus, improved the antimicrobial efficacy and slightly reduced the silver retaining property and hemocompatibility. As shown in Figure 4.6, intensive UV treatment could convert silver-sulfhydryl complex to R-S-S-R' bond and silver elementary substance, therefore reactivate the antimicrobial efficacy of the nanocomposite. Therefore, it was concluded that the presence of silver elementary substance provided the major

contribution to the antimicrobial activity of ALAred-Ag nanocomposite. The MIC/MBC values of the ALAox-Ag nanocomposites kept the same as those of AgNO$_3$ for *E. Coli* but twice as much for *S. aureus* indicating that ALAox had negligible influence of antimicrobial property of silver. Similar studies have been investigated on the antimicrobial efficacy of amino-based biopolymer composites in silver-based antiseptics, including chitosan (Travan, et al., 2009; Wei, Sun, Qian, Ye, & Ma, 2009) and zein(B. Zhang, Y. Luo, & Q. Wang, 2010).

Formation of monoradical triggered by UV radiation:

$$R\text{-}S\text{-}Ag \rightarrow R\text{-}S \cdot + Ag^0$$

Formation of disulfide bond by monoradical scavenging:

$$R\text{-}S \cdot + R'\text{-}S \cdot \rightarrow R\text{-}S\text{-}S\text{-}R'$$
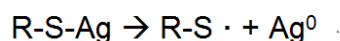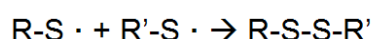
Figure 4.6 Proposed mechanism of monoradical scavenging process of Ag-S coordination bond under intensive UV radiation

4.5   Conclusion.

High cysteine protein, ALA, was modified by reduction or oxidation to produce different cysteine redox states. Silver/protein nanocomposites were formed by both electrostatic attraction and coordination bonds. The cysteine redox states of protein samples had significant impact on the structural and function changes of the silver/protein composites. Overall, ALAred-Ag had the best overall functionalities with low toxicity and high antimicrobial efficacy. Although more research is needed to further prove the therapeutic potential of the novel material, such as *in vivo* animal study of cell liability and antimicrobial efficacy, etc. The promising results from this study would provide an alternative synthetic route of silver-based antimicrobial agent

to substantially reduce the toxicity level of silver and maintains its antimicrobial efficacy.

4.6 Acknowledgement.

CHAPTER 5. Development of Highly-Ordered Nanofillers in Zein Nanocomposites for Improved Tensile and Barrier Properties.

5.1   Abstract

It has been a long-lasting challenge to prepare highly-ordered biopolymer nanocomposites to optimize or tune the desired mechanical and barrier properties of the nanocomposite film. In this study, we developed a simple and cost-effective method to synthesize highly-ordered zein nanocomposites. The method involved the synthesis of magnetic iron oxides (Fe_3O_4) nanofiller and the preparation of highly-ordered structure by *in situ* nanofillers reorientation under external magnetic field. The successful preparation of Fe_3O_4 magnetic nanoplatelets together with exfoliated and highly-ordered zein resin nanocomposites was confirmed by Scanning Electron Microscopy, X-Ray Diffraction, and Vibrating Sample Magnetometer. As a result, in comparison with zein resin film, the exfoliated zein nanocomposites (Fe-Zein) showed dramatic improvement on mechanical and barrier properties. The tensile strength, elongation and Young's modulus of Fe-Zein were increased by 218%, 48% and 264% respectively, while the water vapor and oxygen permeability decreased by 68% and 29%. More importantly, the highly-ordered zein nanocomposites (Fe-Zein-Mag) showed additional improvement on the mechanical and gas barrier properties. Comparing to Fe-Zein, the tensile strength and elongation of Fe-Zein-Mag were increased by 10% and 48% respectively, and a 30% decrease in Young's Modulus was observed, indicating the Fe-Zein-Mag film was more elastic. Besides, the water vapor and oxygen permeability of Fe-Zein-Mag were also decreased by additional 48% and 17 % respectively.

5.2   Introduction

Over the past decades, because of polymers' functionality, light weight, inexpensiveness and ease of processing, they have replaced conventional metal or ceramic materials in ubiquitous packaging areas, where they provide physical, chemical, and biological protection from the environment and prolong product display. However, along with the arisen concern of environmental sustainability, the global sustainable packaging industry is growing much faster than traditional packaging industry (Platt, 2006). Biopolymers are considered as potential replacements for these conventional plastic packaging materials due to their superior biodegradability in nature. Although previous studies have shown their enormous versatility (de Azeredo, 2009; Kriegel, Arrechi, Kit, McClements, & Weiss, 2008; P. Kumar, Sandeep, Alavi, & Truong, 2011; Marsh & Bugusu, 2007; Mukherjee & Kao, 2011; Rhim, 2007), a limiting property of biopolymers using as packaging materials is their intrinsic mechanical property and barrier property to gaseous substances, such as water vapor, oxygen (O_2), carbon dioxide (CO_2), and organic volatile molecules (P. Kumar, Sandeep, Alavi, & Truong, 2011; Rhim, 2007). These physical nature of the biopolymer materials resulted in great interests in developing new materials with enhanced vapor and/or gas barrier property by new preparation strategies and carrying out fundamental research to assist the understanding of the relationship between polymer structure and its properties.

The most frequently adopted strategies to improve mechanical and gas barrier properties are the use of polymer composites, the coating of high barrier materials, and the use of multilayered films consisting a layer of high barrier film (Ray &

Okamoto, 2003). Polymer composite is the most frequently adopted method, which is to add suitable filler into polymers matrix to enhance polymer's properties. Composites typically consist of a polymer matrix as the continuous phase and fillers as the discontinuous phase (Bharadwaj, 2001; de Azeredo, 2009; Ray & Bousmina, 2005; Ray & Okamoto, 2003; B. Zhang, Y. Luo, & Q. Wang, 2011). Nanocomposites are an innovative alternative to traditional technologies for improving polymer properties using nano-scale materials as fillers. Nanocomposites usually exhibit increased mechanical strength, improved gas/vapor barrier properties, and improved heat resistance compared to conventional polymers and polymer composites (Ray & Bousmina, 2005; Ray & Okamoto, 2003; Sorrentino, Gorrasi, & Vittoria, 2007). When dispersed into polymer matrix, nanofillers create a maze-like structure that creates a tortuous path to gaseous molecules, greatly slowing their permeation rates (Bharadwaj, 2001). Besides, traditional composite structures usually require a large quantities of filler (~60 % vol), but the demand of nanofillers has been dramatically reduced in nanocomposites to <2 % vol (Ray & Bousmina, 2005).
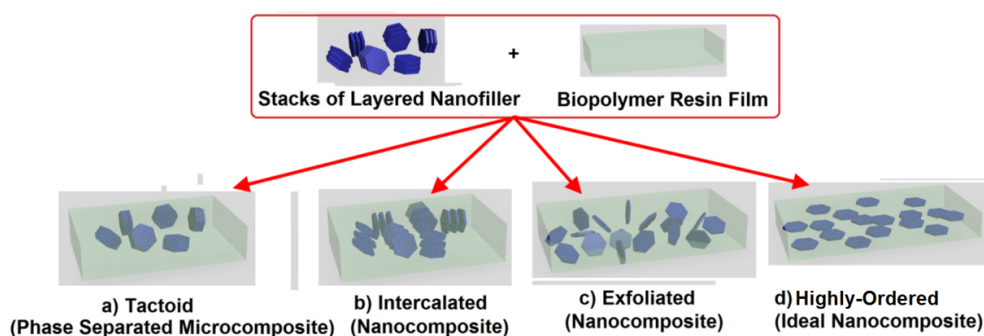

Figure 5.1 The four types of nanocomposite structures.

Plenty of studies have endeavored in the development of nanocomposites materials (Alexandre & Dubois, 2000; Ray & Bousmina, 2005; Ray & Okamoto,

2003; Rhim, 2007; Sorrentino, Gorrasi, & Vittoria, 2007). Currently, three types of polymer-nanofiller structures have been well-achieved and studied: a) tactoid, (b) intercalated and (c) exfoliated (Carrado, 2000; Ray & Okamoto, 2003) (Figure 5.1). Tactoid structures can be found in traditional composites (Alexandre & Dubois, 2000). Intercalated structures have moderate expansion of the clay interlayer, in which polymer chains can penetrate the basal spacing of filler, but the stacked shape of the nanoplatelets remains. In exfoliated structures, clay clusters lose their layered structure and are well dispersed as individual nanoplatelet within the continuous polymer phase (Ray & Bousmina, 2005; Ray & Okamoto, 2003). The current 'ideal' structures for biopolymer nanocomposites are intercalated and exfoliated structures (Alexandre & Dubois, 2000; Bharadwaj, 2001; de Azeredo, 2009; Ray & Bousmina, 2005; Ray & Okamoto, 2003). However, Bharadwaj has theoretically proved that highly-ordered nanofillers (shown in Figure 1d, picture of highly-ordered) could substantially increase the gas barrier properties by up to three fold comparing to the intercalated or exfoliated structure following the Equation 1.1 (Bharadwaj, 2001), where L and W are the length and width of the nanofiller, respectively. S stands for the arrangement of the nanofiller (Equation 1.2), and can be calculated by substituting difference angular value (θ) into Equation 1.2. In a complete disordered filler arrangement, S is assigned as 0. In an ideal orthogonal arrangement, θ is 90°, so S equals to -1/2. In an ideal planar arrangement, where nanofillers are incorporated parallel to the nanocomposite interface, θ is to 0° and S equals to 1. Although the exfoliated structure is consisted of well-distributed nanofillers in biopolymer matrices,

the randomly orientated nanofillers cannot provide the optimized functionalities, including mechanical properties, gas permeability, electronic, and catalytic properties etc. Therefore, a highly-ordered structure should be characterized as the nanofillers are incorporated in polymer matrices in the way of both sufficient distribution and identical orientation. Recently, plenty of studies have pointed out the significance of synthesizing truly highly-ordered nanocomposites (Alexandre & Dubois, 2000; Bharadwaj, 2001; de Azeredo, 2009; Ray & Bousmina, 2005; Ray & Okamoto, 2003; Rhim, 2007; Sorrentino, Gorrasi, & Vittoria, 2007). More importantly, highly-ordered nanocomposites has shown promising capabilities of improving matrix film's mechanical property and gas permeability, which were two critical characteristics to biopolymer-based packaging materials (Bharadwaj, 2001; Salvetat, et al., 1999; Wong, Sheehan, & Lieber, 1997).

Currently, several methods have been established in the formation of highly-ordered nanocomposites, including dip-pen nanolithography (Gao, et al., 2010), and layer-by-layer deposition (Tian, Park, Cheng, Liang, Zhang, & Wang, 2009). Gao et al. established a pulse laser deposition method that incorporated layers of $CoFe_2O_4$ nanoarray in a continuous $Pb(Zn, Ti)O_3$ alloys, and the as-prepared nanocomposite exhibited strong piezoelectric signals and magnetoelectric coupling (Gao, et al., 2010). Tian and his colleagues developed a method adopting electrostatic interaction (Svagan, Åkesson, Cárdenas, Bulut, Knudsen, Risbo, et al., 2012; Tian, Park, Cheng, Liang, Zhang, & Wang, 2009). The highly-ordered structure was obtained by layer-by-layer deposition of positively charged poly(ethylamine) and single wall carbon nanotube

functionalized with negatively charged sodium dodecylbenzenesulfonate. Although these two methods could form highly-ordered structures of nanocomposite coating, their feasibility in sustainable packaging application is questionable due to the complexity of the fabrication techniques and impracticability in the scaled-up production of free standing films. Therefore, to establish a low-cost and fast production of highly-ordered biopolymer nanocomposites, a hydrothermal synthetic route to hexagonal magnetic nanoplatelets has been developed in this study and the formed nanofillers have been characterized as well. Moreover, the highly-ordered nanofillers through in situ reorientation have been produced by external magnet. The mechanical and gas barrier properties of the zein film with or without adding nanofillers have been examined.

Zein was selected as the model biopolymer for its potential application as a structural packaging material (Lai & Padua, 1997, 1998; Lai, Padua, & Wei, 1997). Zein is a storage protein in corn kernel, and is a major co-product from bio-fuel industry. Its film-forming property has been recognized for decades (Lai & Padua, 1997; Lawton, 2002; B. C. Zhang, Y. C. Luo, & Q. Wang, 2010, 2011). However, the poor mechanical and gas barrier properties fundamentally restricted the application of zein and many other biopolymers as well. Scientists have endeavored in developing various methods to improve the properties of zein film, including plasticizer (e.g. polyols, mono-, di-, or oligosaccharides, lipids, and lipid derivatives) (Lai & Padua, 1997, 1998; Lai, Padua, & Wei, 1997; Lawton, 2002; B. C. Zhang, Y. C. Luo, & Q. Wang, 2011), coating of moisture barrier (e.g. tung oil and linseed oil), as well as

lamination (Rakotonirainy & Padua, 2001; Q. Wang & Padua, 2005). Recent studies investigated a nanocomposite method that dramatic improved the properties of zein resin film using silica-based nanofillers (Luecha, Sozer, & Kokini, 2010). However, it is still largely unachieved to form highly-ordered nanocomposites, which would maximize the effects of nanofillers incorporation. Therefore, the objective of this study, is to develop a simple and cost-effective method to synthesize highly-ordered biopolymer nanocomposites to improve tensile and gas barrier properties, using magnetic nanofillers, and zein is selected as the model biopolymer matrix.

5.3 Materials and Methods.

5.3.1 Materials.

Zein was obtained from MP Biomedicals (Solon, OH, USA), with a minimum of 90% of protein. Oleic Acid ($C_{18:1}$) was purchased from Fisher Scientific (Fairlawn, NJ, USA). Hydrazine monohydrate ($N_2H_4 \cdot H_2O$), ferrous sulfate, 7-hydrage ($FeSO_4 \cdot 7H_2O$), sodium hydroxide (NaOH), calcium sulfate anhydrous ($CaSO_4$), magnesium nitrate ($Mg(NO_3)_2$) were purchased from Alfa Aesar (Ward Hill, MA, USA).

5.3.2 Preparation of iron oxide/magnetite (Fe_3O_4) nanoplatelet filler.

Hexagonal Fe_3O_4 nanoplatelet was prepared following Wang's method with some modification (J. Wang, Chen, Zeng, & Hou, 2004). N_2 degassed water was used for the preparation of 0.1 M $FeSO_4 \cdot 7H_2O$ aqueous solution. 15 mL of Fe^{2+} solution was added into Teflon-lined stainless autoclave (Acid Digestion Bomb 4749, Parr

Instrument Company, Moline, IL, USA). 5 mL of sufficiently mixed $N_2H_4 \cdot H_2O$ aqueous solution (50% v/v) with 0.6 g of NaOH was drop-wisely added into the Teflon liner under vigorous stir. N_2 was continuously passed through the solvent to prevent Fe^{2+} oxidation. The autoclave was then placed in an oven at 130^oC for 6 hrs for reaction. After cooled to room temperature, the products were washed three times with water and ethanol, and finally dried by nitrogen evaporator (N-EVAP 111, Organomation Associates Inc., Berlin, MA, USA) at 25^oC for 3 hrs.

5.3.3 Preparation of Fe_3O_4 loaded zein resin film.

Zein resin was first prepared by dissolving granular zein in 70% ethanol aqueous solution (16% w/v). Oleic acid was weighed separately at a ratio of 1 g/g of zein, and homogenized at 10,000 rpm for 2 mins with 2% by weight of as-prepared Fe_3O_4 nanofiller to ensure the filler is well-distributed and protected by oleic acid using a homogenizer (VDI 25, VWR, West Chester, PA, USA). The mixture was then added slowly into heated zein solution at 75^oC and stirred vigorously for 15 mins. Thereafter, the above emulsion was poured into an ice water bath (0^oC) to obtain the zein-based resin. After kneading, zein films were prepared by stretching the dough over the circular rims of petri dish. Films were air-dried for 24 hrs under room condition. After drying, film stacks of 3 ply were laminated (fusion type) at 120 ^oC for 5 mins under a commercial hot-roller (Apache AL-13P) to produce the final specimen with exfoliated filler structure (Fe-Zein) for further characterization. Besides, zein-oliec acid resin films without the addition of Fe_3O_4 nanofiller were prepared as the control, which was denoted as 'Zein'.

5.3.4   Formation of highly-ordered Fe₃O₄ nanofiller in zein resin.

highly-ordered Fe_3O_4 nanofiller in zein resin should be both well-distributed and highly-aligned. To obtain this structure, the as-prepared exfoliated Fe-Zein films were further treated with 4 kG external magnetic field under a permanent magnet (Neodymium Magnets N52, Protage, IN, USA) over a hotplate at $120^{\circ}C$ for 20 mins. The final highly-ordered films (Fe-Zein-Mag) were then cooled to room temperature before the removal of magnet.

5.3.5   Scanning Electron Microscopy (SEM).

The morphology and orientation of nanofillers were examined by a SEM (SU-70, Hitachi, Pleasanton, CA, USA). First, the Fe_3O_4 nanofiller and resin films samples were mounted on a specimen stub by conductive carbon tape, and then the stub was coated with a layer of conductive gold particle (~20 nm) with a sputter-coater (Hummer XP, Anatech, CA, USA). Representative SEM images were then depicted and analyzed in the following section.

5.3.6   X-Ray Diffraction (XRD).

XRD was used to characterize the chemical composition of the nanofiller and the nanofiller orientation inside zein resin films. Nanofiller powder and resin films were attached to specimen stubs by a flat double-sided tape. Powder diffraction was measured using Bruker D8 Advance powder diffractometer operated in Bragg-Brentano mode (theta-theta geometry), equipped with CuKa sealed tube (wavelength 1.54178 A), Ni beta-filter and position sensitive LynxEye detector. After measurement, phase identification was performed using The International Center for Diffraction Data (ICDD) powder diffraction database.

5.3.7   Vibrating Sample Magnetometer (VSM).

The magnetic property of as-prepared Fe_3O_4 nanofiller and nanocomposite film were investigated by VSM (Lakeshore 7400, Westerville, OH, USA). The powdered Fe_3O_4 nanofiller (10mg) was filled inside a Kel-F sample holder cup, while nanocomposites films ($10\times10\times0.76$mm) were attached to a Kel-F thin film bottom sample tail during the measurement. The field intensity was scanned from 5 kG to -5 kG. The homogeneity and anisotropy of the nanofillers were determined by combining in-plane (IP) and out-of-plane (OOP) hysteresis loops. All experiments were performed at 20°C.

5.3.8   Tensile property.

The tensile property, including tensile strength, elongation and Young's modulus were measured using a texture analyzer (TA.XT plus, Stable Micro System, Surrey, UK). The tensile tests were performed according to an ASTM Standard Method D638-10 (Rakotonirainy & Padua, 2001; Q. Wang & Padua, 2005). Film thickness was measured with a graduation micrometer (General Tools, New York City, NY, USA). Zein film specimens were first cut into dumbbell-shape of Type I dimension, and then were preconditioned at 23°C and 53% RH (saturated $Mg(NO_3)_2$) for 48 hrs. The texture analyzer was set to an initial grip of 115 mm and an extension rate of 5 mm/min. Five replicates were measured for each treatment.

5.3.9   Water-vapor permeability.

The water-vapor permeability of zein resin films were measured gravimetrically, according to an ASTM Standard Method E96/E96M-10 (Rakotonirainy & Padua, 2001; Q. Wang & Padua, 2005). Test cells had an exposure area of 10 cm^2 (PO-2300,

BYK, Columbia, MD, USA). CaSO$_4$ anhydrous was used to maintain 0% relative humidity (RH) inside the cells. Saturated solutions of Mg(NO$_3$)$_2$ and deionized water were placed in sorbostats to maintain 53% and 100% RH at 25°C, respectively. Weight gains were plotted versus time, and a steady state was assumed as a straight line fitted six points of the plot. Three replicates were measured for each treatment.

5.3.10 Oxygen gas permeability.

The O$_2$ permeability was measured using a non-invasive oxygen analysis system (Oxy-Sense 101, Dallas, TX, USA) according to an ASTM Standard Method F2714-08 and F2622-08e1 (Rakotonirainy & Padua, 2001; Q. Wang & Padua, 2005). The stainless-steel test cell had an exposure area of 10 cm^2, and the OXYDOT oxygen sensor (Oxysense, Dallas, TX, USA) was attached to the window at the bottom of the test cell. After carefully seal the test cell to avoid film wrinkle, pure nitrogen gas was prefilled at the bottom chamber of the test cell prior to the experiment. Then, the test cell was stored at 20°C and 36% humidity in dark until the equilibrium condition was established.

5.3.11 Statistical Analysis.

The data of tensile and gas barrier properties were reported as mean ± standard error, and the experimental statistics were performed using the SAS software with $\alpha=0.05$ (Version 9.2, SAS Institute Inc., Cary, NC, USA).

5.4   Resuls and Discussion

5.4.1   Synthesis of magnetic nanoplatelet nanofillers.

Figure 5.2 Characterization of Fe3O4 nanofiller
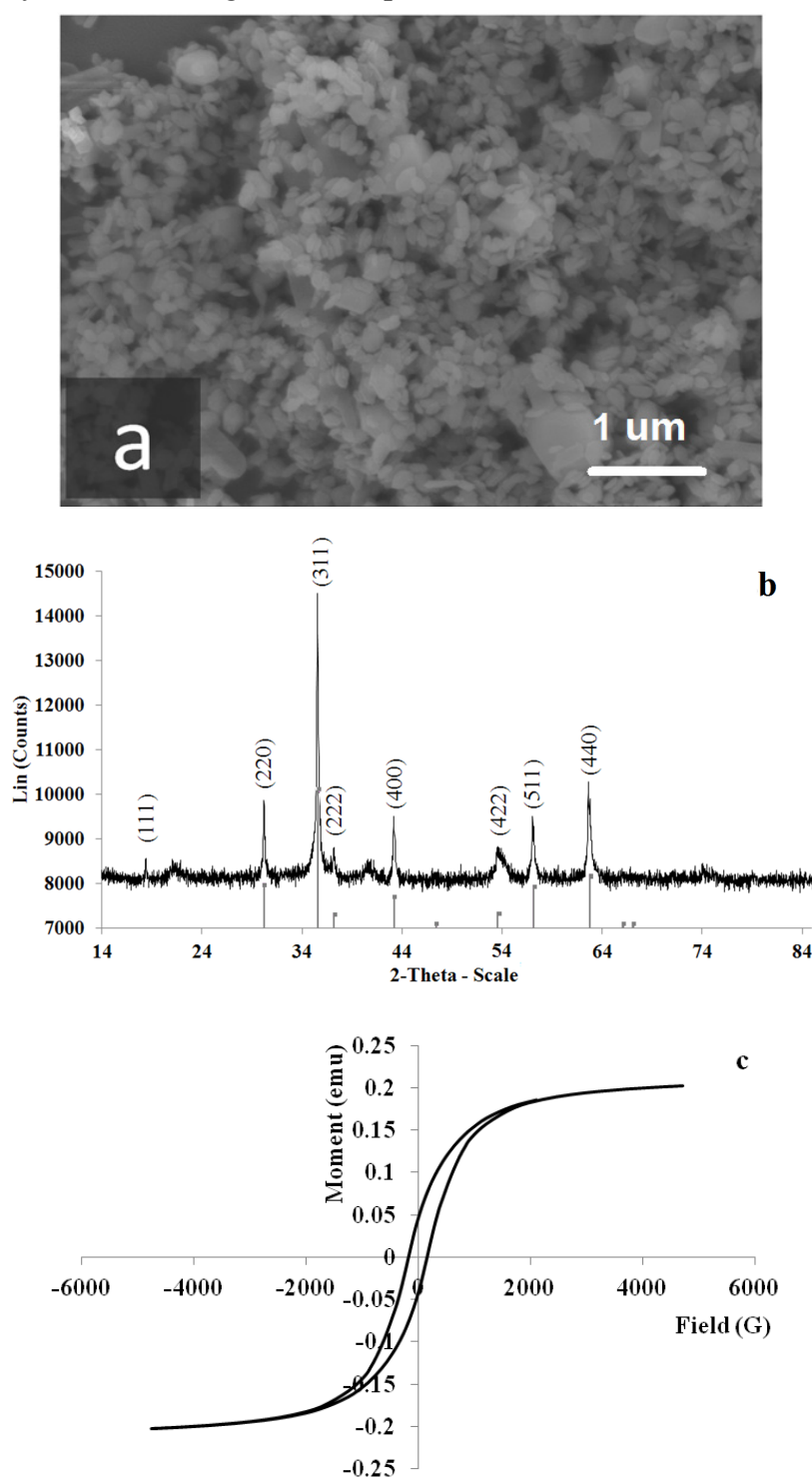(a) SEM image of the nanofiller showing its hexagonal nanocrystal shape; (b) XRD spectrum of the nanofiller and the peaks standard Fe3O4 in ICDD database; (c) Hysteresis loop of the nanofiller determined by VSM.

In this study, Fe_3O_4 hexagonal nanoplatelets were synthesized by the hydrothermal

method and the representative SEM image was shown in Figure 5.2a. The nanofiller

should be specifically prepared to achieve both high aspect ratio and magnetic property. According to Bharadwaj's theoretical model, the high aspect ratio (e.g. nanoplatelet) is critical to provide better gas barrier and mechanical support (Bharadwaj, 2001). As characterized by SEM, the nanofillers showed a shape of hexagonal plate, which had high aspect ratio and the size of individual platelet was around 200 nm × 20 nm (long diagonal × height). Besides, the chemical composition and magnetic property of the nanofiller were determined using XRD and VSM and results were presented in the Figures 5.2b and 5.2c, respectively. The XRD spectrum showed a perfect match over a standard Fe_3O_4 spectrum in ICDD database. The strongest signal peak of plane (311) reflection would be used to identify the presence of Fe_3O_4 nanofiller in the following characterization of nanocomposites. The magnetic property of the filler was also confirmed by the VSM. The thin loop indicated that the Fe_3O_4 nanoplatelet had small coercive force and soft ferromagnetic property (Figure 5.2c). Similar results have been reported for the other Fe_3O_4-based nanomaterials in various shapes (Tan, Zhuang, Peng, & Li, 2008).
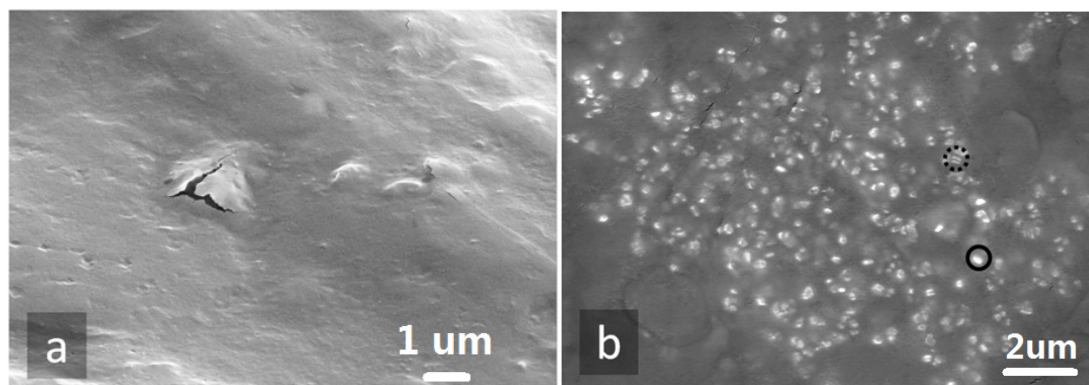
5.4.2   Formation of exfoliated nanocomposites.

Figure 5.3 SEM image of zein and nanocomposite
(a) zein resin film (Zein); (b) exfoliated nanocomposite (Fe-Zein).

123
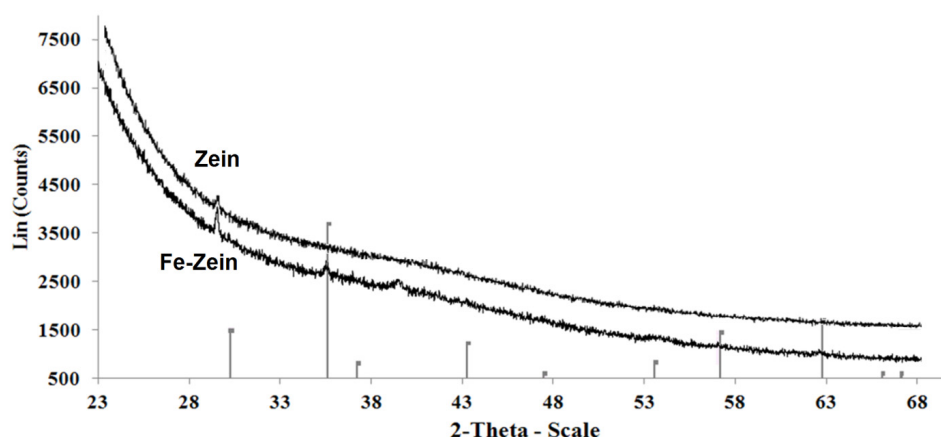
Figure 5.4 XRD spectra of zein resin film (Zein) and exfoliated nanocomposites (Fe-Zein).

In previous studies, it was found that only intercalated and exfoliated nanocomposites could significantly improve the mechanical and gas barrier properties of packaging materials because of the sufficient distribution of nanofillers in the packaging matrix. The tactoid structures were found to be a physical blend of two components due to the poor compatibility between filler and matrix materials (Alexandre & Dubois, 2000; Carrado, 2000; Ray & Bousmina, 2005; Ray & Okamoto, 2003).The shearing forces with high energy (i.e. homogenization process) were applied in this study to enable the sufficient separation of nanoplatelets, among which the primary interplanar interaction was strong magnetic forces rather than weak hydrogen bond and hydrophobic-hydrophobic attraction. Dispersion of nanoplatelets into the polymer matrix is affected by mismatches between the hydrophobic/hydrophilic character of both filler and the biopolymer matrices (Ray & Bousmina, 2005; Ray & Okamoto, 2003). In this study, zein was hydrophobic (Lai & Padua, 1997), and nanofillers (Fe$_3$O$_4$) were hydrophilic. Therefore, in order to prepare exfoliated nanocomposite (Fe-Zein), the surfaces of Fe$_3$O$_4$ nanofillers were modified

with a surface active component that was amphiphilic oleic acid molecules to improve the hydrophobicity and the compatibility with zein matrices. Consequently, an exfoliated nanocomposite was successfully obtained. The formed exfoliated structure was examined by SEM (Figure 5.3b), which showed the magnetic nanofillers were well-distributed and incorporated into the flat zein resin film in a random orientation. Both perpendicular (dashed circle in Figure 5.3b) and parallel (solid circle in Figure 5.3b) orientation of nanofillers to the planar surface were found in the resin film. XRD spectrum further confirmed the successful incorporation of Fe_3O_4 nanofillers by showing a typical plane (311) reflection of a Fe_3O_4 crystal, comparing to the control of zein resin film (Figure 5.4). Besides, the proposed incorporation of magnetic nanofiller in polymer film has also been confirmed by VSM result (Figure 5.5). The hysteresis loops of the IP and OOP scan of the exfoliated nanocomposites showed similar shape. Besides, Fe-Zein-IP and Fe-Zein-OOP showed similar residue flux densities value (Y-axis intercept) around 0.0005 emu. These results indicated that the magnetic nanofillers in exfoliated nanocomposites were well-distributed and randomly orientated. According to the Stoner-Wohlfarth model, an anisotropic material should behave differently in responding to various directions of external magnetic fields (Wouters, Lebedev, Van Tendeloo, Yamada, Sato, Vanacken, et al., 2011). Since the IP and OOP loops in Fe-Zein sample overlapped with each other, the magnetic nanofillers in Fe-Zein were randomly oriented, indicating that a typical exfoliated structure was formed. Therefore, the results of SEM image, XRD spectrum and VSM hysteresis loops proved the successful formation of exfoliated Fe-Zein

nanocomposites filled with well-distributed and randomly oriented Fe_3O_4 nanoplatelets.

Figure 5.5 Hysteresis loops of exfoliated nanocomposites (Fe-Zein) in in-plane (solid loop) and out-of-plane (dashed loop) directions.

5.4.3 Formation of highly-ordered nanocomposites.
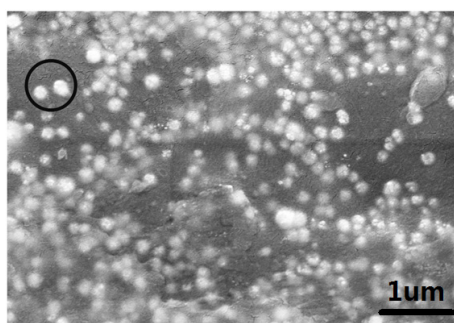
Figure 5.6 SEM image of highly-ordered nanocomposites (Fe-Zein-Mag).

The highly-ordered nanocomposite (Fe-Zein-Mag) was obtained from heat and magnetic-treated exfoliated nanocomposite (Fe-Zein). The nanofillers in Fe-Zein-Mag should have property of both exfoliated structure and highly aligned in orientation. As shown in Figure 5.6, fillers were mostly embedded in one direction, parallel to the resin film (solid circle in the figure), which was very similar to the schematic top view of highly-ordered nanocomposite (Figure 5.1, picture of highly-ordered). The typical

peak of Fe_3O_4 crystal in XRD spectrum was identified from zein resin background

(Figure 5.7a) for Fe-Zein-Mag sample. Besides, a close comparison of the signal of

plane (311) reflection between Fe-Zein and Fe-Zein-Mag further provided supporting

information (Figure 5.7b) to filler orientation. The peak shown in Fe-Zein-Mag

spectrum was narrower and sharper than the one in Fe-Zein spectrum, which indicated

that the Fe_3O_4 filler was more uniformly oriented in the Fe-Zein-Mag sample, and

some anisotropic structures may present (Tomov, 2005). The magnetic property of

Fe-Zein-Mg (Figure 5.8) obtained from VSM was different from that of Fe-Zein

(Figure 5.5). An increase of residue flux density was observed in Fe-Zein-Mag-OOP

to over 0.00065 emu from 0.0005 emu in Fe-Zein-OOP, while the value in

Fe-Zein-Mag-IP decreased to 0.0004 emu. It was reported that the magnetic dipole of

nanoplatelet was perpendicular to the Fe_3O_4 nanocrystal plane (Foss, Proksch,

Dahlberg, Moskowitz, & Walsh, 1996), so that the increase in OOP direction and the

decrease in IP direction indicated that a majority of nanofillers were parallel to the

film with their magnetic dipoles perpendicular to the film plane, which was in

agreement of SEM results. The relationship between nano-magnetite orientation and

the magnetic property was also confirmed by previous studies that the shapes of OOP

and IP loops were significantly different in an anisotropic material (Wouters, et al.,

2011). All together, the SEM, XRD and VSM results confirmed the effects of external

magnetic field on the structure inside nanocomposites. The rearrangement of

highly-ordered nanofillers was achieved by applying an in-situ external magnet.
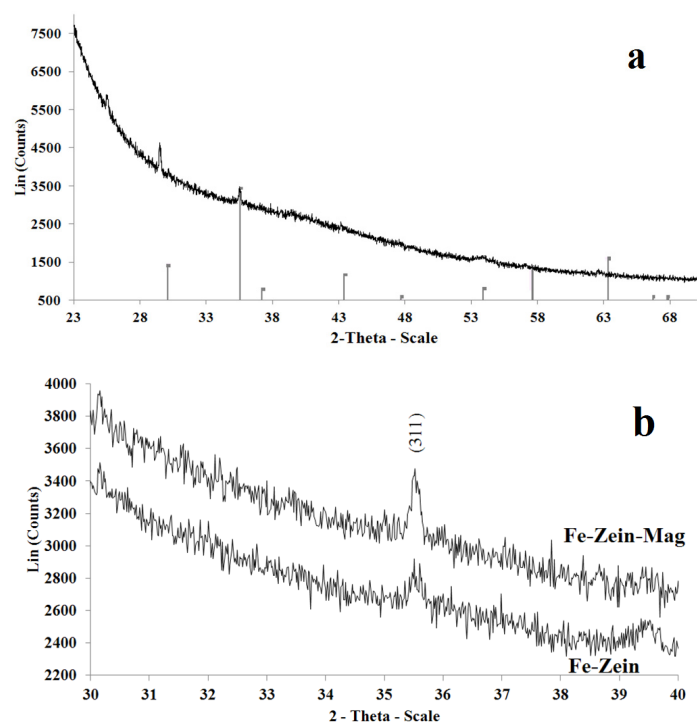
Figure 5.7 XRD spectra of highly-ordered nanocomposites
(a) highly-ordered nanocomposites (Fe-Zein-Mag); (b) comparison of plane (311)
reflection of Fe_3O_4 nanofiller in exfoliated nanocomposites (Fe-Zein) and
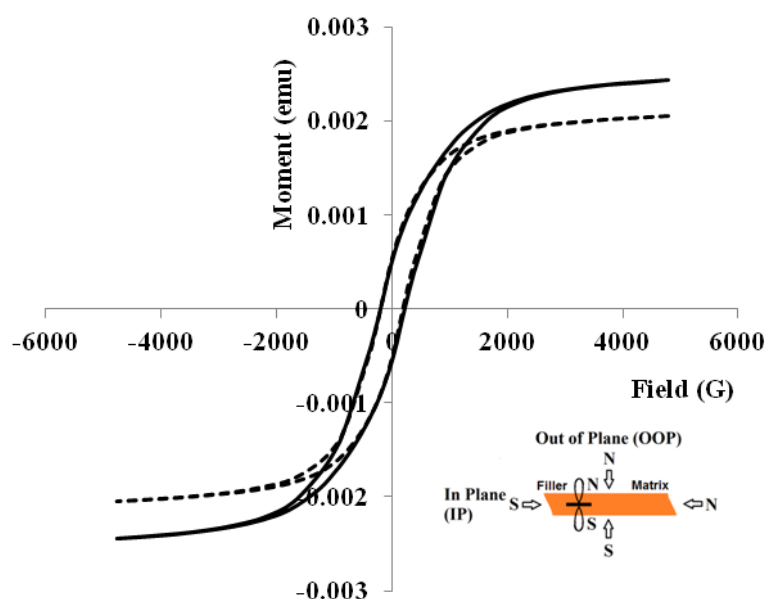highly-ordered nanocomposites (Fe-Zein-Mag).
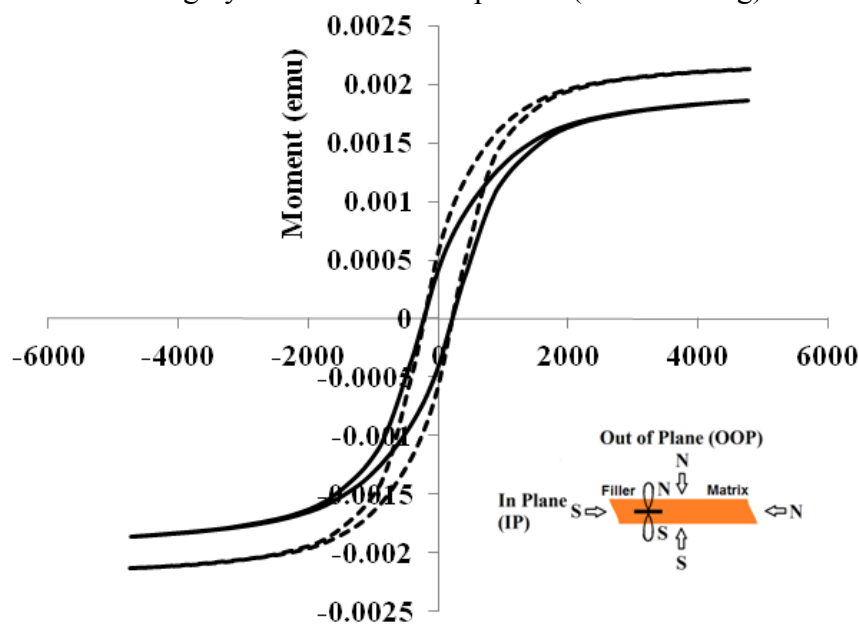
Figure 5.8 Hysteresis loops of highly-ordered nanocomposite (Fe-Zein-Mag) in
in-plane (solid loop) and out-of-plane (dashed loop) directions.

5.4.4   Tensile property.

Table 5.1 Thickness and tensile properties of zein-based nanocomposites.

Sample Name	Thickness	Tensile	Elongation at	Young's

	$(10^{-4}m)$	Strength (MPa)	Break (%)	Modulus (MPa)
Zein	7.95±1.17 b	2.11±0.35 b	24.05±4.73 c	94.50±35.79 c
Fe-Zein	5.69±0.33 c	6.71±0.95 a	35.67±1.67 b	344.57±14.76 a
Fe-Zein-Mag	12.78±0.84 a	7.39±0.36 a	52.67±7.67 a	239.78±10.24 b

* Means with same letter are not significantly different (P>0.05).

The tensile properties, including tensile strength, elongation, and Young's modulus, were measured for treatments of zein films (Zein), zein films with exfoliated nanocomposites (Fe-Zein), and highly-ordered nanocomposite (Fe-Zein-Mag) and results were reported in Table 5.1. The zein resin film was selected as a control. However, the mechanical property of the control zein film obtained in this study was lower than those of previously reported zein resin film (Rakotonirainy & Padua, 2001; Q. Wang & Padua, 2005). This can be attributed to the different conditions in lamination process that low pressure lamination was adopted in this study while high pressure carver press was used in previous studies (Rakotonirainy & Padua, 2001; Q. Wang & Padua, 2005). Nonetheless, after adding the nanofiller, the exfoliated nanocomposites Fe-Zein showed dramatic improvement in both tensile strength (218.0%), Young's modulus (by 264.6%) and elongation (by 48.3%) as compared with the blank zein resin film, which could be attributed primarily to the change of film composition and the formation of exfoliated structure. Similar phenomenon has been discovered by various studies using silica-based nanofillers (Luecha, Sozer, & Kokini, 2010) that the 2% loading of montmorillonite nanofiller in exfoliated

nanocomposite showed approximately 140% and 150% increase in tensile strength and Young's modulus, respectively. After nanofiller reorientation, the Fe-Zein-Mag sample showed more elastic behavior indicated by decreased Young's modulus (from 344 to 240 MPa), while the elongation further increased by another 47.7%. Moreover, the tensile strength of treated films showed an increase, but was not significantly different from that of control zein film. During the tensile testing, the external force was parallel to the resin film, and in the same direction as the orientation of the nanofiller in Fe-Zein-Mag, in which the fillers 'anchored' among different polymer molecules and provided a strengthened intermolecular attraction against deformation. We thought that the synthesized hexagonal Fe_3O_4 nanoplatelet had similar function as the role of silica nanoplatelet on improving mechanical property of biopolymer film, while providing additional magnetic property to manipulate fillers in situ at nano-scale.

5.4.5 Barrier property.

(1) *Water Vapor Permeability:*

The moisture and gas barrier property is another critical feature in determining the applicability of a biopolymer film as a packaging material. Similar to the mechanical properties, the water vapor permeability of zein resin film obtained in this study was also higher than the reported value (Rakotonirainy & Padua, 2001; Q. Wang & Padua, 2005) due to the involvement of low pressure lamination process. However, after forming the nanocomposites, the water vapor permeability of the exfoliated Fe-Zein sample was decreased 32% and 45% comparing to that of the

control zein resin film at 53% and 100% R.H., respectively. Previous study (Luecha, Sozer, & Kokini, 2010) using 2% loading of layered silica in zein film also achieved similar effects that the water vapor permeability decreased by 38% at 52% R.H. Therefore, the result indicated that the Fe_3O_4 nanofillers had similar function as layered silica, commonly used filler. In agreement with the theoretical modeling (Bharadwaj, 2001) and other previous research studies (Luecha, Sozer, & Kokini, 2010), the inorganic nanofillers (e.g. Fe_3O_4, or silica) were impermeable to water and gaseous molecules, due to the close packing substructure in their nanocrystal platelets. Based on Bharadwaj's theoretical model (Bharadwaj, 2001), as shown in Equation 1.2, the vapor permeability of nanocomposites with highly-ordered arrangement (S=1) could be as low as one third of that of exfoliated nanocomposites (S=0). In this study, the highly-ordered nanocomposites only showed an additional 48% and 34% drop of permeation rate at 53% and 100% R.H., respectively. The difference between the experimental results and the theoretical anticipation could be ascribed to the non-homogeneous distribution of the nanofillers inside the resin film (Figure 5.3b), even though most of them faced in the same direction. Besides, it can be seen in Table 5.2 that the water vapor permeability in 100% relative humidity was much higher than that in the 53% environment, and the effects of fillers' incorporation and orientation were also diminished in high moisture circumstance. Similar phenomena were previously reported by Lai et al. (Lai & Padua, 1998), in which they associated the phenomena with the swelling of zein resin film in high moisture environment. The swelling and the moisture adsorption inside the resin film may impair the integrity of

the film and result in defects on the formation of moisture channel for water migration.

Table 5.2 Gas barrier properties of zein-based nanocomposites

Sample Name	Water Vapor Permeability 53% R.H. (pg/Pa·Sec·m)	Water Vapor Permeability 100% R.H. (pg/Pa·Sec·m)	O_2 Permeability (10^{-18} m^2/ Pa·Sec)
Zein	58.51±13.22 a	69.26 ± 17.99 a	685.1 ± 52.8 a
Fe-Zein	18.91±3.66 b	31.58 ± 6.12 b	488.3 ± 44.6 b
Fe-Zein-Mag	9.83±4.29 c	20.95 ± 4.15 c	403.9 ± 39.4 c

* Means with same letter are not significantly different (P>0.05).

(2) *O_2 Permeability:*

Oxygen permeability is another useful characteristic in the application of biopolymer film. Similar to the result of water vapor permeability, Fe_3O_4 nanofillers provided a barrier to oxygen gas. After loading 2% of nanofillers in zein resin film, the O_2 permeability of Fe-Zein dropped 28.7% from that of zein control film. Besides, the highly-ordered nancomposite (Fe-Zein-Mag) showed further improvement by 17.3% to provide a better physical barrier to O_2. The improvement in O_2 barrier property was only half of that in water vapor. An earlier study ascribed this effect to the incorporation of plasticizer oleic acid (Kanig & Goodman, 1962; Rakotonirainy & Padua, 2001). They found that oleic acid can absorb free gaseous oxygen to the resin film and facilitate the permeation of oxygen molecule through the film. Since oleic acid was added into the zein film at the ratio of 1:1 w/w, it may have contributed to

the O_2 permeability and counterbalance the contribution of 2% loaded Fe_3O_4 nanofillers.

5.5 Conclusions

In summary, Fe_3O_4 magnetic nanoplatelets with high aspect ratio were successfully synthesized in this study using a simple hydrothermal reaction. The prepared nanoplatelet was used as nanofillers to form zein nanocomposites and improve mechanical and gas barrier properties of zein films (Figure 5.9). The structure and chemical composition of both random-oriented (exfoliated) and highly-ordered were confirmed by SEM, XRD, and VSM. Further investigation revealed that highly-ordered nanofillers can further improve the elasticity and gas barrier properties of zein films, which was predicted by Bharadwaj's theoretical study. Therefore, this study successfully confirmed the feasibility of preparing highly-ordered nanocomposites using high aspect ratio magnetic nanofillers. Besides, this method was simpler and more cost-effective comparing to the aforementioned lithography and layer-by-layer deposition methods, and may bring an impact on further improvement of the functionality and application of other biopolymer films. Nonetheless, to optimize the mechanical and gas barrier properties of biopolymer films, more work may be endeavored to resolve additional unknown questions, such as the potential environmental impact of the Fe_3O_4 nanofiller, or reduce potential interference of iron oxide filler to the metal detector by developing other magnetic nanofillers using conventional nanofiller materials, such as graphene sheet or layered silica doped with trace amount of iron ions.
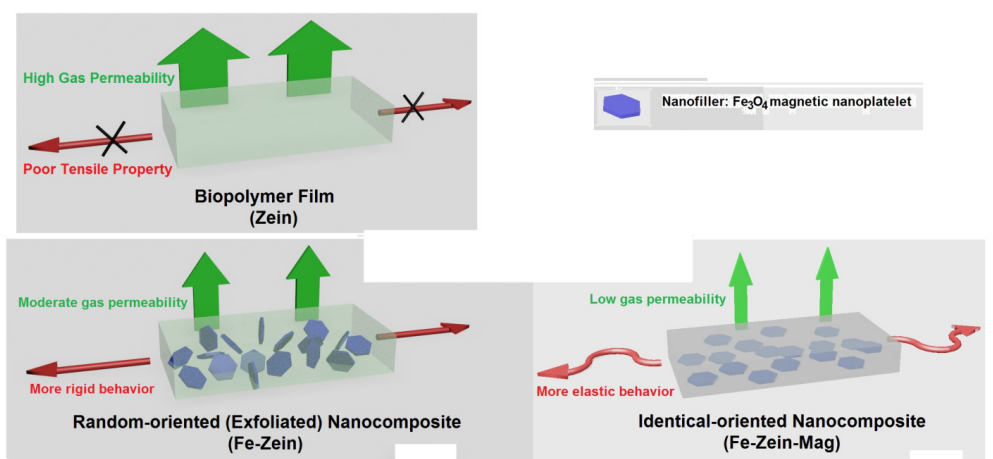
Figure 5.9 Scheme of Zein resin film (left), Fe-Zein exfoliated nanocomposite film (middle), and Fe-Zein-Mag highly-ordered nanocomposites film (right) The size of the red arrow indicated the level of the gas permeability rate (V.P. meant vapor pressure, and R.H. meant relative humidity); The shape of the blue arrow indicated the prominent tensile property of the film (Straight arrow meant rigid property, and curved arrow meant elastic property).

5.6 Acknowledgements

References

Akhavan, O., Abdolahad, M., Abdi, Y., & Mohajerzadeh, S. (2011). Silver nanoparticles within vertically aligned multi-wall carbon nanotubes with open tips for antibacterial purposes. *Journal of Materials Chemistry, 21*(2), 387-393.

Alexandre, M., & Dubois, P. (2000). Polymer-layered silicate nanocomposites: preparation, properties and uses of a new class of materials. *Materials Science & Engineering R-Reports, 28*(1-2), 1-63.

Alomirah, H. F., & Alli, I. (2004). Separation and characterization of beta-lactoglobulin and alpha-lactalbumin from whey and whey protein preparations. *International Dairy Journal, 14*(5), 411-419.

Andrews, J. M. (2001). Determination of minimum inhibitory concentrations. *Journal of Antimicrobial Chemotherapy, 48*, 5-16.

Arakawa, H., Neault, J. F., & Tajmir-Riahi, H. A. (2001). Silver(I) complexes with DNA and RNA studied by Fourier transform infrared spectroscopy and capillary electrophoresis. *Biophysical Journal, 81*(3), 1580-1587.

Argos, P., Pedersen, K., Marks, M. D., & Larkins, B. A. (1982). A STRUCTURAL MODEL FOR MAIZE ZEIN PROTEINS. *Journal of Biological Chemistry, 257*(17), 9984-9990.

Avella, M., De Vlieger, J. J., Errico, M. E., Fischer, S., Vacca, P., & Volpe, M. G. (2005). Biodegradable starch/clay nanocomposite films for food packaging applications. *Food Chemistry, 93*(3), 467-474.

Aymonier, C., Schlotterbeck, U., Antonietti, L., Zacharias, P., Thomann, R., Tiller, J. C., & Mecking, S. (2002). Hybrids of silver nanoparticles with amphiphilic hyperbranched macromolecules exhibiting antimicrobial properties. *Chemical Communications*(24), 3018-3019.

Balogh, L., Swanson, D. R., Tomalia, D. A., Hagnauer, G. L., & McManus, A. T. (2001). Dendrimer-silver complexes and nanocomposites as antimicrobial agents. *Nano Letters, 1*(1), 18-21.

Barone, J. R., Dangaran, K., & Schmidt, W. F. (2006). Blends of cysteine-containing proteins. *Journal of Agricultural and Food Chemistry, 54*(15), 5393-5399.

Berglin, M., Olsson, A., & Elwing, H. (2008). The interaction between model biomaterial coatings and nylon microparticles as measured with a quartz crystal microbalance with dissipation monitoring. *Macromolecular Bioscience, 8*(5), 410-416.

Beveridg.T, Toma, S. J., & Nakai, S. (1974). DETERMINATION OF SH-GROUPS AND SS-GROUPS IN SOME FOOD PROTEINS USING ELLMANS REAGENT. *Journal of Food Science, 39*(1), 49-51.

Bharadwaj, R. K. (2001). Modeling the barrier properties of polymer-layered silicate nanocomposites. *Macromolecules, 34*(26), 9189-9192.

Bollecker, S., Viroben, G., Popineau, Y., & Gueguen, J. (1990). ACID DEAMIDATION AND ENZYMATIC MODIFICATION AT PH-10 OF WHEAT GLIADINS - INFLUENCE ON THEIR FUNCTIONAL-PROPERTIES. *Sciences Des Aliments, 10*(2), 343-356.

Boyle, W. J., Simonet, W. S., & Lacey, D. L. (2003). Osteoclast differentiation and activation. *Nature, 423*(6937), 337-342.

Bruno, T., & Svoronos, P. (2006). *CRC handbook of fundamental spectroscopic correlation charts.* Florida, USA: CRC Press.

Cabedo, L., Feijoo, J. L., Villanueva, M. P., Lagaron, J. M., & Gimenez, E. (2006). Optimization of biodegradable nanocomposites based on aPLA/PCL blends for food packaging applications. *Macromolecular Symposia, 233*, 191-197.

Cabra, V., Arreguin, R., Vazquez-Duhalt, R., & Farres, A. (2007). Effect of alkaline deamidation on the structure, surface hydrophobicity, and emulsifying properties of the Z19 alpha-zein. *Journal of Agricultural and Food Chemistry, 55*(2), 439-445.

Carrado, K. A. (2000). Synthetic organo- and polymer-clays: preparation, characterization, and materials applications. *Applied Clay Science, 17*(1-2), 1-23.

Casella, M. L. A., & Whitaker, J. R. (1990). ENZYMATICALLY AND CHEMICALLY MODIFIED ZEIN FOR IMPROVEMENT OF FUNCTIONAL-PROPERTIES. *Journal of Food Biochemistry, 14*(6), 453-475.

Chan, W. K. M., Decker, E. A., Lee, J. B., & Butterfield, D. A. (1994). EPR SPIN-TRAPPING STUDIES OF THE HYDROXYL RADICAL SCAVENGING ACTIVITY OF CARNOSINE AND RELATED DIPEPTIDES. *Journal of Agricultural and Food Chemistry, 42*(7), 1407-1410.

Charles, A. L., Kao, H. M., & Huang, T. C. (2003). Physical investigations of surface membrane-water relationship of intact and gelatinized wheat-starch systems. *Carbohydrate Research, 338*(22), 2403-2408.

Charlot, A., Sciannamea, V., Lenoir, S., Faure, E., Jerome, R., Jerome, C., Van De Weerdt, C., Martial, J., Archambeau, C., Willet, N., Duwez, A. S., Fustin, C. A., & Detrembleur, C. (2009). All-in-one strategy for the fabrication of antimicrobial biomimetic films on stainless steel. *Journal of Materials Chemistry, 19*(24), 4117-4125.

Chen, B. Q., & Evans, J. R. G. (2005). Thermoplastic starch-clay nanocomposites and their characteristics. *Carbohydrate Polymers, 61*(4), 455-463.

Chen, G. H., Zhao, W. F., Tang, H. T., & Wang, H. Q. (2007). Preparation and surface characterization of highly ordered polymer/graphite nanosheet composites. *Materials and Manufacturing Processes, 22*(5-6), 733-736.

Chen, H., Gu, F., & Huang, Z. G. (2006). Improved Chou-Fasman method for protein secondary structure prediction. *Bmc Bioinformatics, 7*.

Chen, H. M., Muramoto, K., Yamauchi, F., Fujimoto, K., & Nokihara, K. (1998). Antioxidative properties of histidine-containing peptides designed from

peptide fragments found in the digests of a soybean protein. *Journal of Agricultural and Food Chemistry, 46*(1), 49-53.

Chen, H. M., Muramoto, K., Yamauchi, F., & Nokihara, K. (1996). Antioxidant activity of designed peptides based on the antioxidative peptide isolated from digests of a soybean protein. *Journal of Agricultural and Food Chemistry, 44*(9), 2619-2623.

Chen, P., & Zhang, L. (2006). Interaction and properties of highly exfoliated soy protein/montmorillonite nanocomposites. *Biomacromolecules, 7*(6), 1700-1706.

Chiue, H., Iwami, K., Kusano, T., & Ibuki, F. (1994). DECREASED ANTIOXIDATIVE ACTIVITY OF MAIZE ZEIN IN RESPONSE TO DEAMIDATION RATE. *Bioscience Biotechnology and Biochemistry, 58*(1), 198-199.

Chiue, H., Kusano, T., & Iwami, K. (1997). Deamidation-induced fragmentation of maize zein, and its linked reduction in fatty acid-binding capacity as well as antioxidative effect. *Food Chemistry, 58*(1-2), 111-117.

Cho, K. H., Park, J. E., Osaka, T., & Park, S. G. (2005). The study of antimicrobial activity and preservative effects of nanosilver ingredient. *Electrochimica Acta, 51*(5), 956-960.

Cserhati, T., Forgacs, E., & Illes, Z. (2003). TLC study of the binding of nonionic surfactants to the corn protein zein. *Journal of Liquid Chromatography & Related Technologies, 26*(16), 2751-2761.

Cuq, B., Gontard, N., & Guilbert, S. (1998). Proteins as agricultural polymers for packaging production. *Cereal Chemistry, 75*(1), 1-9.

Cyras, V. P., Manfredi, L. B., Ton-That, M. T., & Vazquez, A. (2008). Physical and mechanical properties of thermoplastic starch/montmorillonite nanocomposite films. *Carbohydrate Polymers, 73*(1), 55-63.

de Azeredo, H. M. C. (2009). Nanocomposites for food packaging applications. *Food Research International, 42*(9), 1240-1253.

Dean, K., & Yu, L. (2005). *Biodegradable polymers for industrial application*. FL, USA: CRC Press LLC.

Del Nobile, M. A., Conte, A., Incoronato, A. L., & Panza, O. (2008). Antimicrobial efficacy and release kinetics of thymol from zein films. *Journal of Food Engineering, 89*(1), 57-63.

do Nascimento, E. G., Sampaio, T. B. M., Medeiros, A. C., & de Azevedo, E. P. (2009). Evaluation of chitosan gel with 1% silver sulfadiazine as an alternative for burn wound treatment in rats. *Acta Cirurgica Brasileira, 24*(6), 460-465.

Dubas, S. T., & Pimpan, V. (2008). Green synthesis of silver nanoparticles for ammonia sensing. *Talanta, 76*(1), 29-33.

Dzwolak, W., Kato, M., Shimizu, A., & Taniguchi, Y. (2001). FTIR study on heat-induced and pressure-assisted cold-induced changes in structure of bovine alpha-lactalbumin: Stabilizing role of calcium ion. *Biopolymers, 62*(1), 29-39.

El-Gamel, N. E. A., Seyfarth, L., Wagler, J., Ehrenberg, H., Schwarz, M., Senker, J., & Kroke, E. (2007). The tautomeric forms of cyameluric acid derivatives. *Chemistry-a European Journal, 13*(4), 1158-1173.

Fink, H., Faxalv, L., Molnar, G. F., Drotz, K., Risberg, B., Lindahl, T. L., & Sellborn, A. (2010). Real-time measurements of coagulation on bacterial cellulose and conventional vascular graft materials. *Acta Biomaterialia, 6*(3), 1125-1130.

Forato, L. A., Bernardes, R., & Colnago, L. A. (1998). Protein structure in KBr pellets by infrared spectroscopy. *Analytical Biochemistry, 259*(1), 136-141.

Forato, L. A., Bicudo, T. C., & Colnago, L. A. (2003). Conformation of alpha Zeins in solid state by Fourier transform IR. *Biopolymers, 72*(6), 421-426.

Foss, S., Proksch, R., Dahlberg, E. D., Moskowitz, B., & Walsh, B. (1996). Localized micromagnetic perturbation of domain walls in magnetite using a magnetic force microscope. *Applied Physics Letters, 69*(22), 3426-3428.

Fratzl, P., Gupta, H. S., Paschalis, E. P., & Roschger, P. (2004). Structure and mechanical quality of the collagen-mineral nano-composite in bone. *Journal of Materials Chemistry, 14*(14), 2115-2123.

Furno, F., Morley, K. S., Wong, B., Sharp, B. L., Arnold, P. L., Howdle, S. M., Bayston, R., Brown, P. D., Winship, P. D., & Reid, H. J. (2004). Silver nanoparticles and polymeric medical devices: a new approach to prevention of infection? *Journal of Antimicrobial Chemotherapy, 54*(6), 1019-1024.

Gao, X. S., Rodriguez, B. J., Liu, L. F., Birajdar, B., Pantel, D., Ziese, M., Alexe, M., & Hesse, D. (2010). Microstructure and Properties of Well-Ordered

Multiferroic Pb(Zr,Ti)O-3/CoFe2O4 Nanocomposites. *Acs Nano, 4*(2), 1099-1107.

Goldstein, S., Meyerstein, D., & Czapski, G. (1993). THE FENTON REAGENTS. *Free Radical Biology and Medicine, 15*(4), 435-445.

Gong, S. J., Wang, H. J., Sun, Q. S., Xue, S. T., & Wang, J. Y. (2006). Mechanical properties and in vitro biocompatibility of porous zein scaffolds. *Biomaterials, 27*(20), 3793-3799.

Gordon, O., Slenters, T. V., Brunetto, P. S., Villaruz, A. E., Sturdevant, D. E., Otto, M., Landmann, R., & Fromm, K. M. (2010). Silver Coordination Polymers for Prevention of Implant Infection: Thiol Interaction, Impact on Respiratory Chain Enzymes, and Hydroxyl Radical Induction. *Antimicrobial Agents and Chemotherapy, 54*(10), 4208-4218.

Gucbilmez, C. M., Yemenicioglu, A., & Arslanoglu, A. (2007). Antimicrobial and antioxidant activity of edible zein films incorporated with lysozyme, albumin proteins and disodium EDTA. *Food Research International, 40*(1), 80-91.

Guo, H. X., Heinamaki, J., & Yliruusi, J. (2008). Stable aqueous film coating dispersion of zein. *Journal of Colloid and Interface Science, 322*(2), 478-484.

Guo, H. X., & Shi, Y. P. (2009). A novel zein-based dry coating tablet design for zero-order release. *International Journal of Pharmaceutics, 370*(1-2), 81-86.

Hamouda, T., & Baker, J. R. (2000). Antimicrobial mechanism of action of surfactant lipid preparations in enteric Gram-negative bacilli. *Journal of Applied Microbiology, 89*(3), 397-403.

Hernandez-Izquierdo, V. M., & Krochta, J. M. (2008). Thermoplastic processing of proteins for film formation - A review. *Journal of Food Science, 73*(2), R30-R39.

Hernandez-Ledesma, B., Amigo, L., Recio, I., & Bartolome, B. (2007). ACE-inhibitory and radical-scavenging activity of peptides derived from beta-lactoglobulin f(19-25). Interactions with ascorbic acid. *Journal of Agricultural and Food Chemistry, 55*(9), 3392-3397.

Ho, C. H., Tobis, J., Sprich, C., Thomann, R., & Tiller, J. C. (2004). Nanoseparated polymeric networks with multiple antimicrobial properties. *Advanced Materials, 16*(12), 957-+.

Hoffman, K. L., Han, I. Y., & Dawson, P. L. (2001). Antimicrobial effects of corn zein films impregnated with nisin, lauric acid, and EDTA. *Journal of Food Protection, 64*(6), 885-889.

Hu, Y. J., Fu, H. B., & Bernstein, E. R. (2006). IR plus vacuum ultraviolet spectroscopy of neutral and ionic organic acid molecules and clusters: Acetic acid. *Journal of Chemical Physics, 125*(18).

Huang, J. C., He, C. B., Liu, X. M., Xu, J. W., Tay, C. S. S., & Chow, S. Y. (2005). Organic-inorganic nanocomposites from cubic silsesquioxane epoxides: direct characterization of interphase, and thermomechanical properties. *Polymer, 46*(18), 7018-7027.

Hurtado-Lopez, P., & Murdan, S. (2005). Formulation and characterisation of zein microspheres as delivery vehicles. *Journal of Drug Delivery Science and Technology, 15*(4), 267-272.

Hurtado-Lopez, P., & Murdan, S. (2006). Zein microspheres as drug/antigen carriers: A study of their degradation and erosion, in the presence and absence of enzymes. *Journal of Microencapsulation, 23*(3), 303-314.

Jiang, B., Guo, T., Peng, L. W., & Sun, Z. R. (1998). Folding type-specific secondary structure propensities of amino acids, derived from alpha-helical, beta-sheet, alpha/beta, and alpha+beta proteins of known structures. *Biopolymers, 45*(1), 35-49.

Jonas, L., Bloch, C., Zimmermann, R., Stadie, V., Gross, G. E., & Schad, S. G. (2007). Detection of silver sulfide deposits in the skin of patients with argyria after long-term use of silver-containing drugs. *Ultrastructural Pathology, 31*(4-6), 379-384.

Joshi, A. B., Sawai, M., Kearney, W. R., & Kirsch, L. E. (2005). Studies on the mechanism of aspartic acid cleavage and glutamine deamidation in the acidic degradation of glucagon. *Journal of Pharmaceutical Sciences, 94*(9), 1912-1927.

Kanig, J. L., & Goodman, H. (1962). Evaluative procedures for film-forming materials used in pharmaceutical applications. *Journal of Pharmaceutical Sciences, 51*(1), 77-83.

Kim, J. S., Kuk, E., Yu, K. N., Kim, J. H., Park, S. J., Lee, H. J., Kim, S. H., Park, Y. K., Park, Y. H., Hwang, C. Y., Kim, Y. K., Lee, Y. S., Jeong, D. H., & Cho, M. H. (2007). Antimicrobial effects of silver nanoparticles. *Nanomedicine-Nanotechnology Biology and Medicine, 3*(1), 95-101.

Kim, J. Y., Lee, C., Cho, M., & Yoon, J. (2008). Enhanced inactivation of E. coli and MS-2 phage by silver ions combined with UV-A and visible light irradiation. *Water Research, 42*(1-2), 356-362.

Kriegel, C., Arrechi, A., Kit, K., McClements, D. J., & Weiss, J. (2008). Fabrication, functionalization, and application of electrospun biopolymer nanofibers. *Critical Reviews in Food Science and Nutrition, 48*(8), 775-797.

Krishnaraj, C., Jagan, E. G., Rajasekar, S., Selvakumar, P., Kalaichelvan, P. T., & Mohan, N. (2010). Synthesis of silver nanoparticles using Acalypha indica leaf extracts and its antibacterial activity against water borne pathogens. *Colloids and Surfaces B-Biointerfaces, 76*(1), 50-56.

Ku, K., & Song, K. B. (2007). *J. Microbiol. Biotechnol., 17*, 520.

Kumar, P., Sandeep, K. P., Alavi, S., & Truong, V. D. (2011). A Review of Experimental and Modeling Techniques to Determine Properties of Biopolymer-Based Nanocomposites. *Journal of Food Science, 76*(1), E2-E14.

Kumar, R., & Munstedt, H. (2005). Silver ion release from antimicrobial polyamide/silver composites. *Biomaterials, 26*(14), 2081-2088.

Lai, H. M., & Padua, G. W. (1997). Properties and microstructure of plasticized zein films. *Cereal Chemistry, 74*(6), 771-775.

Lai, H. M., & Padua, G. W. (1998). Water vapor barrier properties of zein films plasticized with oleic acid. *Cereal Chemistry, 75*(2), 194-199.

Lai, H. M., Padua, G. W., & Wei, L. S. (1997). Properties and microstructure of zein sheets plasticized with palmitic and stearic acids. *Cereal Chemistry, 74*(1), 83-90.

Lawton, J. W. (2002). Zein: A history of processing and use. *Cereal Chemistry, 79*(1), 1-18.

Lee, P. C., & Meisel, D. (1982). ADSORPTION AND SURFACE-ENHANCED RAMAN OF DYES ON SILVER AND GOLD SOLS. *Journal of Physical Chemistry, 86*(17), 3391-3395.

Liu, X. M., Sun, Q. S., Wang, H. J., Zhang, L., & Wang, J. Y. (2005). Microspheres of corn protein, zein, for an ivermectin drug delivery system. *Biomaterials, 26*(1), 109-115.

Luecha, J., Sozer, N., & Kokini, J. L. (2010). Synthesis and properties of corn zein/montmorillonite nanocomposite films. *Journal of Materials Science, 45*(13), 3529-3537.

Lunt, J. (1998). Large-scale production, properties and commercial applications of polylactic acid polymers. *Polymer Degradation and Stability, 59*(1-3), 145-152.

Marcuse, R. (1960). ANTIOXIDATIVE EFFECT OF AMINO-ACIDS. *Nature, 186*(4728), 886-887.

Marsh, K., & Bugusu, B. (2007). Food packaging - Roles, materials, and environmental issues. *Journal of Food Science, 72*(3), R39-R55.

Mastromatteo, M., Barbuzzi, G., Conte, A., & Del Nobile, M. A. (2009). Controlled release of thymol from zein based film. *Innovative Food Science & Emerging Technologies, 10*(2), 222-227.

Matsushima, N., Danno, G., Takezawa, H., & Izumi, Y. (1997). Three-dimensional structure of maize alpha-zein proteins studied by small-angle X-ray scattering. *Biochimica Et Biophysica Acta-Protein Structure and Molecular Enzymology, 1339*(1), 14-22.

McGowan, B. A., Padua, G. W., & Lee, S. Y. (2005). Formulation of corn zein chewing gum and evaluation of sensory properties by the time-intensity method. *Journal of Food Science, 70*(7), S475-S481.

Melaiye, A., Sun, Z. H., Hindi, K., Milsted, A., Ely, D., Reneker, D. H., Tessier, C. A., & Youngs, W. J. (2005). Silver(I)-imidazole cyclophane gem-diol complexes encapsulated by electrospun tecophilic nanofibers: Formation of nanosilver particles and antimicrobial activity. *Journal of the American Chemical Society, 127*(7), 2285-2291.

Miller, K. S., & Krochta, J. M. (1997). Oxygen and aroma barrier properties of edible films: A review. *Trends in Food Science & Technology, 8*(7), 228-237.

Mizutani, Y., Matsumura, Y., Imamura, K., Nakanishi, K., & Mori, T. (2003). Effects of water activity and lipid addition on secondary structure of zein in powder systems. *Journal of Agricultural and Food Chemistry, 51*(1), 229-235.

147

Mohungoo, M. J., & Gawkrodger, D. J. (2009). Allergy to silver in a patient with oral lichenoid reaction, with a review of patch testing experience in 27 cases of oral lichenoid reaction. *British Journal of Dermatology, 161*, 79-79.

Morgado, E. (1992). ELECTRONEGATIVITY EFFECTS ON THE FREQUENCY OF THE N-H STRETCHING MODE IN PLASMA DEPOSITED A-SI-N-H ALLOYS. *Journal of Non-Crystalline Solids, 139*(3), 248-256.

Mukherjee, T., & Kao, N. (2011). PLA Based Biopolymer Reinforced with Natural Fibre: A Review. *Journal of Polymers and the Environment, 19*(3), 714-725.

Nelson, D., & Cox, M. (2004). *Lehninger Principles of Biochemistry*. New York, USA: W. H. Freeman.

Ogrady, F., Murphy, B., & Pearson, N. J. (1983). SEMIAUTOMATED DETERMINATION OF MINIMUM BACTERICIDAL CONCENTRATIONS OF ANTIBIOTICS. *Journal of Clinical Pathology, 36*(2), 208-212.

Ozkaya, E. (2009). A rare case of allergic contact dermatitis from silver nitrate in a widely used special patch test marker. *Contact Dermatitis, 61*(2), 120-122.

Panacek, A., Kvitek, L., Prucek, R., Kolar, M., Vecerova, R., Pizurova, N., Sharma, V. K., Nevecna, T., & Zboril, R. (2006). Silver colloid nanoparticles: Synthesis, characterization, and their antibacterial activity. *Journal of Physical Chemistry B, 110*(33), 16248-16253.

Pena-Ramos, E. A., Xiong, Y. L. L., & Arteaga, G. E. (2004). Fractionation and characterisation for antioxidant activity of hydrolysed whey protein. *Journal of the Science of Food and Agriculture, 84*(14), 1908-1918.

Peters, B., & Trout, B. L. (2006). Asparagine deamidation: pH-dependent mechanism from density functional theory. *Biochemistry, 45*(16), 5384-5392.

Petruccelli, S., & Anon, M. C. (1995). PARTIAL REDUCTION OF SOY PROTEIN ISOLATE DISULFIDE BONDS. *Journal of Agricultural and Food Chemistry, 43*(8), 2001-2006.

Platt, D. (2006). *Biodegradable Polymer - Market Report*. Shropshire, UK: Smithers Rapra Limited.

Pomes, A. (1971). **Zein**. In H. Mark (Ed.), *Encyclopedia of polymer science and technology*, vol. 15 (pp. 125–132): Wiley.

Rakotonirainy, A. M., & Padua, G. W. (2001). Effects of lamination and coating with drying oils on tensile and barrier properties of zein films. *Journal of Agricultural and Food Chemistry, 49*(6), 2860-2863.

Ramanathan, T., Abdala, A. A., Stankovich, S., Dikin, D. A., Herrera-Alonso, M., Piner, R. D., Adamson, D. H., Schniepp, H. C., Chen, X., Ruoff, R. S., Nguyen, S. T., Aksay, I. A., Prud'homme, R. K., & Brinson, L. C. (2008). Functionalized graphene sheets for polymer nanocomposites. *Nature Nanotechnology, 3*(6), 327-331.

Ray, S. S., & Bousmina, M. (2005). Biodegradable polymers and their layered silicate

   nano composites: In greening the 21st century materials world. *Progress in*

   Materials Science, 50(8), 962-1079.

Ray, S. S., & Okamoto, M. (2003). Polymer/layered silicate nanocomposites: a review

   from preparation to processing. *Progress in Polymer Science, 28*(11),

   1539-1641.

Rhim, J. W. (2007). Potential use of biopolymer-based nanocomposite films in food

   packaging applications. *Food Science and Biotechnology, 16*(5), 691-709.

Rhim, J. W., Lee, J. H., & Hong, S. I. (2007). Increase in water resistance of

   paperboard by coating with poly(lactide). *Packaging Technology and Science,*

   20(6), 393-402.

Rhim, J. W., Lee, J. H., & Kwak, H. S. (2005). Mechanical and water barrier

   properties of soy protein and clay mineral composite films. *Food Science and*

   Biotechnology, 14(1), 112-116.

Rissa, K., Lepisto, T., & Yrjola, K. (2006). Effect of kaolin content on structure and

   functional properties of water-based coatings. *Progress in Organic Coatings,*

   55(2), 137-141.

Romanov, V., Siu, C. K., Verkerk, U. H., Hopkinson, A. C., & Siu, K. W. M. (2010).

   Bond Dissociation Energies of Solvated Silver(I)-Amide Complexes:

   Competitive Threshold Collision-Induced Dissociations and Calculations.

   Journal of Physical Chemistry A, 114(26), 6964-6971.

Saiga, A., Tanabe, S., & Nishimura, T. (2003). Antioxidant activity of peptides obtained from porcine myofibrillar proteins by protease treatment. *Journal of Agricultural and Food Chemistry, 51*(12), 3661-3667.

Salvetat, J. P., Kulik, A. J., Bonard, J. M., Briggs, G. A. D., Stockli, T., Metenier, K., Bonnamy, S., Beguin, F., Burnham, N. A., & Forro, L. (1999). Elastic modulus of ordered and disordered multiwalled carbon nanotubes. *Advanced Materials, 11*(2), 161-165.

Sanpui, P., Murugadoss, A., Prasad, P. V. D., Ghosh, S. S., & Chattopadhyay, A. (2008). The antibacterial properties of a novel chitosan-Ag-nanoparticle composite. *International Journal of Food Microbiology, 124*(2), 142-146.

Sellborn, A., Andersson, M., Fant, C., Gretzer, C., & Elwing, H. (2003). Methods for research on immune complement activation on modified sensor surfaces. *Colloids and Surfaces B-Biointerfaces, 27*(4), 295-301.

Sellborn, A., Andersson, M., Hedlund, J., Andersson, J., Berglin, M., & Elwing, H. (2005). Immune complement activation on polystyrene and silicon dioxide surfaces Impact of reversible IgG adsorption. *Molecular Immunology, 42*(5), 569-574.

Selling, G. W., Biswas, A., Patel, A., Walls, D. J., Dunlap, C., & Wei, Y. (2007). Impact of solvent on electrospinning of zein and analysis of resulting fibers. *Macromolecular Chemistry and Physics, 208*(9), 1002-1010.

Selling, G. W., Lawton, J., Bean, S., Dunlap, C., Sessa, D. J., Willett, J. L., & Byars, J. (2005). Rheological studies utilizing various lots of zein in

N,N-dimethylformamide solutions. *Journal of Agricultural and Food Chemistry, 53*(23), 9050-9055.

Sessa, D. J., Selling, G. W., Willett, J. L., & Palmquist, D. E. (2006). Viscosity control of zein processing with sodium dodecyl sulfate. *Industrial Crops and Products, 23*(1), 15-22.

Shewry, P. R., & Tatham, A. S. (1990). THE PROLAMIN STORAGE PROTEINS OF CEREAL SEEDS - STRUCTURE AND EVOLUTION. *Biochemical Journal, 267*(1), 1-12.

Shi, K., Kokini, J. L., & Huang, Q. R. (2009). Engineering Zein Films with Controlled Surface Morphology and Hydrophilicity. *Journal of Agricultural and Food Chemistry, 57*(6), 2186-2192.

Sinclair, R. G. (1996). The case for polylactic acid as a commodity packaging plastic. *Journal of Macromolecular Science-Pure and Applied Chemistry, A33*(5), 585-597.

Singh, N., Georget, D. M. R., Belton, P. S., & Barker, S. A. (2009). Zein-Iodine Complex Studied by FTIR Spectroscopy and Dielectric and Dynamic Rheometry in Films and Precipitates. *Journal of Agricultural and Food Chemistry, 57*(10), 4334-4341.

Sondi, I., & Salopek-Sondi, B. (2004). Silver nanoparticles as antimicrobial agent: a case study on E-coli as a model for Gram-negative bacteria. *Journal of Colloid and Interface Science, 275*(1), 177-182.

Sorrentino, A., Gorrasi, G., & Vittoria, V. (2007). Potential perspectives of bio-nanocomposites for food packaging applications. *Trends in Food Science & Technology, 18*(2), 84-95.

Stoimenov, P. K., Klinger, R. L., Marchin, G. L., & Klabunde, K. J. (2002). Metal oxide nanoparticles as bactericidal agents. *Langmuir, 18*(17), 6679-6686.

Stuart, B. (2004). *Infrared spectroscopy: fundamentals and applications* (Vol. 14, Analytical techniques in the sciences). West Sussex, <st1:country-region w:st="on"><st1:place w:st="on">UK</st1:country-region>: John Wiley and Sons.

Svagan, A., **Åkesson, A.**, **Cárdenas, M.**, **Bulut, S.**, **Knudsen, J.**, **Risbo, J.**, & **Plackett, D.** (2012). Transparent Films Based on PLA and Montmorillonite with Tunable Oxygen Barrier Properties. *Biomacromolecules*.

Tan, Y., Zhuang, Z., Peng, Q., & Li, Y. (2008). Room-temperature soft magnetic iron oxide nanocrystals: Synthesis, characterization, and size-dependent magnetic properties. *Chemistry of Materials, 20*(15), 5029-5034.

Tian, Y., Park, J. G., Cheng, Q. F., Liang, Z. Y., Zhang, C., & Wang, B. (2009). The fabrication of single-walled carbon nanotube/polyelectrolyte multilayer composites by layer-by-layer assembly and magnetic field assisted alignment. *Nanotechnology, 20*(33), 7.

Tomov, I. (2005). Accounting for secondary extinction in XRD characterizations of texture and microstructure with anisotropy - Responsive methods. *Archives of Metallurgy and Materials, 50*(1), 147-157.

Travan, A., Pelillo, C., Donati, I., Marsich, E., Benincasa, M., Scarpa, T., Semeraro, S., Turco, G., Gennaro, R., & Paoletti, S. (2009). Non-cytotoxic Silver Nanoparticle-Polysaccharide Nanocomposites with Antimicrobial Activity. *Biomacromolecules, 10*(6), 1429-1435.

Triebel, C., Vasylyev, S., Damm, C., Stara, H., Ozpinar, C., Hausmann, S., Peukert, W., & Munstedt, H. (2011). Polyurethane/silver-nanocomposites with enhanced silver ion release using multifunctional invertible polyesters. *Journal of Materials Chemistry, 21*(12), 4377-4383.

Tu, J. W., Wang, H. J., Li, H. W., Dai, K. R., Wang, J. Y., & Zhang, X. L. (2009). The in vivo bone formation by mesenchymal stem cells in zein scaffolds. *Biomaterials, 30*(26), 4369-4376.

Uyama, H., Kuwabara, M., Tsujimoto, T., Nakano, M., Usuki, A., & Kobayashi, S. (2003). Green nanocomposites from renewable resources: Plant oil-clay hybrid materials. *Chemistry of Materials, 15*(13), 2492-2494.

Valappil, S. P., Pickup, D. M., Carroll, D. L., Hope, C. K., Pratten, J., Newport, R. J., Smith, M. E., Wilson, M., & Knowles, J. C. (2007). Effect of silver content on the structure and antibacterial activity of silver-doped phosphate-based glasses. *Antimicrobial Agents and Chemotherapy, 51*(12), 4453-4461.

Vanaman, T. C., Brew, K., & Hill, R. L. (1970). DISULFIDE BONDS OF BOVINE ALPHA-LACTALBUMIN. *Journal of Biological Chemistry, 245*(17), 4583-&.

Walling, C. (1998). Intermediates in the reactions of Fenton type reagents. *Accounts of Chemical Research, 31*(4), 155-157.

Wang, H. J., Gong, S. J., Lin, Z. X., Fu, J. X., Xue, S. T., Huang, J. C., & Wang, J. Y. (2007). In vivo biocompatibility and mechanical properties of porous zein scaffolds. *Biomaterials, 28*(27), 3952-3964.

Wang, H. J., Gong, S. J., & Wang, J. Y. (2008). Mechanical improvement of zein protein as scaffold for bone tissue engineering. *Materials Science and Technology, 24*(9), 1045-1052.

Wang, J., Chen, Q. W., Zeng, C., & Hou, B. Y. (2004). Magnetic-field-induced growth of single-crystalline Fe3O4 nanowires. *Advanced Materials, 16*(2), 137-+.

Wang, Q., & Padua, G. W. (2005). Properties of zein films coated with drying oils. *Journal of Agricultural and Food Chemistry, 53*(9), 3444-3448.

Wang, Q., Yin, L. L., & Padua, G. W. (2008). Effect of hydrophilic and lipophilic compounds on zein microstructures. *Food Biophysics, 3*(2), 174-181.

Wang, Y., & Padua, G. W. (2003). Tensile properties of extruded Zein sheets and extrusion blown films. *Macromolecular Materials and Engineering, 288*(11), 886-893.

Wei, D. W., Sun, W. Y., Qian, W. P., Ye, Y. Z., & Ma, X. Y. (2009). The synthesis of chitosan-based silver nanoparticles and their antibacterial activity. *Carbohydrate Research, 344*(17), 2375-2382.

Winters, E. P., & Deardorff, D. L. (1958). ZEIN AS A FILM-TYPE COATING FOR MEDICINAL TABLETS. *Journal of the American Pharmaceutical Association, 47*(8), 608-612.

Wong, E. W., Sheehan, P. E., & Lieber, C. M. (1997). Nanobeam mechanics: Elasticity, strength, and toughness of nanorods and nanotubes. *Science, 277*(5334), 1971-1975.

Wouters, J., Lebedev, O. I., Van Tendeloo, G., Yamada, H., Sato, N., Vanacken, J., Moshchalkov, V. V., Verbiest, T., & Valev, V. K. (2011). Preparing polymer films doped with magnetic nanoparticles by spin-coating and melt-processing can induce an in-plane magnetic anisotropy. *Journal of Applied Physics, 109*(7).

Wright, J. B., Lam, K., & Burrell, R. E. (1998). Wound management in an era of increasing bacterial antibiotic resistance: A role for topical silver treatment. *American Journal of Infection Control, 26*(6), 572-577.

Yong, Y. H., Yamaguchi, S., Gu, Y. S., Mori, T., & Matsumura, Y. (2004). Effects of enzymatic deamidation by protein-glutaminase on structure and functional properties of alpha-zein. *Journal of Agricultural and Food Chemistry, 52*(23), 7094-7100.

Yu, J. G., Yang, J. W., Liu, B. X., & Ma, X. F. (2009). Preparation and characterization of glycerol plasticized-pea starch/ZnO-carboxymethylcellulose sodium nanocomposites. *Bioresource Technology, 100*(11), 2832-2841.

Zhang, B., Luo, Y., & Wang, Q. (2010). Development of Silver−Zein Composites as a Promising Antimicrobial Agent. *Biomacromolecules, 11*(9), 2366-2375.

Zhang, B., Luo, Y., & Wang, Q. (2011). Development of silver/alpha-lactalbumin nanocomposites: a new approach to reduce silver toxicity. *International Journal of Antimicrobial Agents, 38*(6), 502-509.

Zhang, B. C., Luo, Y. C., & Wang, Q. (2010). Development of Silver-Zein Composites as a Promising Antimicrobial Agent. *Biomacromolecules, 11*(9), 2366-2375.

Zhang, B. C., Luo, Y. C., & Wang, Q. (2011). Effect of acid and base treatments on structural, rheological, and antioxidant properties of alpha-zein. *Food Chemistry, 124*(1), 210-220.

Zhao, R. X., Torley, P., & Halley, P. J. (2008). Emerging biodegradable materials: starch- and protein-based bio-nanocomposites. *Journal of Materials Science, 43*(9), 3058-3071.

Zhong, Q. X., & Jin, M. F. (2009). Nanoscalar Structures of Spray-Dried Zein Microcapsules and in Vitro Release Kinetics of the Encapsulated Lysozyme As Affected by Formulations. *Journal of Agricultural and Food Chemistry, 57*(9), 3886-3894.

Zhong, Q. X., Jin, M. F., Davidson, P. M., & Zivanovic, S. (2009). Sustained release of lysozyme from zein microcapsules produced by a supercritical anti-solvent process. *Food Chemistry, 115*(2), 697-700.

Zhu, L. J., Chen, J., Tang, X. Y., & Xiong, Y. L. L. (2008). Reducing, radical

scavenging, and chelation properties of in vitro digests of alcalase-treated zein

hydrolysate. *Journal of Agricultural and Food Chemistry, 56*(8), 2714-2721.